DISPLACEMENT DEMANDS FOR PERFORMANCE BASED DESIGN OF SKEWED BRIDGES WITH SEAT TYPE ABUTMENTS

Seku Samory Catacoli Mosquera

M.A.Sc., Del Valle University, Colombia, 2008

B.A., Del Valle University, Colombia, 2002

A THESIS SUBMITTED IN PARTIAL FULFILLMENT OF

THE REQUIREMENTS FOR THE DEGREE OF

DOCTOR OF PHILOSOPHY

in

THE FACULTY OF GRADUATE STUDIES AND POSTDOCTORAL STUDIES

(Civil Engineering)

THE UNIVERSITY OF BRITISH COLUMBIA

(Vancouver)

February 2014

Abstract

Skewed bridges are irregular structures due to the geometry of the deck and bents. Past earthquakes indicate that skewed bridges with seat type abutments exhibit greater damage than their non-skewed pairs. The damage has been attributed to in-plane rotations caused by pounding between the skewed deck and its abutments during strong ground shaking.

This thesis combines experimental and analytical approaches to understanding the displacement demands on skewed bridges. As part of the experimental studies, results from ambient vibrations tests help to better understand the importance of directionality in the lateral response of skewed bridges. The predominant direction of the transverse response occurs in the direction of the skew bents; whereas the predominant direction of the longitudinal response is perpendicular to the skew. In addition, the analysis of records from an instrumented skewed bridge confirmed accelerations that could produce in-plane rotations of the deck.

A comprehensive parametric study based on nonlinear dynamic analyses was performed to evaluate the effects of different skew angles, abutments types, and soil-foundation-structure interaction. The results demonstrated that elastic methods recommended by current seismic design provisions, and commonly used in standard practice, do not properly capture the in-plane rotations of the deck due to pounding. To overcome this shortcoming, a simple and effective method is proposed here to evaluate the displacement demands of skewed piers accounting for in-plane deck rotations.

The proposed method uses validated simplified nonlinear models to generate torsional sensitivity charts for specific bridge prototypes. The charts provide peak in-plane deck rotation estimates as a function of bridge skew angle and the in-plane rotational period. An advantage of this approach is that it requires the designer to only conduct a linear dynamic analysis of the bridge. Nonlinear analysis required to assess the in-plane deck rotation is replaced here by torsional sensitivity charts. The proposed approach is able to predict the displacement response for a comprehensive range of skewed bridge prototypes by capturing the effects of the main parameters controlling the response. The information presented in this thesis will help improve the existing recommendations for performance based design of skewed bridges.

Preface

This work was part of a research project entitled "Seismic Response of Skewed Bridges" carried on in a professional partnership between the University of British Columbia (UBC) and the British Columbia Ministry of Transportation and Infrastructure (BCMoT) to provide practical guidelines for the seismic assessment of skewed bridges. Professor Carlos E. Ventura was the Project Leader and also the Supervisor of this research work.

Parts of the materials included in Chapters 1 and 2 of this document were published in three conference articles, listed below:

- Catacoli S., Ventura C.E., Finn, W.D.L. (2012) Displacement Demands for Performance Based Design of Skewed Bridges. Proceedings of the Fifteenth World Conference on Earthquake Engineering, Lisbon, Portugal. Paper ID: 3586, 9 pages. I wrote the paper, conducted the analyses and formulated the models. Professors Ventura and Finn were the reviewers and provided important feedback.

- Catacoli S., Ventura C.E., McDonald S (2013) System Identification and Displacements Profiles of Multi-Span Skewed Bridges with Seat Type Abutments. Topics in the Dynamics of Civil Structures, Volume 4. Conference Proceedings of the Society for Experimental Mechanics Series 2013, pp 127-135. McDonald, S. was a member of the field team conducting the test and helped to process the data. I conducted the analysis, prepared the computational models to check the results and wrote the paper.

- Catacoli S., Ventura C.E. (2013) Dynamic Response of a Multi-Span Skewed Bridge with Seat Type Abutments to Moderate Ground Motions. Proceedings of the International Operational Modal Analysis Conference 2013, Minho, Portugal. Paper ID: 219, 9 pages. I processed the data, conducted the analysis and wrote the paper. Professor Ventura was the main reviewer and as director of the Earthquake Engineering Research Facility (EERF) granted access to hardware and software available at the EERF.

.

Table of Contents

List of Tables

List of Figures

List of Abbreviations

AASTHO: American Association of State Highway and Transportation Officials

BCMoT: British Columbia Ministry of Transportation and Infrastructure

CHBDC: Canadian Highway Bridge Code

EASI : Embankment- Abutment- Structure Interaction

EFDD: Enhanced Frequency Domain Decomposition

Mw: Earthquake Moment Magnitude

MSEW: Mechanically Stabilized Walls

PGA: Peak Ground Acceleration

SSI: Soil Structure Interaction

SSI : Stochastic Subspace Identification (modal identification technique)

SFSI: Soil-Foundation-Structure Interaction

List of Symbols

CM: Center of mass of the deck

D: Pier diameter

dd, bb: Distance between columns in X and Y directions

F_u: Maximum passive capacity of the abutment-backfill

f : Frequency of vibration in hertz

H: Pier height

I_o: Mass moment of inertia of superstructure

K_{abut} : Stiffness of the abutment-backfill

$K_{abut\text{-}eff}$: Effective stiffness of the abutment-backfill

k_{colx} , k_{coly}: Pier stiffness in the transverse and longitudinal directions

$K_{sh\text{-}eff}$: Effective stiffness of the abutment-shear key

K_{11}, K_{22}, K_{33}, K_{44}, K_{55}, K_{66}: Pile cap stiffnesses

$K_{LONG\text{-}O}$: Longitudinal stiffness of the bridge when the gap at expansion joints is open

$K_{ROT\text{-}O}$: In-plane rotational stiffness of the bridge when the longitudinal gap at expansion joints is open

K_{TRAN}: Transverse stiffness of the bridge (stiffness at the center of mass in the transverse direction due to columns and shear keys contributions)

L: Total bridge span

L_C: Maximum horizontal distance from the pier to center of stiffness

m: Mass of superstructure (deck + cap beams)

N_C: Number of piers in the bridge

P_u: Maximum capacity of the abutment-shear key

S_a : Spectral acceleration

S_D: Spectral displacement

T_{Long}: Longitudinal period of the bridge

T_{Long-o}: Longitudinal period of the bridge when the gap at expansion joints is open

T_{rot}: In-plane rotational period of the bridge

T_{rot-o}: In-plane rotational period of the bridge when the longitudinal gap at expansion joints is open.

T_{Tran}: Transverse period of the bridge

ε_{50}: Strain at 50% stress level of clay

ϕ: Skew angle

Δ_{rot}: Additional pier drift due to in-plane deck rotation

Δ_{trans}: Pier drift due to lateral translation of deck

Δ_{Total}: Total drift of the pier

ξ: Damping ratio

θ: Peak in-plane rotation of the deck

Acknowledgements

I want to thank my Supervisor Dr. Carlos Ventura for opening the doors of the UBC- Earthquake Engineering Research Facility (EERF) to me. My expectation of working with the best in a wide variety of earthquake engineering topics has been fulfilled. Thank for the constant challenge, the positive reinforcement, and the personal advice, especially during the hard times. I am honored by your trust and for always believing that I would make it to this point. Working together, I learned to be a problem solver instead of a trouble maker, this along with the critical thinking and research independence have become a strong foundation in my career.

I am deeply grateful to one of the greatest earthquake engineering minds I have ever met: Dr. Liam Finn. His co-supervision and personal support have been fundamental throughout. I feel so blessed for the opportunity to work with Dr. Finn, and listening to his countless experiences was always among the most delightful academic moments at UBC. I am highly indebted to Dr. Finn's advice.

I would like to thank Dr. Don Anderson for his dedication and sharp comments during my research process, particularly when the research problems became especially challenging. Dr. Anderson's observations and review were fundamental to achieve the quality and objectives of this work. I would also like to thank Dr. Mahdi Taiebat for his kind support, and constant interest in the modeling aspects of this research. Dr. Taiebat was instrumental in facilitating the computer server required to run the large amount of analyses conducted in this work and he provided comments that enhanced the quality of the presentation of this thesis. I am also grateful to Dr.

Ken Elwood for a research assistantship provided during the initial part of my PhD program and his great support for my adjustment to the bridge engineering world and the Canadian education system.

I am thankful to the external examiner Prof. Mervyn Kowalsky from North Carolina State University, as well as the examiners Prof. Farrokh Sassani and Prof. Siegfried F. Stiemer from UBC, for conducting an insightful and detailed evaluation of this thesis.

This research is funded by the British Columbia Ministry of Transportation and Infrastructure. The support provided by Senior Bridge Engineer Sharlie Huffman is acknowledged with thanks and was very instrumental to ensure the practical deliverables of this research.

I would also like to thank the recommendations of Dr. Anoosh Shamsabadi from the California Ministry of Transportation (CALTRANS), as well as briefings regarding bridge engineering practice in British Columbia given by the Senior Engineer Don Kennedy from Associated Engineering. Acknowledgements are also extended to the Central Weather Bureau of Taiwan (CWB), the Ministry of Transportation and Communications of Taiwan, and Mr. Jason Ching for providing strong motion data and drawings of an instrumented skewed bridge analyzed in this research.

I want to express my gratitude to my mentors at Del Valle University in Colombia for their hard work and envisioning my enrollment in a PhD program: Doctors Jose Garcia, Patricia Guerrero, and Peter Thomson. Also to the memory of Esteban Vanegas, Earthquake Engineering Lab Manager, a great friend, and a talented researcher.

Special thanks to Miguel Fraino for helping me to shape the graphics in this thesis and to my friends Jason Dowling, Sheri Molnar, Jose Centeno, Manuel Archila, and Brook Robazza for kindly proofreading different parts of this manuscript.

Many thanks to all the members of the UBC- Soil Structure Interaction Group for their collaboration and comments during the regular presentations of this work. My gratitude to the executive members of the Structural Engineers Association of British Columbia (SEABC) for the opportunity to work in the certificate program in structural engineering. Also, thanks to the staff and the beautiful people that I met at my residence, St John's College: the best place on earth, which provided an essential balance during my PhD Program.

During this process I met and counted on with the support of people that will always be stamped in my heart: Manuel Archila, Miguel Fraino, Jose Centeno, Freddy Pina, Illiana Mijares, Sotonye Godwin, Leah Mwai, Sheri Molnar, Jose Florez, Tom Peotto, Daniel Archila, Abhijit Pandary, Kara Shin, Katherine Mendez, Sandra Mejia, Dawn Wong, Juan Serpa, Juan Carvajal, Hugon Juarez, Leopoldo Gutierrez, Bishnu Pandey, Felix Yao, Fermin Caicedo, Thapelo Vundula, Edwin Guerra and the members of the Ortiz and Sanchez families. Special thanks also to my Colombian friends: Nohemy Galindez, Carlos Rangel, Fabio Rivera, Isabel Cuadros, Carlos Jaramillo, and Sandro Rivas for their permanent support. My gratitude is also extended to my colleagues Martin Turek, Yavuz Kaya, Armin Bebamzadeh, Majid Baradaran, Mehrtash Motamedi and Steve McDonald for the experiences shared at the UBC-EERF facility.

A profound gratitude to my Pastors along this process: Reverends Milton Cuero, Anibal Diaz, Jair Montenegro, Carlos Arias and Christtian Orozco for always being there. Special thanks to all my former Pastors in Colombia, represented by Senior Pastor Jimmy Chamorro, for their unworldly support from the very beginning.

My utmost and deepest gratitude is to my family for taking care of me and their countless efforts to bring me all the way to this point. All my love to Valentina, the light of my eyes.

To Jesus Christ my inspiration and strength.

To my Mother Marleny and my Grandmother Melba

for their lovely care and for teaching me

the importance of education.

Chapter 1: INTRODUCTION

Given their deck and bents geometry, skewed bridges are classified as irregular structures (Figure 1.1). A good understanding of the lateral displacement demands is needed in the current displacement-based design procedures for skewed bridges (AASHTO, 2011), in which the displacement demand is directly compared with the provided displacement capacity to ensure the desirable seismic performance. This is particularly important in skewed bridges with seat type abutments, in which, given their support details, pounding between the deck and its abutments is more likely to happen in many cases leading to the unseating of the superstructure or collapse of the piers.

Figure 1.1 Typical multi-span skewed bridge

1.1 Terminology

Skew Angle (ϕ): Difference between the horizontal alignment of the abutment or an intermediate bent with respect to the transverse axis of the bridge (Figure 1.2).

Longitudinal Gap: Expansion joint between the bridge deck and abutment support designed to accommodate movements of the superstructure due to temperature (expansion/contraction) variations, live loads or shrinkage.

Abutment Backwall: Retaining wall that provides support to the bridge approach.

Abutment Backfill: Soil behind the abutment backwall to provide passive resistance against longitudinal displacements.

Abutment Shear Keys: Transverse restraint at the ends of the superstructure of the bridge.

Bearings: Devices between the pier and deck to support the superstructure of the bridge (not shown in Figure 1.2).

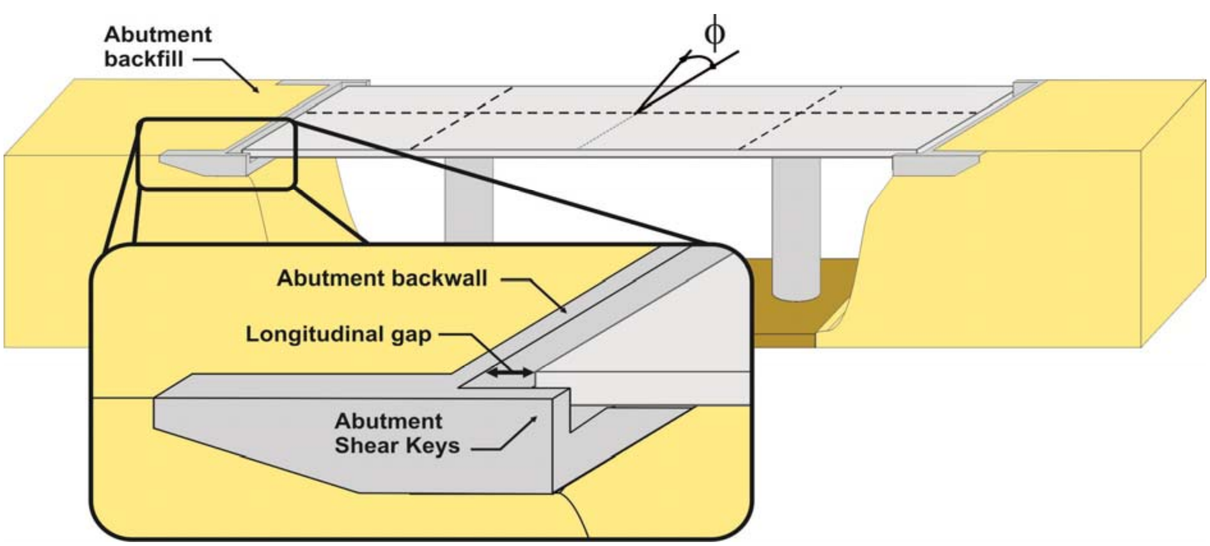

Figure 1.2 Terminology used in skewed bridges

1.2 Seismic Damage of Skewed Bridges

The susceptibility of skewed bridges to exhibit more significant seismic damage than straight bridges was identified first during the 1971 San Fernando earthquake (Housner et al., 1971) and has been clearly observed in many major earthquakes since then. The performance of 21 bridges that were damaged during nine major earthquakes since the 1971 San Fernando earthquake was investigated in this research. The objective of this damage investigation was to identify the structural components and types of skewed bridges that have exhibited more damage during past earthquakes. It is acknowledged that the damage was caused not only by the skewness of the bridges, but by multiple factors.

The damage investigation highlighted that damage have occurred to short and medium multi-span skewed bridges with: more than two spans, equal and unequal skew angles greater than 30°, seat type abutments, concrete piles, poor transverse restraint, and rocker or elastomeric bearings. The primary cause of collapse was failure of columns and the second cause was unseating of superstructure. Some of these bridges had been retrofitted with longitudinal restrainers.

The types of damages observed include unseating of the superstructure, failure of bearings, breakdown of transversal and longitudinal restrainers, cracking of girders, shear failure of piers, excessive displacement of abutments, slumping of the backfill, cracking of embankments and failure of piles (Figure 1.3). The consequences of failure of skewed bridges vary from disruption of bridge serviceability due to large permanent displacements at expansion joints, to bridge closure due to collapse of superstructure or loss of gravity load capacity in columns. A summary of some relevant failures is provided in the following paragraphs. Additional details of each failure are reported in Appendix A.

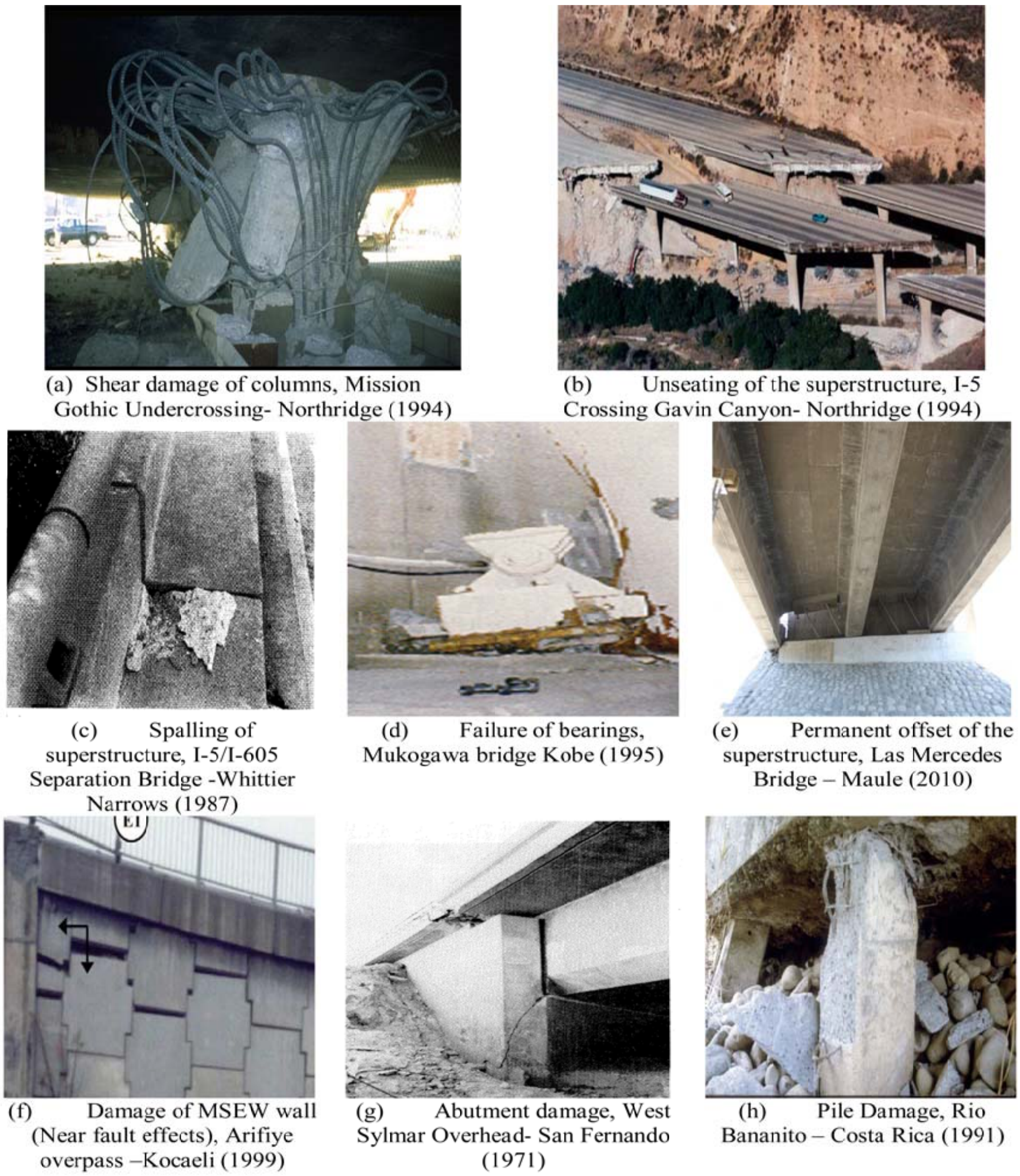

(a) Shear damage of columns, Mission Gothic Undercrossing- Northridge (1994)

(b) Unseating of the superstructure, I-5 Crossing Gavin Canyon- Northridge (1994)

(c) Spalling of superstructure, I-5/I-605 Separation Bridge -Whittier Narrows (1987)

(d) Failure of bearings, Mukogawa bridge Kobe (1995)

(e) Permanent offset of the superstructure, Las Mercedes Bridge – Maule (2010)

(f) Damage of MSEW wall (Near fault effects), Arifiye overpass –Kocaeli (1999)

(g) Abutment damage, West Sylmar Overhead- San Fernando (1971)

(h) Pile Damage, Rio Bananito – Costa Rica (1991)

Figure 1.3 Damage to skewed bridges

In bridges designed prior to the dissemination of ATC-6-2 (1983), which contains comprehensive seismic provisions, considerable deck rotations led to permanent deck offset or unseating of the superstructure. For instance, although retrofitted with longitudinal restrainer cables to supplement its short support length (200 mm), the Gavin Canyon Undercrossing fell down during the 1994 Northridge earthquake (Priestley et al. 1994, Moehle et al. 1995, Klosek et al. 1995). This example indicates the importance of the in-plane rotation and transverse displacement demands in the seismic assessment of skewed bridges.

Brittle failures have occurred in rocker and roller bearings on skewed bridges; the failure of the I-5/I-605 overpasses during the 1987 Whittier-Narrows earthquake (Priestley, 1988) and the Mukogawa bridge during the 1995 Hyogo Ken Nambu earthquake are good illustrations of this (NIST, 1996). During the 2010 Maule earthquake permanent offset and unseating of the superstructure occurred in short span skewed bridges with laminated elastomeric bearings and poor transverse restraint (MAE, 2010). Las Mercedes bridge and Route 5 overpass are examples of this failure. Other damage observed in superstructures of skewed bridges include: spalling of girders, as observed in the West Sylmar Overhead during the San Fernando earthquake; cracking of concrete box girders, as observed in the Fairfax-Washington Undercrossing during the Northridge earthquake; and plastic distortion of steel girders at abutments, as presented in the Mukogawa bridge in the Hyogo Ken Nambu earthquake.

Damage in the substructure of skewed bridges has been clearly evidenced in past earthquakes. Columns of the Foothill Boulevard and the Northbound Truck Route Undercrossings suffered extensive shear damage during the 1971 San Fernando earthquake (Housner et al., 1971).

Although columns at that time had inadequate confinement and insufficient transverse reinforcement, the damage was possibly aggravated by the increment in displacement demand due to skewness of the bridge. Similarly, the increasing demand at the base of the architectural flares in the columns of the Mission Gothic Undercrossing most likely exacerbated the shear and flexural damage of the bents during the 1994 Northridge earthquake (Priestley et al. 1994, Moehle et al. 1995). Shear failure caused by torsion due to deck skewness was also observed in the wall piers of the Kawaraginishi Bridge during the 1995 Hyogo Ken Nambu earthquake (NIST, 1996).

Near fault ground motions have also caused major damage to skewed bridges built in recent times. Both the Arifiye overpass built in 1988 in Turkey according to AASHTO-1975 and the Shie Wie bridge built in 1994 in Taiwan according to AASHTO-1977 collapsed during the 1999 Kocaeli earthquake and the 1999 Chi-Chi earthquake, respectively. The Arifiye overpass transversally crosses the fault near the northern abutment where large longitudinal displacement (1 m) occurred, which caused unseating of the simple supported spans, damage to the abutments, tilting of columns and damage to the mechanically stabilized earth walls (MSEW) at the approaches. The Shie Wie bridge crosses the fault near the southern abutment, where spans collapsed, columns tilted including caissons, and the southern retaining wall collapsed.

During the 1989 Loma Prieta earthquake, the Struve Slough Bridge, a skewed bridge supported on extended pile shafts, collapsed mainly due to effects of foundation flexibility. As explained in more detail in the next section, this case might provide an illustration of the effects that soil structure interaction (SSI) might have in the seismic performance of skewed bridges.

The Struve Slough Bridge Case

Description: The bridge, located in Watsonville, CA was built in 1964 and, is comprised of two independent structures carrying northbound and southbound traffic. Each structure has a skew of 30.5° and has a total length of 226 m over 22 spans. The abutments are integral with the deck; and the superstructure has five concrete T-beams supporting the deck slab and three equally spaced expansion joints with cable restrainers, installed in 1984 to prevent unseating of the spans. As shown in Figure 1.4a, each bent is made of four 381 mm diameter extended pile shafts driven to about 24.4 m below ground and cast inside steel jackets (EERI, 1990). As typical of the 1960's construction era, the extended pile shaft section above ground has insufficient transverse reinforcement and inadequate confinement (Jablonski et al., 1992).

The soil profile varies along the length of the bridge. At the south abutment, it consists of compact silty sand up to 12.8 m in depth overlying stiff silty clays. At mid-span, the soil profile is composed of very soft clay and peat, up to 19.5 m in depth, overlying dense sand and stiff silty clay. At the north abutment, the profile is similar to that of the south abutment, but the layers are of different thicknesses (Jablonski et al., 1992, Mitchell et al., 1991).

Observed Damage: The central part of both the northbound and the southbound structures collapsed (Figure 1.4 a). A significant displacement demand as much as 600 mm was identified at the top of columns leading to combined shear and flexural failure. In fact, some columns slid off from the cap beams and punched through the deck. In spite of the large displacements caused by the collapsed structures, the cable restrainers were intact and held the superstructure together

(Housner, 1990). The earthquake induced geotechnical damage, producing gaps from about 30 – 45 cm wide around the piles (Figure 1.4 b), and ground settlements as large as 50.8 cm (Mitchell et al., 1991, EERI, 1990). Some piles might have failed underground. There was no evidence of abutment translation or pounding at expansion joints (Housner, 1990). Also, there was no indication of liquefaction (Jablonski et al., 1992).

(a) Collapse due to failure of extended pile shafts

(b) Gaps around the piles (30-45 cm wide)

Figure 1.4 Damage observe at the Struve Slough Bridge

Soil Structure Interaction Aspects: The damage observed points out the influence of the following soil structure interaction aspects:

- ✓ The large displacement demand at the top of the columns was attributed to foundation flexibility; especially at mid-span, where the long extended pile shafts were surrounded by a thick layer of very soft soils. In addition, the ground motions were amplified by the soft soil profile.

- ✓ The reduction in column capacity was caused by the P-Delta effect, which in turn was caused by the large displacement demand at the top of the columns (Mitchell et al., 1991). In fact, the column capacity was already very limited due to insufficient transverse reinforcement and inadequate confinement.

- ✓ The foundation type, single extended pile shaft, tends to cause greater displacement at the top of columns than the displacement caused by other foundations (Mitchell et al., 1991).

In addition, the skewness of the bridge most likely worsened the effects of the above elements. For example, the additional displacement demand induced by skewed decks could have further reduced the column capacity.

1.3 Background on the Seismic Response of Skewed Bridges

1.3.1 Research on the Effects of Earthquake-induced Pounding

Maragakis and Jennings (1987) investigated the seismic response of short skewed bridges with seat type abutments and found that the in-plane rotational vibration of the superstructure is mainly caused by the impact between the skewed deck and the abutments. Initially, a simple analytical model was formulated in which the bridge deck is assumed to be rigid, skewed at an angle θ, the columns fixed at the base, and the system undamped. This preliminary analytical model enabled the identification of basic parameters involved in the rigid body motions of skewed decks, namely the initial skew angle, the stiffness of abutments, the gap at expansion joints and the location of the bridge columns relative to the center of mass of the deck. Subsequently, Maragakis and Jennings formulated a more detailed analytical model. Although it retained the rigid deck assumption, the refined model included damping, elastomeric bearings, and yielding of columns and abutments. This detailed model captured the fact that impact forces are induced after the closure of either of the gaps between the deck and the abutments or at the expansion joints. The impact force causes rotation of the deck, which results in significant transverse displacement in addition to the transverse component of the ground motion. Additional research by Bjornsson et al. (1997) showed that a high probability of unseating is associated with skewed angles between 45 and 60 degrees.

McCallen and Romstad (1994) studied embankment-abutment-structure interaction (EASI) effects of a short span bridge with skewed concrete box girder superstructure and integral abutments. Two different models were used. In the first approach a simplified stick model represented the structure. In the second approach a finite element model including solid elements to represent the backfill was used to provide a detailed representation of the entire system. The results of the study indicated that even if the superstructure undergoes linear response during strong shaking the nonlinearity in the backfill could result in nonlinear response of the entire system. The parametric study undertaken showed that the overall response of the system is sensitive to both the stiffness and the inertia of soil embankments.

Shamsabadi and Kapuskar (2006) investigated EASI in short span skewed bridges with seat type abutments using near field ground motions and nonlinear springs to represent the backfill behind the abutment walls. The nonlinear abutment springs, which account for near field embankment deformations, were developed using a strain hardening constitutive model. Findings indicated that the deck rotation is the result of a nonuniform passive pressure behind the abutment wall, and also demonstrated that near fault ground motions can cause large displacements at abutments and columns that are not considered in current bridge design provisions.

Tirasti and Kawashima (2008) investigated the torsional response of skewed bridge piers. They analyzed a typical medium span Japanese bridge comprised of 4 spans, 3 piers with steel bearings at each pier, and seat type abutments using nonlinear time history analysis. The bridge was represented by a stick model that accounts for torsional stiffness in the foundations, pounding at abutments, locking of bearings and hinging of piers. The results of this study demonstrated the higher ductility and torsional demands of skewed bridge piers compared to straight bridge piers, as well as a potential increment in the demand at the middle piers due to damage of bearings.

An accurate representation of the impact between the deck and the abutments was modeled by Dimitrakopoulos (2010). Unlike traditional models which consider the impact as concentrated in a single point at the middle of the deck, this model considered either single impact at the corner of the deck or multipoint impact along the deck. The bridge deck was assumed rigid and pounding against an inelastic half space representing the abutment. The study demonstrated that the potential of a skewed deck to rotate after an impact with its abutments not only depends on the skew angle, but also on the width-to-length ratio of the deck. In addition, the tendency observed during earthquakes of single span skewed decks to rotate in such a way that the skew angle increases was explained.

1.3.2 Research on the Identification of Dynamic Properties

Using ambient vibration, Ventura et al. (1996) studied the dynamic parameters of three short span bridges with integral abutments skewed at 39°, 19° and 6°. The first five vertical frequencies and mode shapes were clearly identified indicating that for higher order frequencies, the vertical and torsional modes of vibration of the deck have significant coupling. Also, the first five transverse frequencies and mode shapes were identified, indicating that the transverse mode shapes do not have significant coupling with the vertical and torsional-vertical modes.

A number of authors have conducted analytical studies to identify the dynamic parameters of skewed bridges in the vertical directions; Ghobarah (1974) found a closed form solution for the vertical frequencies and modes of vibration of a two-span skewed bridge. As observed by Ventura et al., the analytical vertical modes exhibit significant coupling with the torsional components. Other empirical studies included using an orthotropic plate to represent the skewed deck (Srinivasan and Munaswamy 1976) and considering the stiffness effects of bearings and diaphragms (Maleki 2001). Further research is needed in the identification of the dynamic properties of skewed bridges with seat type abutments in the lateral direction.

1.3.3 Research on the Effects of Soil-Foundation-Structure Interaction (SFSI)

Despite the fact that Soil-Foundation-Structure Interaction could play a significant role in the in-plane rotations of skewed bridges during strong earthquakes, limited research on this topic is available in the literature. Chen and Penzien (1977) investigated the SFSI effects in the response of short spans skewed bridges using nonlinear time history analysis. The bridge studied is similar to the San Fernando Road Overhead, which collapsed during the 1971 San Fernando earthquake. The structure consisted of three spans and was skewed at 37.5°. Each backfill was modeled using solid elements, and the contact between abutment walls and backfills is represented with friction elements. The foundation was represented by translational and rotational springs in all three directions and the spring constants were estimated using elastic half space theory. The analysis indicated that maximum displacements and accelerations of the bridge deck, accounting for both Soil-Foundation-Structure interaction (SFSI) and Embankment-Abutment-Structure-interaction (EASI), are greater than those obtained accounting only for EASI.

1.4 Code Provisions for the Calculation of Displacement Demands of Skewed Bridges

Given their geometry, skewed bridges are classified as irregular bridges by most seismic specifications. AASTHO (2011) uses a displacement approach to assess the seismic demands of the bridge. Bridges of standard importance with a skew angle smaller than 30 degrees may be represented with two-degrees of freedom models to evaluate the longitudinal and transverse demands. The estimation of seismic demand in bridges with a skew angle greater than 30 degrees requires 3D models and linear elastic multimodal spectral analysis. When the bridge is essential or a higher level of accuracy is required nonlinear time history analysis must be performed. In any case, the transverse demands are obtained in the direction of the skew and are then compared to the capacity of the bent to assess its seismic performance.

Similarly, the Canadian Highway Bridge Code, CAN/CSA-S6-06 (CHBDC) requires linear elastic multimodal spectral analysis for standard bridges and nonlinear dynamic time history for essential bridge, but the minimum skew angle required to call for these analyses is 15 degrees. Other guidelines, such as the Seismic Retrofitting Manual for Highway Structures (FHWA, 2006) allow the elastic time history analysis as an alternative to the multimodal spectral analysis.

1.5 Limitation of Elastic Analysis for Skewed Bridges

In an elastic analysis, the nonlinear effects of the longitudinal gap and the properties of the abutment are approximately accounted for by examining two bounding models: the tension model and the compression model. In the tension model the superstructure is free to move longitudinally at both ends, while in the compression model both ends are partially restrained to simulate the effects when the gap is closed.

These elastic models are commonly used in practice. However, the in-plane rotations in skewed bridges due to earthquake-induced pounding are not captured by the elastic models since the linear springs at both abutments are always engaged and transfer tension and compression forces. Figure 1.5 helps to illustrate this limitation; for simplicity the bridge is symmetric and the abutments are represented by a single linear spring at both ends. As the deck moves in the longitudinal direction (Figure 1.5 b), it activates reactions at both ends (Figure 1.5 c), each reaction produces opposite moments around the center of mass that counteract each other (Figure 1.5 d), and as a result, the model cannot capture in-plane rotations due to pounding.

The in-plane rotation induced by earthquake pounding is captured using nonlinear models, in which the gap is accurately modeled and the springs at abutments transfer only compression forces when the gap is closed. It is noted, however, that elastic analysis can capture the rotations produced by other irregularities such as unequal skew angles or variable pier heights.

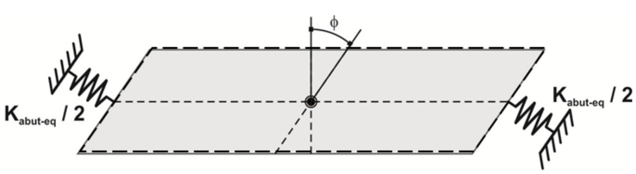

(a) Top view- for simplicity abutments are represented by a single spring at both ends

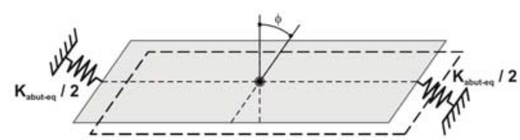

(b) Deck displacement in longitudinal direction

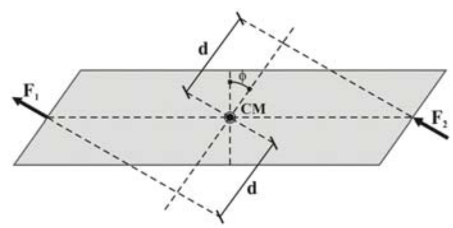

(c) Reaction forces at both ends

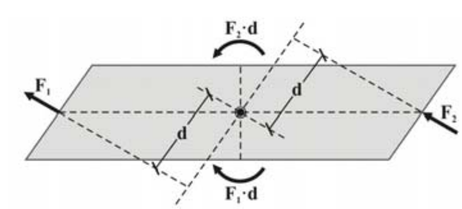

(d) Counteracting moments around the center of mass

Figure 1.5 Pounding forces in linear elastic models

1.6 Statement of Problem and Motivation

Displacement based design of new and retrofit of existing skewed bridges require a clear understanding of the seismic demands that these structures will be subjected to during earthquake shaking. Seismic damage from past earthquakes illustrates that skewed bridges with seat type abutments tend to rotate during earthquakes, and the rotations increase the probability of transverse unseating at joints and the displacement demands of skewed piers. As explained previously, linear elastic analyses widely used in engineering practice do not capture the in-plane rotation of the deck due to earthquake-induced pounding and designers currently face a challenge to quantify the expected displacement demands.

On the other hand, the primary cause of collapse of skewed bridges during earthquake shaking is failure of columns. However, the parameters that drive the displacement demands on the piers are not fully defined and understood. In particular, the effects of different type of abutments and foundation conditions of the bridge, whether rigid-base or flexible, and their relation with the skew angle of the deck and the acting ground motion needs further investigation.

1.7 Objectives and Scope

This thesis is the result of a professional partnership between the University of British Columbia (UBC) and the Ministry of Transportation and Infrastructure (BCMoT) to provide practical guidelines for the seismic assessment of skewed bridges. In order to achieve this goal, this thesis has two main objectives: one related to research and one related to engineering practice.

1.7.1 Research Objective

The research objective of this thesis is to examine the effect of deck skewness on the displacement demands of piers. The goal is to identify the conditions that trigger in-plane rotational demands, their contribution to the total demands of the piers, and the effects of Soil-Foundation-Structure Interaction.

1.7.2 Engineering Practice Objective

The engineering practice objective of this thesis is to develop a tool to evaluate the torsional sensitivity of skewed bridges and a simplified method to calculate the demands of the piers due to earthquake-induced pounding.

1.7.3 Scope

This study is limited to the response of symmetric, short and medium, multi-span skewed bridges with seat type abutments and continuous superstructures built according to the current BCMoT specifications.

1.8 Organization of the Thesis

This thesis combines experimental and analytical approaches to understanding the displacement demands of skewed bridges. The subsequent paragraphs describe the content of each chapter:

Chapter 2 discusses the dynamic properties and the directionality in the lateral response of skewed bridges based on the results of ambient vibrations tests performed on four skewed bridges in British Columbia, and in the analysis of acceleration records from the instrumented Second Northern Freeway (TCUBAB) in Taiwan.

Chapter 3 presents the results of a comprehensive analysis that used nonlinear finite element models to study the influence of the skew angle to the deck rotation of bridges with different types and structural response at abutments. The contributions of the deck rotation to the total pier drift as well as the effects of Soil-Foundation-Structure interaction are discussed.

Chapter 4 describes a proposed method to calculate the displacement demands of the piers. The method uses validated simplified nonlinear models to generate torsional sensitivity charts for selected bridge prototypes. The method involves using the torsional sensitivity charts to estimate the lateral displacement of the piers due to deck rotation, which is then added to the deck-translation displacement to obtain the total pier demand. In addition, a discussion of the critical skew angle to call for nonlinear analysis, and the effects of different levels of transverse restraint is presented in this chapter.

Chapter 5 summarizes the conclusions of this thesis, and provides recommendations for displacement-based design and suggestions for future work.

Chapter 2: DYNAMIC PROPERTIES OF MULTI-SPAN SKEWED BRIDGES

2.1 Introduction

Skewed bridges have different stiffnesses and strengths depending upon the orientation of the axes along which these properties are determined. An accurate estimation of the transverse and longitudinal demands is connected to a proper identification of the so called "preferred response directions". The preferred response directions are the directions in which the critical transverse and longitudinal demands respectively occur (Steward et al., 2011). These directions are given by the predominant directions of the transverse and longitudinal modes of vibration. A number of authors have conducted experimental and analytical studies to identify the dynamic parameters of skewed bridges with integral abutments (Carvajal et al. 2009, Maleki 2001, Srinivasan 1978, Ghobarah 1974). However, a better understanding of the dynamic properties and the displacement profiles of skewed bridges with seat type abutments is required, and will improve the evaluation of the maximum displacement demands for these structures.

2.2 Ambient Vibration Studies

This section discusses the results of the ambient vibration tests conducted on four multi-span skewed bridges with seat type abutments.

2.2.1 Description of the Bridges

Highway 99 and 24th Avenue Underpass (HWY 24th): The structure was built in 2006 and is located along Highway 99 in Surrey, British Columbia, Canada (Figure 2.1). The bridge is 48 m long, 19 m wide, and has two continuous spans with seat-type abutments. The superstructure consists of a concrete deck slab supported on 0.8 m deep precast concrete box stringers. The substructure consists of 0.8 m diameter, 3.3 m high multi-column frames with concrete cap beams. The abutment and pier foundations consist of strip footings.

Figure 2.1 Highway 99 and 24th Avenue Underpass (HWY 24th)

Highway 10 Underpass (HWY 10): The structure was built in 1985 and is located along Annacis Highway in Surrey, British Columbia, Canada (Figure 2.2). The bridge is 71 m long, 22.1 m wide, and has two spans with seat-type abutments. The superstructure consists of a concrete deck slab supported on nine 1.9 m deep, concrete I-girders. The superstructure is discontinuous and connected to the cap beam at midspan. The substructure consists of a multicolumn frame with a set of five concrete columns which are 1 m in diameter. The foundations consist of steel pipe piles filled with concrete.

Figure 2.2 Annacis Highway and Highway 10 Underpass (HWY 10th)

Highway 1 and Lougheed Highway Underpass (LHH-EB Underpass): The underpass was built in 2012. It is located in Burnaby, B.C. at Highway 1 and Lougheed Highway. The three-span bridge is approximately 135 m long and 26 m wide. Its construction consists of a concrete deck slab supported on 2.2 m deep steel girders, which are supported by multicolumn frames with a set of eight columns which are 1.22 m diameter. Both ends rest on bent abutments, and are connected by approach slabs. There are also expansion joints on all four spans. The foundation consists of 1.22 m diameter steel pipe piles (Figure 2.3).

Figure 2.3 Highway 1 and Lougheed Highway Underpass (LHH-EB Underpass)

Douglas Road Underpass (Douglas Rd): The underpass, built in 1962, is located at Highway 1 and Douglas Road. It has four spans with a total length of 83 m and a width of 17 m (Figure 2.4). The superstructure consists of a concrete slab deck with precast post-tensioned box girders. The substructure has multicolumn frames with four columns, which are 0.6m in diameter. Pad footings are used for the piers. The abutments are seat-type; and the slab is discontinuous at midspan, whereas the girders are discontinuous at all supports. At the internal piers, expansion bearings exist; but at the abutments there are fixed bearings.

Figure 2.4 Douglas Road Underpass (Douglas Rd)

The following table summarizes the characteristics of the structures tested (Table 2.1).

Structure	Length (m)	Spans		Width (m)	Clearance (m)	Skew Angle (degrees)	Substructure		Superstructure Type
		No.	Lengths (m)				Type	Abutments	
HWY 24TH	48	2	23-23	19	4.9	37	multi-column-frames (D= 0.8m)	seat type	Continuous – concrete box girders
HWY 10TH	71	2	36-36	22.1	9.1	31	multi-column-frames (D = 1.0m)	seat-type	Discontinuous - reinforced concrete I-girders
LHH-EB Underpass	135	3	37-58-37	26	5.0	54-57	multi-column-frames (D = 1.22m)	bent seat-type	Continuos – concrete steel girders
Douglas Rd	83	4	12-22-21-21	17	4.6	28	multi-column-frames (D = 0.6m)	seat-type	Disontinuous – concrete box girders

Table 2.1 Summary of the characteristics of the bridges tested

2.2.2 Field Testing

Ambient Vibration Testing involves measuring a structure’s response to typical excitations that it is subjected to every day. These ambient excitations can be wind, traffic, human activities, etc. This method of testing provides a cheap, non-invasive, and non-destructive method for obtaining modal parameters of large structures. With Ambient Vibration Testing one avoids having to physically excite the structure with heavy equipment, which results in the disruption of the structure’s typical operation. The response that one obtains from these tests is characteristic of the true operating conditions of the structure. To obtain the modal parameters of the structure, Output-Only Modal Analysis algorithms are used to process the data.

Ambient vibration testing is typically carried out by using sensitive accelerometers or other types of sensors, along with a multi-channel data acquisition system. Some inconveniences in using the sensors involve cable handling, sensor balancing, signal clipping, and power supply issues. At the present time the Earthquake Engineering Research Facility (EERF) at the University of British Columbia (UBC) carries out ambient vibration tests using nine wireless Tromino sensors. These instruments were set to record simultaneously high gain velocities, low gain velocities and accelerations at 128 samples per second. The Trominos are equipped with GPS and radio antennas for time synchronization.

In 2012, members of the EERF team carried out ambient vibration tests on the HWY 24th, HWY 10th, LHH-EB Underpass and Douglas Rd bridges. During the tests, one unit stayed at the same location (reference sensor), while the others are moved along the bridge to cover different testing locations (roving sensors). Figure 2.5 shows a typical test setup for HWY 24th. All the bridges were open to traffic. There were 20 testing locations along the sidewalks of HWY 24th, 32 along HWY 10th, 59 along LHH-EB Underpass and 38 along Douglas Rd. In addition to this, there were two testing locations at each approach and at least one free field measurement for all bridges. All measurements were taken for 30 minutes in each setup.

It is important to point out that LHH-EB underpass was partially open to traffic, and did not have sidewalks. As a result, the test could only be conducted on the two southbound lanes that were closed to traffic.

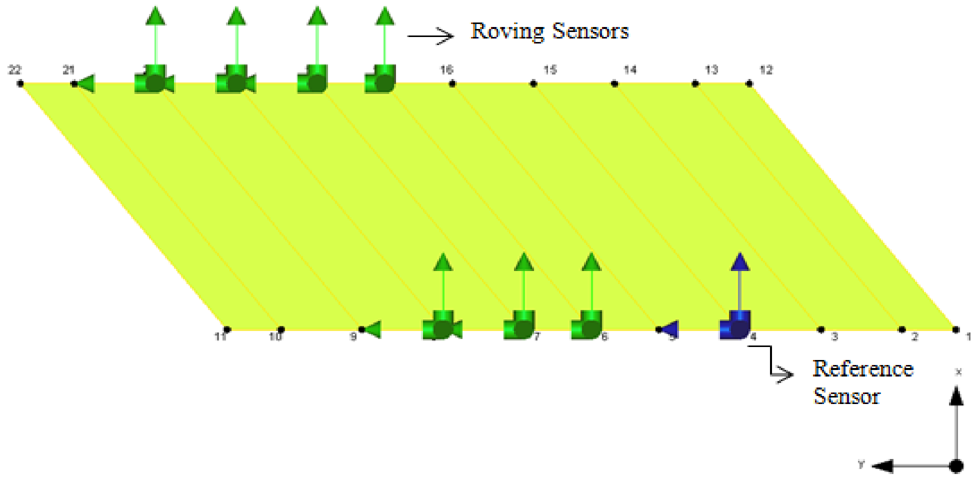

Figure 2.5 Typical test setup for HWY 24th

2.2.3 Data Analysis and Results

The natural frequencies, mode shapes, and damping of the bridges were identified using the program ARTeMIS Extractor (SVS, 2011). The results of the system identification in the vertical direction are given in Appendix B. This section presents the identification of the in-plane dynamic properties.

2.2.3.1 In-plane System Identification

As traffic was the main excitation on the bridges, mainly the vertical modes are excited during the test and the identification of the in-plane motions (transverse, longitudinal and rotation) becomes more challenging. In order to identify the in-plane modes of vibrations, which are fundamental for seismic assessment, the Stochastic Subspace Identification (SSI) technique available in ARTeMIS was used, in addition to the Enhanced Frequency Domain Decomposition (EFDD) technique.

The frequencies and modes of vibration obtained using both techniques are similar (Table 2.2 and Table 2.3). The frequencies are consistent with the boundary conditions of the bridges in each direction. For instance, HWY 24th has strong shear keys at the abutments in the transverse direction and is seated on expansion bearings in the longitudinal direction. Consistently, the transverse frequency of vibration is 10.66 Hz, and the longitudinal is 0.97 Hz. Similarly, HWY 10th, which is also a two-span bridge seated on expansion joints but with weaker shear keys, has a transverse frequency of 4.76 Hz, and a longitudinal frequency of 1.09 Hz. The consistency observed between the frequency of vibration and the level of lateral restraint in each direction, also suggests that the modal response of skewed bridges could be uncoupled in these directions.

The frequency of vibration for in-plane rotation could only be identified with confidence for the HWY 24Th (Table 2.2). The value obtained (11.72 Hz) is considered high, and is close to the transverse frequency identified (10.66 Hz). The damping ratios of the bridges tested are also similar in both techniques, EFDD and SSI. The estimated modal dampings vary from 0.24 to 3.63% (Table 2.2 and Table 2.3). These in-plane damping ratios are similar to the values reported for straight bridges using ambient vibration tests (Turek and Ventura, 2005).

	Mode of Vibration	Freq. (Hz)	ξ %	Description (Plan View)
HWY 24th	1st Longitudinal	0.97	1.96	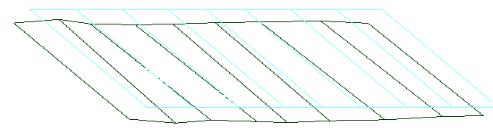
	1st Transverse	10.66	1.53	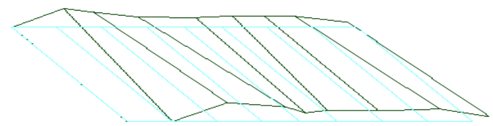
	In-plane Rotation	11.72	0.51	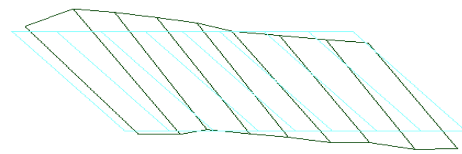
HWY 10th	1st Longitudinal	1.09	0.57	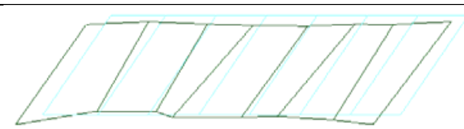
	1st Transverse	4.67	1.71	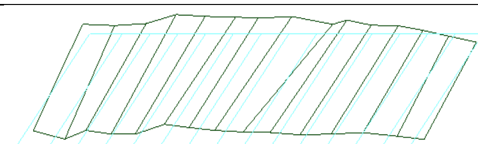
LHH-EB Underpass	1st Transverse	1.72	3.05	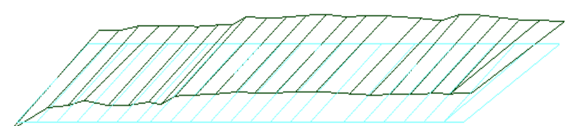
Douglas Rd	1st Longitudinal	2.31	2.36	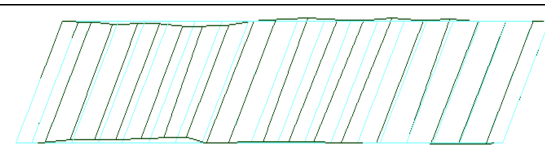
	1st Transverse	0.42	0.90	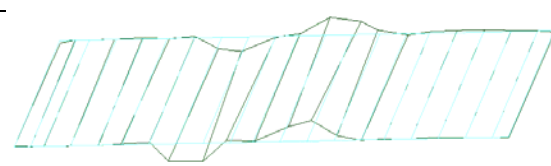

Table 2.2 Summary of in-plane system identification using the EFDD technique

	Mode of Vibration	Freq. (Hz)	ξ %
HWY 24th	1st Longitudinal	--------	------
	1st Transverse	10.52	2.15
	In-plane Rotation	12.44	3.63
HWY 10th	1st Transverse	4.69	1.96
LHH-EB Underpass	1st Transverse	1.96	1.90
Douglas Rd	1st Transverse	0.42	0.75
	1st Longitudinal	2.32	0.24

Table 2.3 Summary of in-plane system identification using the SSI technique

The transverse and longitudinal modes of vibration are used to study the lateral displacement profiles of skewed bridges for different configurations and boundary conditions. As presented in Table 2.2, the transverse and longitudinal displacement profiles of a two-span skewed bridge with seat type abutments and continuous deck as HWY 24th, are in agreement with a rigid deck assumption. In the same way, the transverse displacement profile of a three-span skewed bridge with bent type abutments, expansion bearings, and continuous deck as LHH-EB Underpass, is consistent with a rigid deck profile.

In contrast, the transverse displacement profiles of a two-span skewed bridge with discontinuous deck as HWY 10th, has a parabolic shape, more in agreement to what is expected for a flexible deck. A similar flexible transverse profile is observed for Douglas Rd which is a four spans skewed bridge with discontinuous deck.

2.2.3.2 Directionality of the Lateral Response

The transverse and longitudinal modes of vibration are also used to study the directionality in the lateral response of skewed bridges. The predominant direction of the mode is defined as the azimuth in which the mode tends to move. The predominant direction for each mode was estimated by comparing, at abutments and at mid-span, the nodal coordinates of the undeformed geometry with respect to the nodal coordinates of the mode of vibration (Table 2.4). The evaluation of the predominant direction of response for the bridges tested illustrates that the predominant direction of the transverse response occurs in the azimuth of the skew bents, whereas the predominant direction of the longitudinal response is perpendicular to the azimuth of the skew bents (Table 2.2 and Figure 2.6).

	Azimuth of transverse mode (degrees)	Skew Angle, ϕ (degrees)
HWY 24^{th}	39 to 42	37
HWY 10^{th}	32 to 34	31
LHH-EB Underpass	54 to 56	54-57

Table 2.4 Predominant direction of transverse response

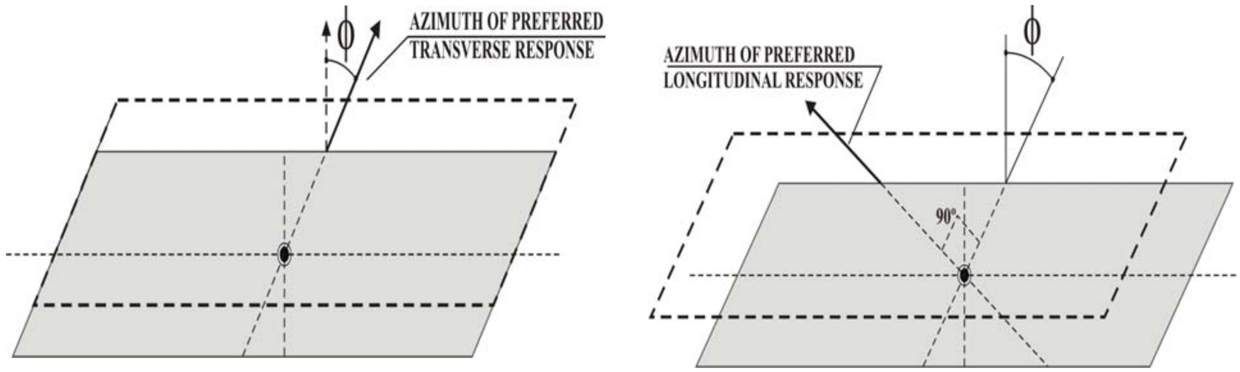

(a) Transverse direction **(b) Longitudinal direction**

Figure 2.6 Directionality of the lateral response of skewed bridges

2.3 Strong Motion Case Study

Data obtained from instrumented bridges offers a unique opportunity to study the actual performance of skewed bridges. A number of authors have conducted studies for skewed bridges with integral or semi-integral abutments (Ventura et al. 2005, Goel and Chopra 1995, Mosquera et al. 2009). But, the performance of instrumented skewed bridges with seat type abutments during moderate or strong earthquakes has not been reported.

The Second Northern Freeway (TCUBAB) located in Taiwan is a three-span skewed bridge with discontinuous girders that was shaken by the September 1999 Chi-Chi earthquake (M_s=7.6) and the October 1999 Chiayi earthquake (M_s=6.4). Although lightly skewed (13 degrees), the bridge is symmetric and heavily instrumented, including sensors at the pile caps, piers, abutments and deck girders. Data available from instrumented skewed bridge with seat type abutments is very scarce, so this case offers a opportunity to examine the performance of skewed bridges during seismic events and their response in terms of rotational and lateral demands.

This section identifies the dynamic properties of the bridge and discusses the displacement and acceleration demands at different locations on the deck. These analyses provide evidence to understand the displacement profiles and the rotational sensitivity of the deck. The pier drift as well as the longitudinal displacements at abutments joints are also studied. These analyses provide an idea of the type of response exhibited whether linear elastic with no structural damage or nonlinear due to the gaps at abutments or structural damage.

2.3.1 Bridge Description and Strong Motion Instrumentation

The Second Northern Freeway (TCUBAB) on the Hsinchu System Interchange is located in Taiwan and is composed by two concrete bridges with a skew angle of 13 degrees (Figure 2.7). Each bridge is 89.07m long, 15.25 m wide, and has three spans with seat type abutments. Each superstructure consists of a concrete deck slab supported on four 1.80 m deep, simply supported prestressed U-girders. Each substructure consists of two pier bents, which are 2 m in diameter and approximately 8 m in height. The foundations consist of concrete pile footings with pile caps.

Simply supported girders are typical on Taiwanese bridges. In order to prevent longitudinal unseating of the superstructure during seismic events, the deck diaphragms at the ends of TCUBAB are anchored to the abutment backwalls, however it has thermal expansion joints on the deck slab at both ends (Figure 2.8). To prevent transverse unseating, the TCUBAB has internal shear keys at bents and abutments. The bridge characteristics are summarized in Table 2.5.

Figure 2.7 The Second Northern Freeway (TCUBAB) in Taiwan (provided by the Ministry of Transportation and Communications of Taiwan)

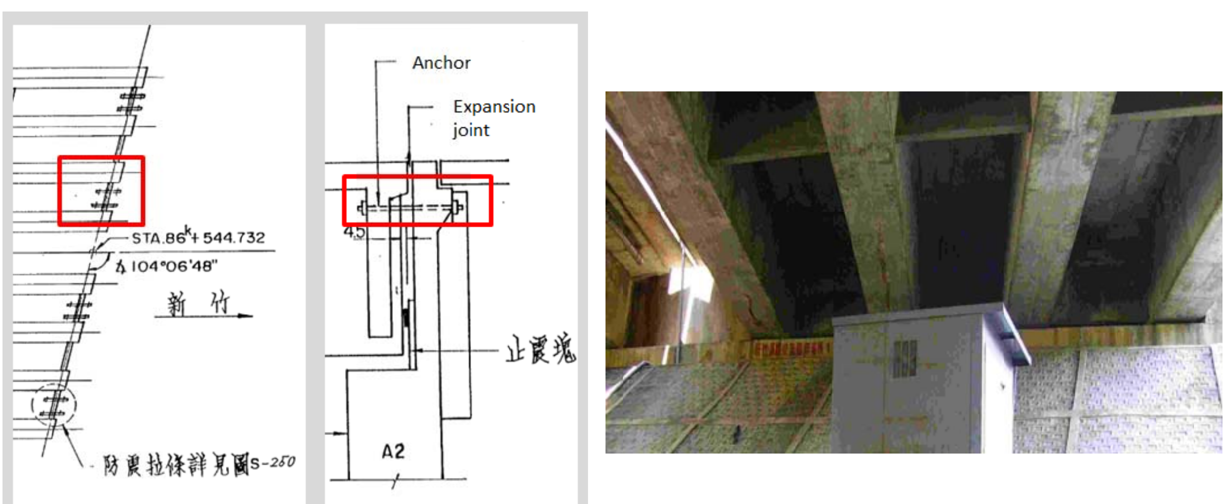

(a) Plan View **(b) Side View** **(c) 3D View**

Figure 2.8 Longitudinal anchors at abutments backwalls (provided by the Ministry of Transportation and Communications of Taiwan)

Bridge Type	Length (m)	Spans		Width (m)	Clearance (m)	Skew Angle (degrees)	Substructure		Superstructure Type	Foundation Type
		No.	Lengths (m)				Type	Abutments		
Twin	89.02	3	29.51-30-29.51	15.25 (each)	8.00	13	multi-column-frames (D = 2.0m)	seat type	discontinuous – U girders	Pile footing with pile caps

Table 2.5 Characteristics of the Second Northern Freeway (TCUBAB)

The strong motion instrumentation in Taiwan is monitored by the Central Weather Bureau (Shin et al., 2002). TCUBAB is instrumented with 29 strong motion accelerometers installed at different locations: free field (3), pile caps (8), abutments (6), pier caps (6), deck girders (3) and lateral barriers (3). As indicated in Figure 2.9 most sensors are located in such a way that the "x-direction" (longitudinal) is along the centerline of the bridge and the "y-direction" (transverse) is perpendicular to this direction.

2.3.2 Strong Motion Data

The instrumentation at the Second Northern freeway (TCUBAB) recorded the accelerations from two events that hit Taiwan in 1999: The Chi-Chi earthquake and the Chiayi earthquake. The September 21 Chi-Chi earthquake (M_s=7.6, depth 7 km) was caused by a major thrust fault along the western foothills of central Taiwan (EERI, 2001). TCUBAB is located about 110 km North from the epicentre (Figure 2.10 a). According to the free field data (Channels 1 and 2), the dominant direction of the motion was in the S-N direction. The 5% damping response spectrum for this direction (CH 2) is presented in Figure 2.10 b. The peak ground acceleration was 0.13g and the dominant periods were 0.51, 0.85, and 2.54 seconds (1.95, 1.17 and 0.39 Hz).

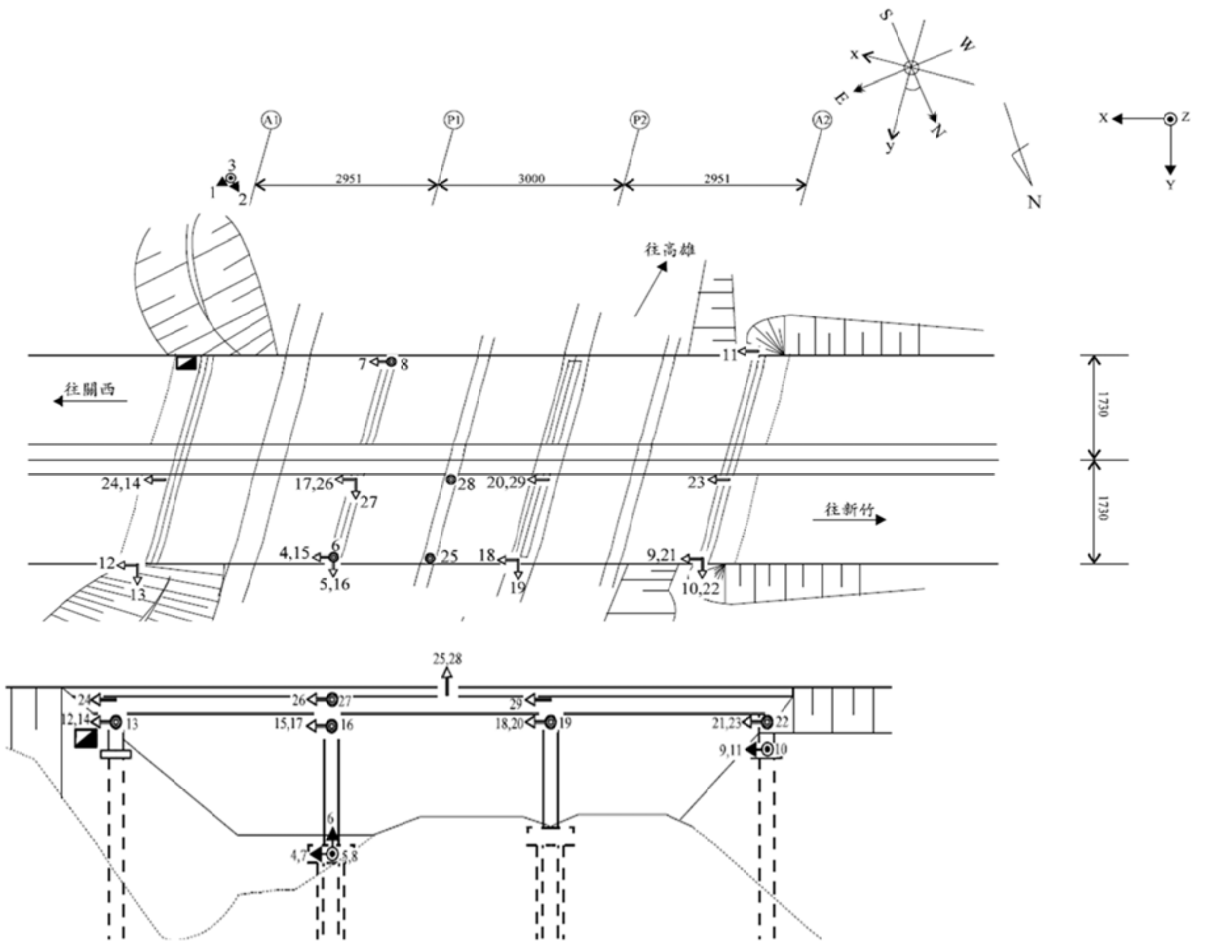

Figure 2.9 TCUBAB strong motion instrumentation (retrieved from http://gdms.cwb.gov.tw)

The October 22, 1999 Chiayi earthquake (M_L=6.4, depth 17.7 km) is the result of a reverse thrust fault located 55 km south-west from the epicentre of the Chi-Chi earthquake (Chao et al. 2011). The dominant trace of the motion is in the S-N direction. The response spectrum for this direction at TCUBAB is shown in Figure 2.10 b. The peak ground acceleration is 0.09g and the dominant periods were 0.47, 0.64 and 1.03 seconds (2.14, 1.56, and 0.97 Hz).

Large coseismic displacements were recorded at different sites during the Chi-Chi earthquake in Taiwan. However, TCUBAB is located outside the fault plane of the earthquake (Yoshioka 2001) and near fault effects such as coseismic displacements did not occurr, as expected. For instance, the station M379, which is the closest GPS station located at 8 km from the bridge, recorded displacements in the east, north and vertical direction of 0.8, 4.5, and 4.5 cm, respectively (Yang et al. 2000). In addition, according to the author's knowledge, no damage has been reported for this bridge. The closest bridge with significant damage was the Shin Wei Bridge, which is located 50 km south-west of TCUBAB (EERI 2001). As a result, no permanent displacement and elastic structural response are expected for TCUBAB.

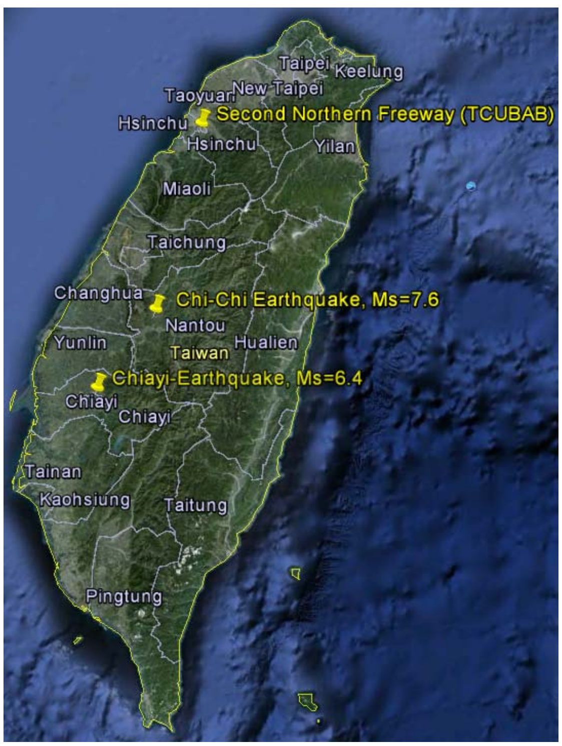

(a) Epicentre and Magnitude (Adapted from Google Earth)

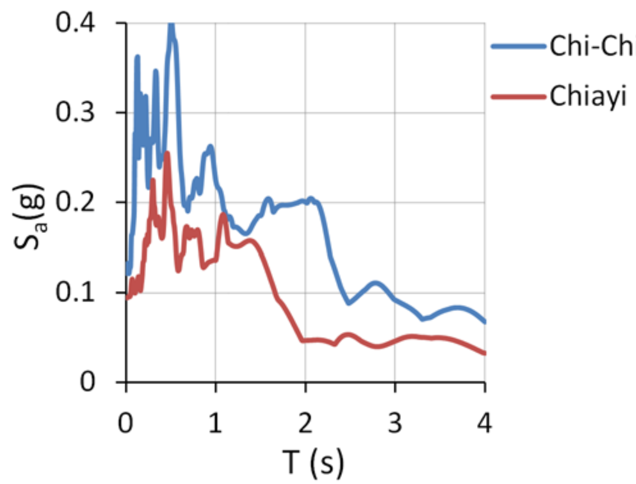

(b) Response Spectra

Figure 2.10 Recorded earthquakes at the TCUBAB

2.3.3 Modal Identification

The instrumented points at the pier caps and abutments in the transverse and longitudinal direction (channels 12, 13, 15, 16, 18, 19, 21, 22) were used to identify the damping ratios and natural frequencies of the modes of vibration excited by the recorded ground motions. In this way, using the EFDD technique two frequencies of vibration were identified at 2.24 and 2.93 Hz. A 6.3 % damping ratio was estimated for the Chi-Chi earthquake and 4.3 % damping was estimated for the Chiayi earthquake. The greater damping ratio for the Chi-Chi earthquake is in agreement to the greater amplitude of this record compared to the Chiayi earthquake.

The plan views of the corresponding transverse modes of vibration with the deformed shape of bridge deck represented as a green line are shown in Figure 2.11. The mode profiles identified are consistent with the profiles expected for a skewed bridge with discontinuous girders and illustrate a predominant direction of the modes parallel to the skew angle. These results are similar to those obtained for discontinuous bridges by using ambient vibration tests. In addition, rigid body motions at 0.39 Hz for the Chi-Chi earthquake and at 0.97 Hz for the Chiayi earthquake were identified; these motions are associated to the dominant frequency of each ground motion.

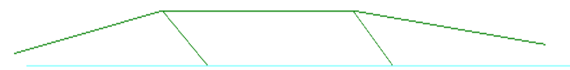

(a) Mode 1- 2.24 Hz (Plan View) **(b) Mode 2- 2.93 Hz (Plan View)**

Figure 2.11 TCUBAB – Modes of vibration predominantly excited

2.3.4 Accelerations and Displacements Demands

2.3.4.1 Bridge Superstructure

The peak accelerations of the deck were 0.6g (Ch 24) for the Chi-Chi earthquake and 0.35g (Ch 27) for the Chiayi earthquake. The Fast Fourier Transforms (FFT) of the recorded accelerations for both earthquakes at different locations on the superstructure and the transmissibility between them are shown in Figure 2.12 to Figure 2.15. The dominant frequencies at the east abutment (Ch 13) and the pier cap 1 (Ch 16) during the Chi-Chi earthquake are 0.39 and 2.34 Hz (Figure 2.12). For these frequencies the transmissibility between the two locations has a magnitude of one and a phase angle of approximately zero radians, indicating that accelerations at these points are in phase and have almost the same amplitude. Similar results are observed for the Chiayi Earthquake (Figure 2.13).

At the deck girder (Ch 27) the dominant frequencies during the Chi-Chi earthquake were 1.56, 2.34 and 2.93 Hz (Figure 2.14). The transmissibility of this point with respect to the east abutment (Ch 13) indicates that at 1.56 Hz the two locations are vibrating in the same direction; however the transmissibility for vibrations at 2.34 and 2.93 Hz has a phase angle of almost 180 degrees (π radians), which indicates vibrations of the first span in opposite direction at these frequencies. These rotational accelerations are in good agreement with the profiles described by the identified modes of vibration at 2.24 and 2.93 Hz. For the Chiayi Earthquake similar results are observed, but the phase difference at 2.34 Hz is smaller (Figure 2.15).

A comparison of the relative peaks of the FFT at the deck girder (Ch 27) suggests that the vibrations at 2.34 Hz, which are associated with rotational accelerations of the deck, have higher energy than the vibrations at 1.56 Hz, which are associated with linear accelerations of the deck. This could be used as evidence of the rotational sensitivity of the spans of skewed bridges with discontinuous girders (Figure 2.14).

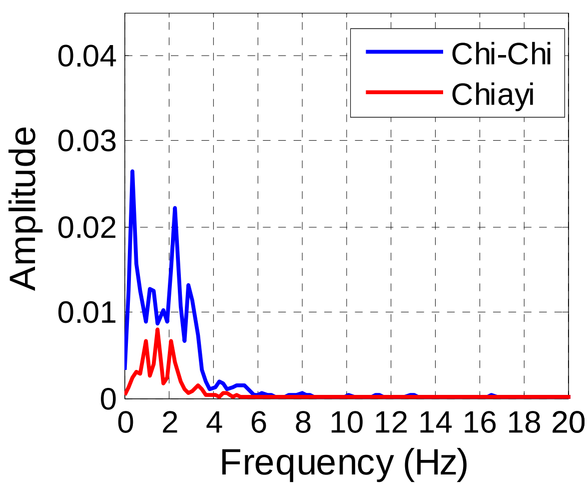

(a) East abutment-Ch 13

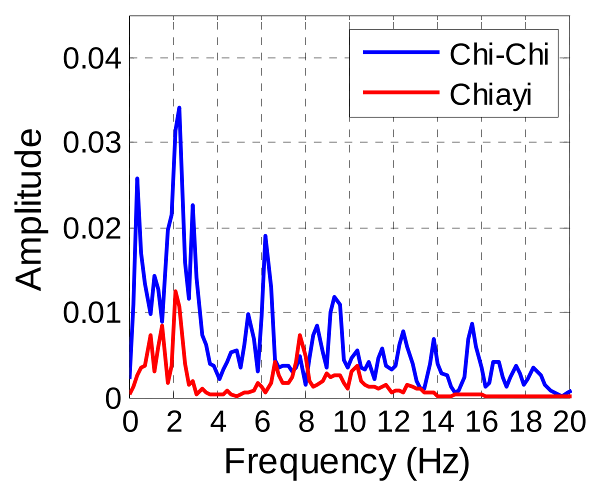

(b) Pier cap 1- Ch 16

Figure 2.12 Fourier Transform of recorded motions at east abutment and pier cap 1

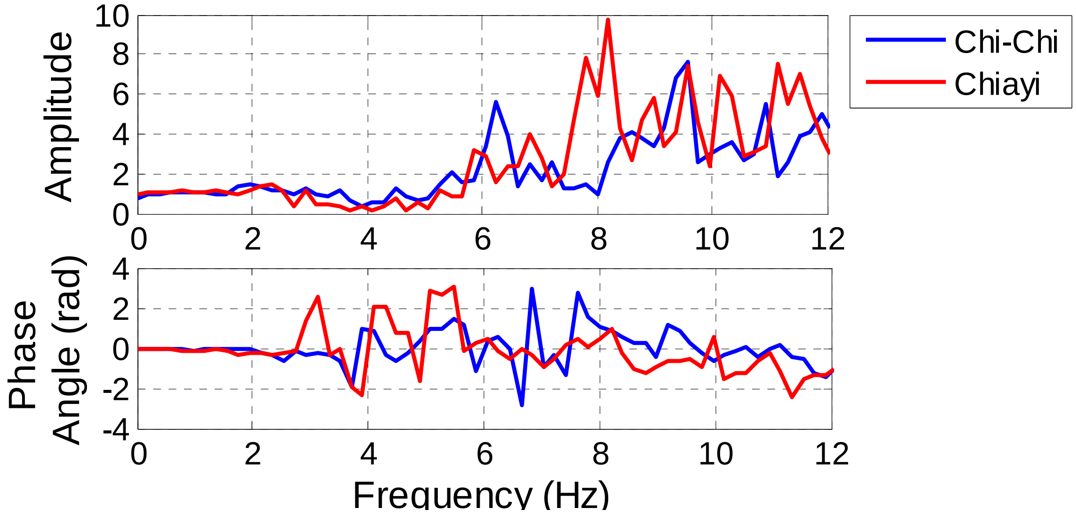

Figure 2.13 Transmissibility from east abutment to pier cap 1 (Ch 13 to Ch 16)

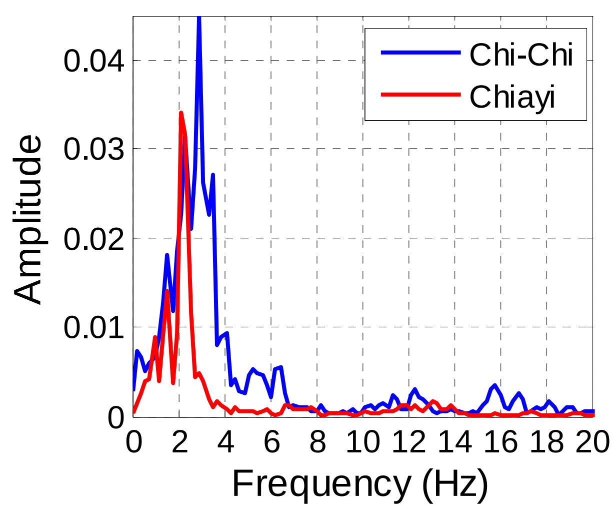

Figure 2.14 Fourier Transform of recorded motion at deck girder - Ch 27

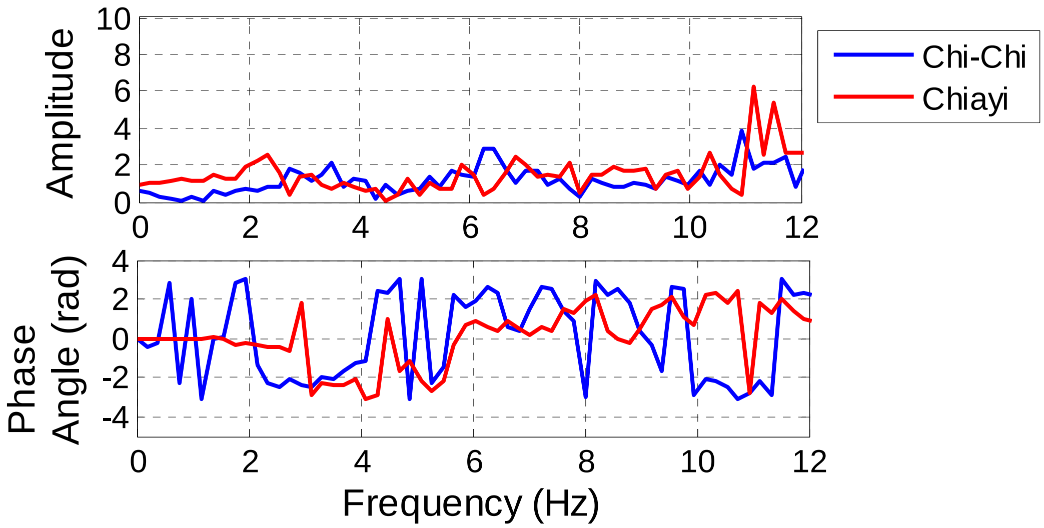

Figure 2.15 Transmissibility from east abutment to deck girder (Ch 13 to Ch 27)

2.3.4.2 Pier Drift

The accelerations recorded on Pier 1 at the base (CH 4 and 5) and the top (CH 15, 16) were used to obtain the pier drift. To obtain the displacements an integration procedure in frequency domain was applied to the relative accelerations. The procedure consists of the following steps:

1. Adding zeros at the end of the signal (zero padding) to reduce the cyclic convolution of the data during the integration.

2. Baseline correction and high pass filtering of the signal (cutoff frequency 0.1 Hz).

3. Calculating Fast Fourier Transform (FFT).

4. Calculating negative FFT divided by frequency squared to obtain displacement in the frequency domain.

5. Using inverse FFT and high pass filter to obtain relative displacement in time domain.

For the Chi-Chi Earthquake the maximum drift in the transverse direction (0.32 %) is slightly higher than the drift in the longitudinal direction (0.24 %) (Figure 2.16). The dominant frequency of the displacement response of pier 1 is 0.39 Hz (Figure 2.17). This low frequency, which coincides with the dominant frequency of the recorded ground motion, is associated with a rigid body motion of the bridge. For the Chiayi Earthquake the maximum drifts found are 0.08 % and 0.07 % in the transverse and longitudinal direction, respectively. As in the Chi-Chi earthquake, the displacement is dominated by a frequency of 0.97 Hz which is associated to the dominant frequency of the ground motion and rigid body motion of the bridge.

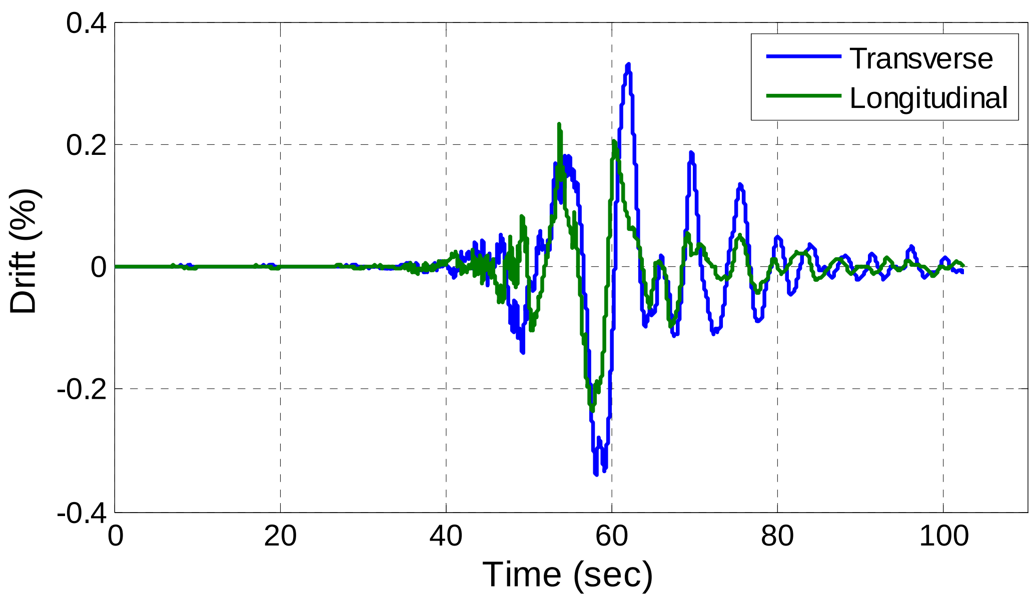

Figure 2.16 Transverse and longitudinal drift demands at pier 1 during the Chi-Chi Earthquake drift

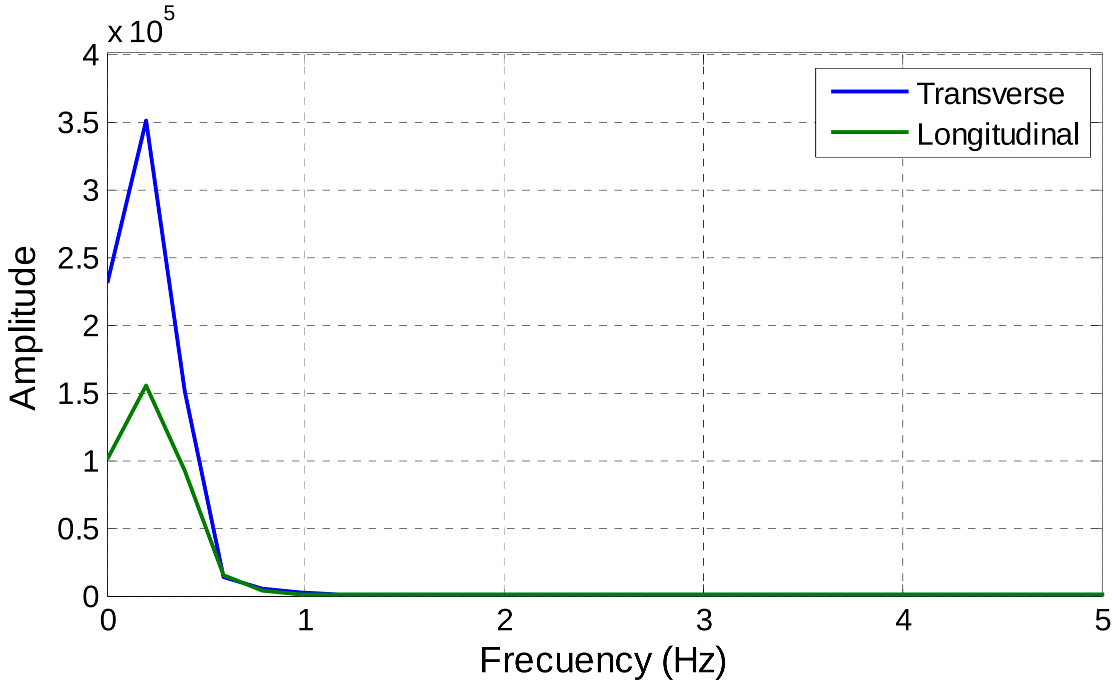

Figure 2.17 Fourier Transform-Displacements at pier 1 during the Chi-Chi Earthquake

2.3.4.3 Abutment Seats

The amount of longitudinal displacement at the abutments is a key parameter to evaluate the probability of superstructure unseating on seat type abutments bridges, as well as the occurrence of pounding between the abutments and the deck. Longitudinal accelerometers at the abutment (CH 14) and at the deck girder by the abutment (CH 24) were used to evaluate the relative displacements at the abutment seats during the 1999 Chi-Chi and Chiayi Earthquakes. Figure 2.18 a shows that the relative displacement at abutments during both events was very small (< 3 mm). One of the reasons for this result is the fact that the deck diaphragms of the bridge are anchored to the abutment's backwalls.

The Transmissibility of the accelerations illustrates that during both earthquakes the signals at the abutments and at the girders are in phase for the range of frequencies controlling the displacements (f < 2 Hz). In addition, the amplitudes of the vibrational components associated to rotational accelerations (2.34 Hz and 2.93 Hz) are higher at the deck's girder than at the abutments (Figure 2.18 b).

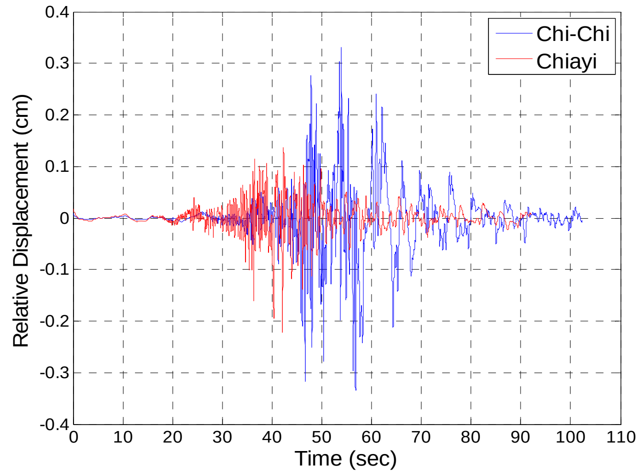

(a) Relative displacements at abutments

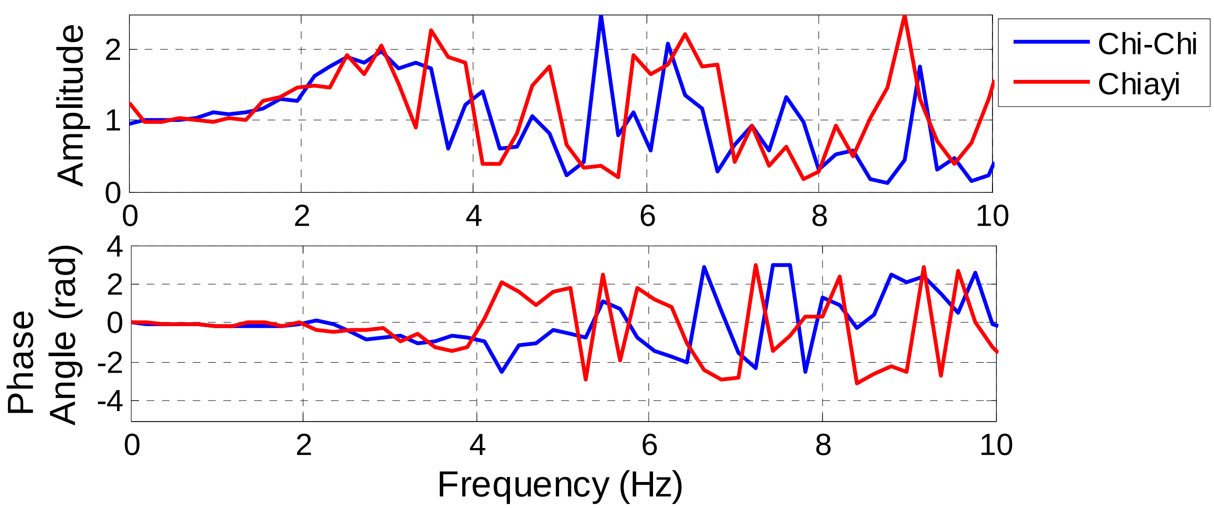

(b) Transmissibility of accelerations from abutment (CH 14) to deck girder (CH 24)

Figure 2.18 Demands at abutments seats during the 1999 Chi-Chi and Chiayi Earthquakes

2.4 Discussion

The most important finding of the ambient vibration tests conducted in this research was the illustration of the directionality in the lateral response of skewed bridges with seat type abutments. The results illustrate that the predominant direction of the transverse mode occurs in the azimuth of the skew bents; whereas the predominant direction of the longitudinal mode is perpendicular to the azimuth of the skew. The results also indicate that the lateral response can be uncoupled by using the transverse and longitudinal modes of vibration and their predominant orientations.

In addition, the instrumentation at Second Northern Freeway (TCUBAB) provided an opportunity to examine the response of multi-span skewed bridges with seat type abutments during actual earthquakes. In terms of deck rotations, the analysis identified rotational accelerations that could potentially produce in-plane rotations of the deck; however these rotations were actually prevented by the internal shear keys of the bridge. The displacement profile during both events predominantly corresponded to longitudinal and transverse rigid body motions of the entire bridge, driven by the dominant frequency of vibration of each ground motion.

The results indicate that the bridge exhibited a linear elastic response in both events. The maximum pier drifts (0.37 %) occurred during the Chi-Chi earthquake and was similar in the longitudinal and transverse directions. The relative displacement at the abutment seats in the longitudinal direction was very small (< 3mm), which is explained by the Taiwanese seismic strategy of anchoring the deck diaphragms and the abutments backwalls to prevent superstructure unseating.

Chapter 3: NONLINEAR RESPONSE OF SKEWED BRIDGES TO EARTHQUAKE-INDUCED POUNDING

3.1 Introduction

Earthquake-induced pounding occurs when the expansion gap at an abutment is closed during a seismic event leading to a deck-abutment collision. The collision generates a coupled system. The study of this system requires consideration of the Embankment-Abutment-Structure Interaction (EASI) effects. The EASI effects are particularly relevant in the case of skewed bridges with seat type abutments, as seismic damage due to past earthquakes illustrates that the superstructure tends to rotate as a result of the pounding between the deck and its abutment. The rotations increase the probability of superstructure unseating and the lateral demands of the piers.

The EASI effects depend on the soil passive pressure mobilized by pounding and the seismic design strategy of the bridge, which includes the amount of deformation expected at the abutments, piers, and foundations. Pounding is principally a short duration mechanism, in which only compression forces are transferred once the longitudinal gap is closed. This mechanism can be properly represented using nonlinear models. Kavianijopari (2011) and Shamsabadi (2007) progressed the study of EASI effects for skewed bridges with ductile abutments. So far, there are no studies that examine the contribution of the in-plane rotation of the deck to the total drift of the pier for different levels of deformations at abutments and Soil-Foundation-Structure Interaction effects (SFSI).

This chapter presents a parametric study of the nonlinear displacement demands of skewed bridges with different structural response at abutments and SFSI effects. The study is applied to short and medium multi-span bridges with continuous superstructure and representative of the bridge inventory in the province of British Columbia (BC), Canada.

3.2 Description of the Models

3.2.1 Bridge Types

Past earthquakes have predominantly damaged skewed bridges with two and three spans. The four bridge types considered in this research are selected to represent standard two and three span bridges with different cross sections, pier types and clear heights located in British Columbia. The bridges are continuous and symmetric. The superstructure is supported at the two ends on seat type abutments with two-inch (5 cm) expansion gaps. Each bridge is studied at skew angles of 15, 30, 45 and 60 degrees. A description of the configurations selected is given in the following subsections.

3.2.1.1 Bridge Type 1

Bridge type 1 is a 120 m long and 12 m wide three-span structure (Figure 3.1 a). The superstructure consists of a concrete deck slab supported on six 1.72 m deep, concrete I-girders.

The superstructure is continuous and rigidly connected to the cap beams. The substructure consists of two bents supported by two piers per bent. The piers are 1.20 m in diameter and 10 m in height.

3.2.1.2 Bridge Type 2

Bridge type 2 is also a 12 m wide three-span structure. The superstructure consists of continuous concrete I-girders, but unlike bridge type 1, the total span is 80m and the substructure consists of two bents, each supported by a single 1.5m diameter, 10 m high pier (Figure 3.1 b).

3.2.1.3 Bridge Type 3

Bridge type 3 is a 46 m long and 20 m wide two-span structure (Figure 3.1 c). The superstructure consists of a concrete deck slab supported on 0.8 m deep precast concrete box stringers. The substructure consists of a multicolumn frame with a set of four concrete columns, each 1.2 m in diameter and 5 m in height. The cap beam is rigidly connected to the superstructure.

3.2.1.4 Bridge Type 4

Bridge type 4 is a 46 m long two-span structure. The superstructure consists of concrete box stringers, but unlike bridge type 3, the width is 12 m and the substructure consists of a bent supported by two piers, which are 1.2 m in diameter and 10 m in height (Figure 3.1 d). The characteristics of the selected bridge configurations are summarized in Table 3.1.

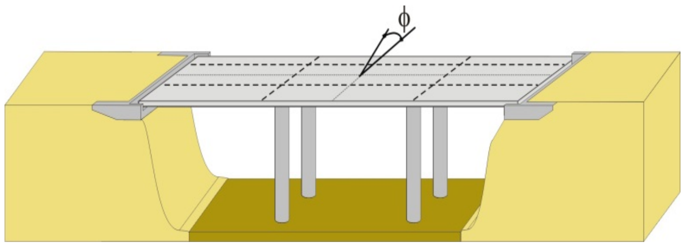

(a) Bridge Type 1

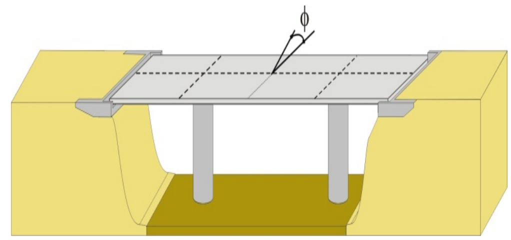

(b) Bridge Type 2

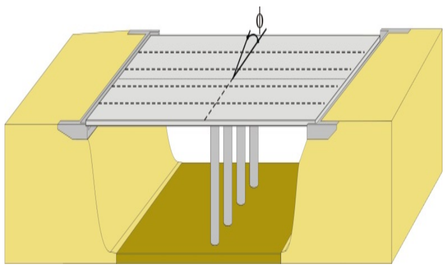

(c) Bridge Type 3

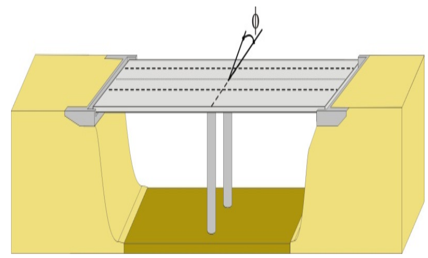

(d) Bridge Type 4

Figure 3.1 Sketches of bridge types analyzed

Bridge	Length (m)	Spans		Width (m)	Clearance (m)	Skew Angle (degrees)	Substructure		Superstructure Type
		No.	Lengths (m)				Type	Abutments	
Type 1	120	3	40-40-40	12	10	15-30-45-60	multi-column-frames (ϕ = 1.20 m)	seat type	Continuous – reinforced concrete I-girders
Type 2	80	3	20-40-20	12	10	15-30-45-60	Single column bent (ϕ = 1.50 m)	seat type	Continuous – reinforced concrete I-girders
Type 3	46	2	23-23	20	5	15-30-45-60	multi-column-frames (ϕ = 1.20 m)	seat type	Continuous – concrete box stringers
Type 4	46	2	23-23	12	10	15-30-45-60	multi-column-frames (ϕ = 1.20 m)	seat type	Continuous – concrete box stringers

Table 3.1 Summary of bridge properties

3.2.2 Detailed Nonlinear Spline Models

Three dimensional spline models are developed in order to study the different bridge types at the selected skewed angles (Figure 3.2). In the spline models the abutment shear keys are represented by four springs in the direction of the skew, and the abutment backfill longitudinal response is represented by a set of springs perpendicular to the face of the skewed abutment. The deck and pier bent are modeled using 3D beam elements. Rigid elements are used to represent the cap beams and the abutment-caps. The models are developed using the computer program SAP 2000 (Computers and Structures, 2012). A detailed description of the properties of the models is given in following sections.

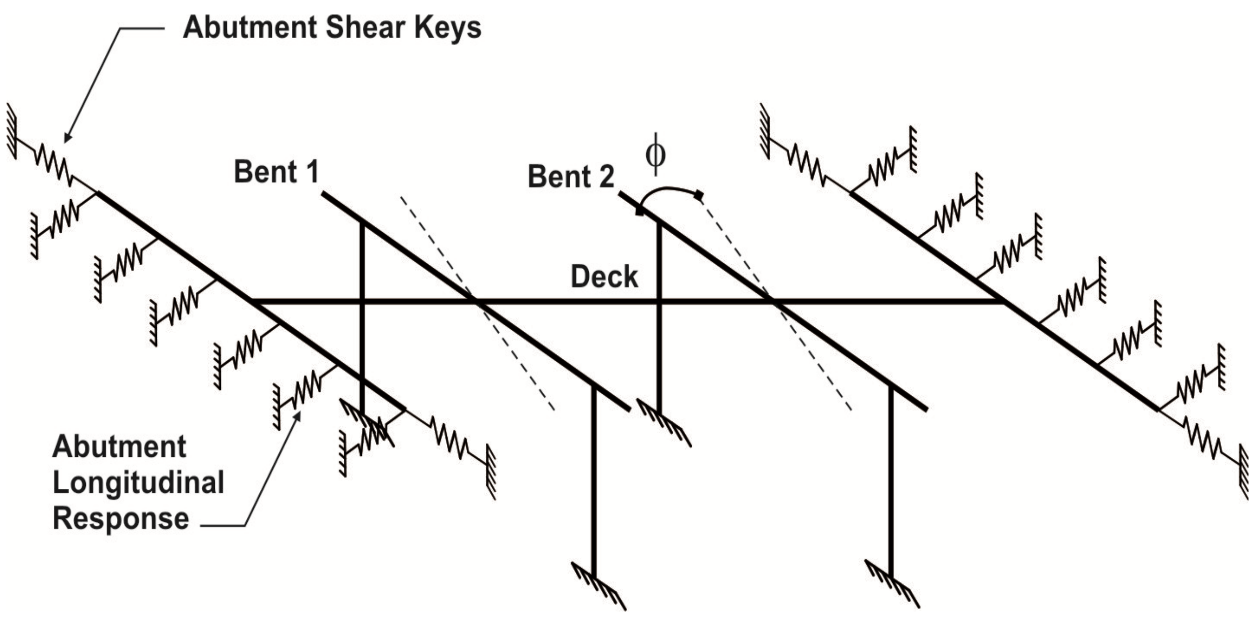

Figure 3.2 Spline model Bridge Type 1

3.2.3 Abutment Models

3.2.3.1 Abutment Design Approaches

The level of deformation and extent of damage expected for the abutments depends on the seismic design approach of the bridge. Some jurisdictions take into consideration the contribution of the abutments to resist seismic demands. In this scenario, the expected response of the abutment backfill in the longitudinal direction might be elastic when the abutment deformations are small or inelastic when the deformations are large enough to reach the maximum capacity of the abutment backfill. In the transverse direction an elastic performance of the abutment is assumed (AASHTO, 2011).

In contrast, other jurisdictions consider only the bridge piers to resist the seismic demands and the abutments are considered only an additional source of structural redundancy. In this approach, the abutment is designed to be capacity protected in the transverse direction by making use of shear keys that act as fuses and have a brittle failure (AASHTO, 2011). In this research, three abutment models that combine the longitudinal deformations of the abutment-backfill with the structural response of the abutment-shear keys are used to represent the design approaches previously mentioned.

3.2.3.1.1 Linear Abutment with Longitudinal Gap

In the longitudinal direction, this model represents an elastic abutment-backfill in which only compression forces are transferred once the gap is closed. In the transverse direction an elastic response of the abutment is considered (Figure 3.3). This model is hereafter called “linear abutment”.

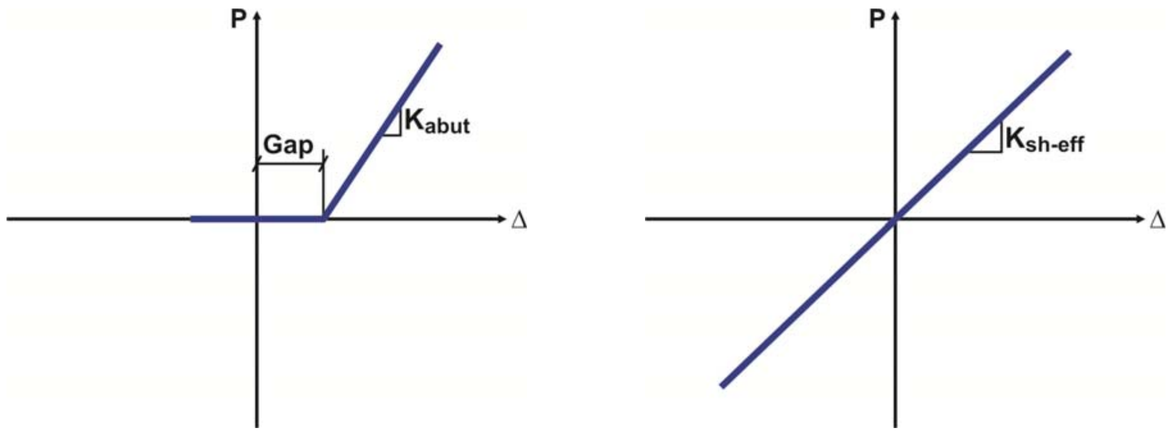

(a) Longitudinal direction **(b) Transverse direction**

Figure 3.3 Linear abutment

3.2.3.1.2 Bilinear Abutment

In the longitudinal direction, the backbone represents an abutment-backfill with elasto-plastic response, in which only compression forces are transferred once the gap is closed. The plateau corresponds to the abutment backfill capacity. In the transverse direction, the model represents an elastic response of the abutment (Figure 3.4).

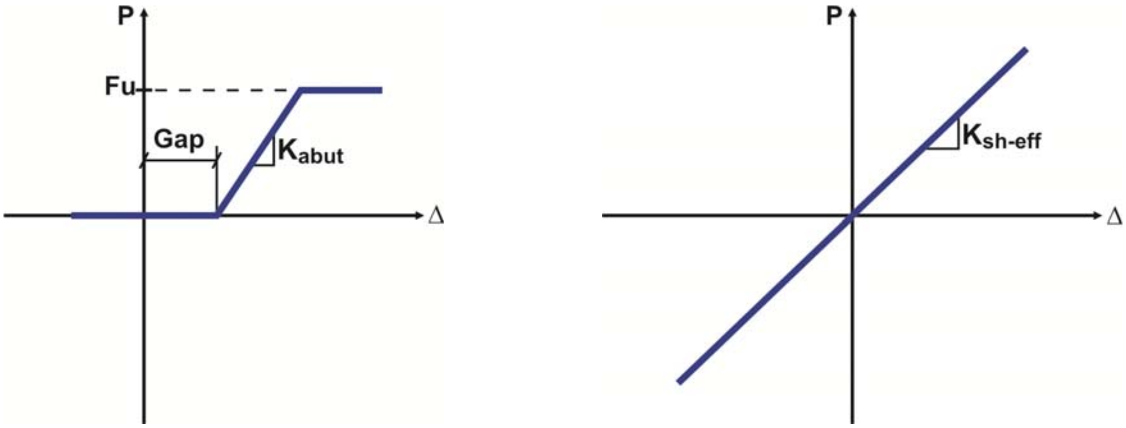

(a) Longitudinal direction **(b) Transverse direction**

Figure 3.4 Bilinear abutment

3.2.3.1.3 Fusing Abutment

In the longitudinal direction this model represents an abutment-backfill with an elasto-plastic response. In the transverse direction, the backbone curve represents an abutment with a lateral restraint system that only transfers forces in one direction and fuses by having a brittle failure once its maximum capacity is reached (Figure 3.5).

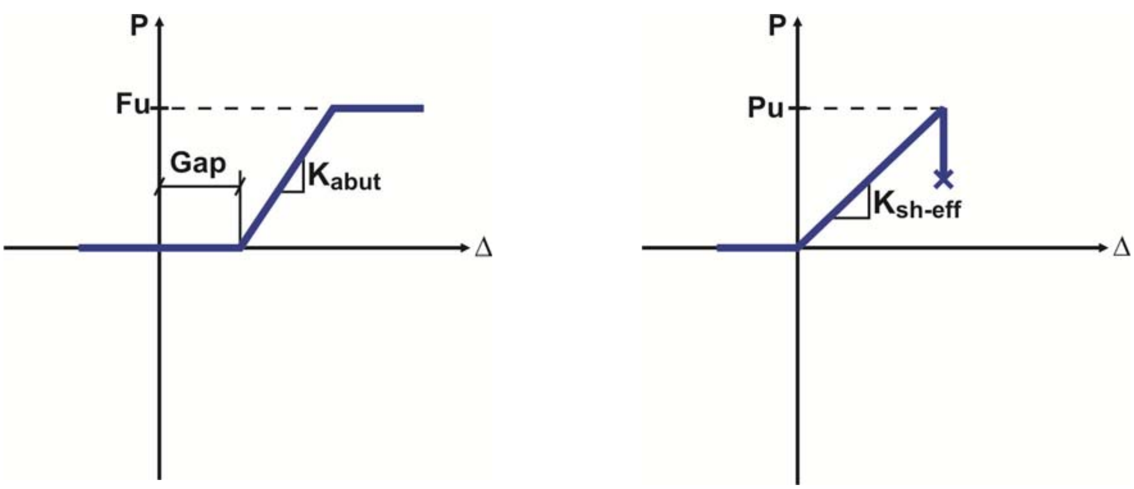

(a) Longitudinal direction **(b) Transverse direction**

Figure 3.5 Fusing abutment

3.2.3.1.4 Elastic Abutment

The elastic abutment represents the traditional model used in linear analysis, in which the longitudinal gap is linearized and the effective abutment stiffness obtained ($K_{abut\text{-}eff}$) is used in tension and compression (Figure 3.6). In the transverse direction the response is also elastic and the effective shear key stiffness is used ($K_{sh\text{-}eff}$).

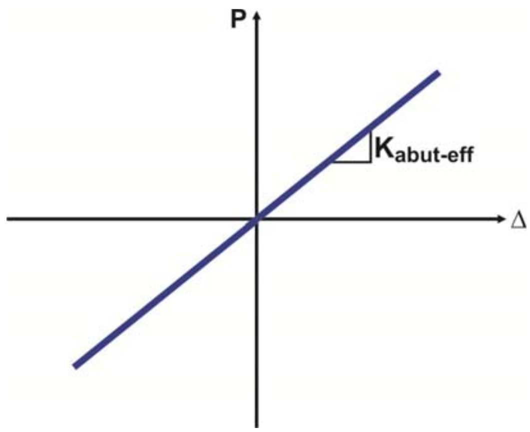

(a) Longitudinal direction

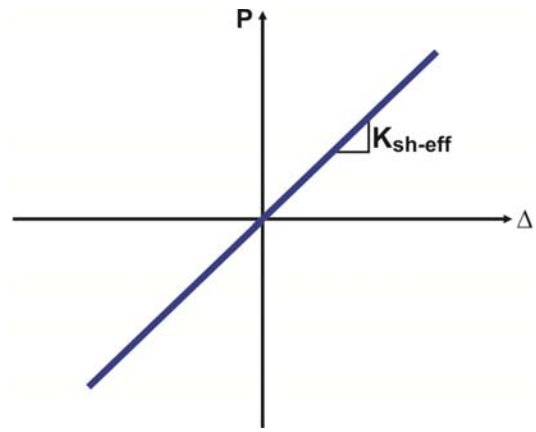

(b) Transverse direction

Figure 3.6 Elastic abutment

3.2.3.2 Abutment Parameters

The input parameters to define the backbone curve in the longitudinal direction for the abutment models are calculated according to the recommendations given in the Caltrans Seismic Design Criteria Version 1.6 (Caltrans, 2010). The values recommended correspond to an elasto-plastic model and are based on force-deflection results from large-scale pseudostatic abutment's tests. The recommendations of Caltrans are in good agreement with the values recommended by Shamsabadi's Hyperbolic Model (Shamsabadi, 2007). Table 3.2 presents the values recommended per meter of abutment by Caltrans for seat type abutments with a backwall height of 1.7m.

In the transverse direction, the input parameters used to define the abutment shear key response are based on the experiments by Silva et al. (2009), who conducted large-scale monotonic and cyclic tests to internal and external shear keys designed for seat type abutment bridges. The effective shear key stiffness ($K_{sh\text{-}eff}$) used in the abutment models is 18 MN/m and the maximum capacity (P_u) was 0.90 MN for each shear key. The effective shear key stiffness includes the effect of the one-inch (2.5 cm) gap between shear keys and deck. The results of Silva's experiments have also been used by other authors to define the abutment shear keys parameters (Kavianijopari, 2011; Shamsabadi, 2007).

Backbone Sketch	Abutment Stiffness K_{abut} $\frac{(MN/m)}{m}$	Effective Abutment Stiffness $K_{abut\text{-}eff}$ $\frac{(MN/m)}{m}$	Maximum Passive Capacity F_u $\frac{(MN)}{m}$
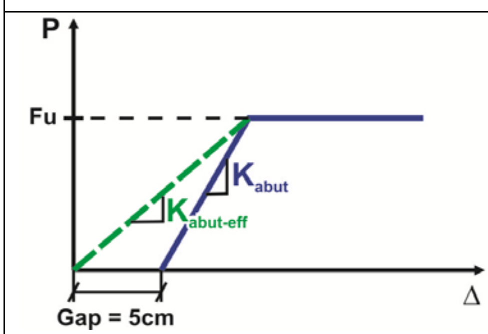	29.35	6.33	0.41

Table 3.2 Input values for the longitudinal response of the abutment models

3.2.4 Superstructure Model

The superstructure is expected to respond elastically during a ground motion. Each superstructure is represented by beam elements with equivalent section properties. The use of beam elements enables considering the effect of superstructure's flexibility (Figure 3.2).

3.2.5 Bent Model

Nonlinear displacements of bridges are the coupled effect of pier damage, pounding at expansion joints and soil-structure interaction. As previously explained, pounding induces in-plane rotations of the superstructure exclusively in skewed bridges. The intention of this research was to focus on the nonlinear effects induced by pounding, which are represented in the nonlinear abutments models considered. In order to allow uncoupling the contribution of pounding from the overall non-linear response, effective section properties were used to approximate the nonlinear effects of pier damage. This approach is allowed by AASHTO (2011) and is based on the principle of equal displacement. Bents were then modeled using beam elements with effective cracked section properties ($I_{effective} = 0.5 \times I_{gross}$). This effective inertia is taken from the values suggested by FHWA (2006).

Initially, the piers are modeled rigidly connected (fixed) to the base. Section 3.4.4 will present results accounting for foundation flexibility. The cap beams are modeled by rigid elements and are assumed to be rigidly connected to the superstructure.

3.2.6 Damping Characterization

As noted earlier in the ambient vibration results (section 2.2), the damping ratios of standard bridges for low levels of shaking are mostly below 3 %. On the other hand, the damping ratio estimated in the strong motion case study (section 2.3) was 6.3 % for the Chi-Chi earthquake and 4.3 % for the Chiayi earthquake. These results are in agreement with the sensitivity study conducted by Ortiz et al. (2013) using a larger database of experimental data, which suggests an increment of the damping ratio with the amplitude of the external excitation. In view of these observations, a damping ratio of 5% is used in this research. Damping at abutments was represented by the multi-linear kinematic hardening model available in the program SAP 2000 (Computers and Structures, 2012).

3.3 Selected Ground Motions

The ground motions considered correspond to crustal, subcrustal, and subduction earthquakes. The records were selected from the suite of representative ground motions recommended in a comprehensive study of the seismic hazard in south-western British Columbia (BC), developed as part of the project for the seismic retrofit of existing school buildings in BC (Pina et al., 2010).

The crustal and subcrustal records were scaled to match the Uniform Hazard Spectra (UHS) for Vancouver and the subduction records were scaled to match the UHS for Victoria, using a probability of exceedance of 2% in 50 years at a site class C. The frequency match was performed for periods from 0 to 2 seconds. The displacement and acceleration spectra are given in Appendix C. The records are applied parallel and perpendicular to the direction of the skewed bents. A summary of the selected records is shown in Table 3.3.

Source	Earthquake Name	Date	Station Name	Mw	Epicentral Distance (km)	PGA (g)
Crustal	Loma Prieta	18-Oct-1989	CDMG 57007 Corralitos	6.9	18.9	0.35
	Northridge	17-Jan-1994	USGS 5108 Santa Susana Ground	6.7	22.8	0.30
Subcrustal	Nisqually	28-Feb-2001	Seattle (EVA)	6.8	80.7	0.25
	El Salvador	13-Jan-2001	Unidad de Salud, Panchimalco (PA)	7.6	95.7	0.36
Subduction	Maule, Chile	27-Feb-2010	Santiago Maipu (E-W)	8.8	78.9	0.32
	Michoacan, Mexico	19-Sept-1985	La Union (UNIO)	8.1	83.9	0.41
	Tokachi-oki, Japan	25-Sept-2003	Noya (HDK107)	8.0	126.4	0.30

Table 3.3 Selected ground motions

3.4 Displacement Demands

This section presents a discussion of the in-plane rotations due to earthquake-induced pounding and the resulting additional pier drift for different types of structural response at abutments. In addition, the contribution of this additional drift to the total magnitude of the pier drift is discussed.

Table 3.4 shows the transverse, longitudinal and in-plane rotational periods of the bridges types analyzed skewed at 45 degrees, with and without elastic abutment backfill. The modes of vibrations observed were similar to those observed in the experimental studies.

	Bridge Type 1			Bridge Type 2			Bridge Type 3			Bridge Type 4		
Boundary Condition	**T_{Tran} (s)**	**T_{Long} (s)**	**T_{rot} (s)**	**T_{Tran} (s)**	**T_{Long} (s)**	**T_{rot} (s)**	**T_{Tran} (s)**	**T_{Long} (s)**	**T_{rot} (s)**	**T_{Tran} (s)**	**T_{Long} (s)**	**T_{rot} (s)**
With elastic Abutment-backfill	1.04	0.95	0.75	1.15	0.85	0.67	0.41	0.45	0.49	0.82	0.69	0.53
Without elastic abutment-backfill	1.04	2.25	0.81	1.11	1.83	1.13	0.41	0.54	0.76	0.82	1.94	0.95

Table 3.4 Periods of vibrations of the bridges types analyzed skewed at 45 degrees

It is important to note that for the lateral displacements presented in this research, the transverse direction is assumed to be in the direction of the skew and the longitudinal direction is normal to this (Figure 3.7). This coordinate system is adopted here as it is consistent with the predominant directions of lateral response of skewed bridges indicated by the experimental evidence (section 2.2.3.2). Also, it is convenient when comparing the demand and capacity of the bents, as AASHTO (2011) requires a comparison with demands obtained at the azimuth of the skewed bents.

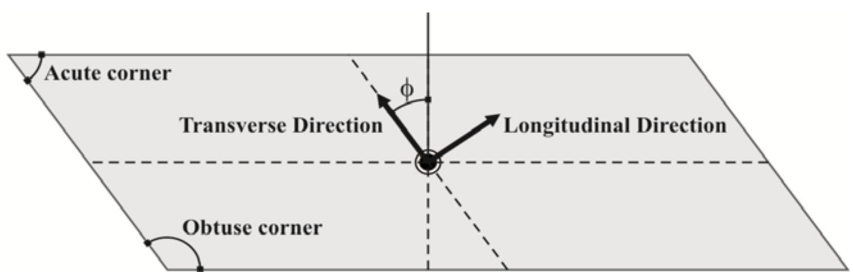

Figure 3.7 Directionality of the lateral response of skewed bridges

A critical parameter in the seismic response of skewed bridges is the in-plane rotation of the deck as it defines the additional demands that piers will be subject to. As discussed previously in the problem statement (section 1.6) the in-plane rotation due to earthquake-induced pounding is not properly captured by linear elastic analysis and requires the use of nonlinear models to be quantified.

3.4.1 Response History of In-plane Deck Rotation

The time histories of the deck rotation at the center of mass of the bridge Type 1, skewed at 45 degrees, during the 1989 Loma Prieta earthquake are used to highlight common features observed in the in-plane rotational response. Figure 3.8 illustrates the strong influence of the abutment design approach in the magnitude and characteristics of the in-plane rotational response.

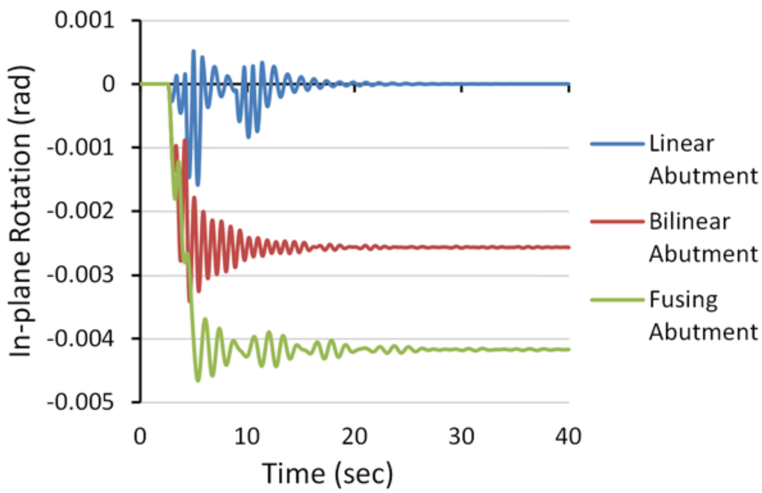

Figure 3.8 Response history of the in-plane rotations at the center of mass of the deck for different abutment's design approaches (Bridge Type 1 skewed at 45 degrees – Loma Prieta Earthquake)

Linear abutments with longitudinal gap, in which the backfill remain elastic, have the lowest in-plane rotations and do not show any residual rotation. The first collision between the abutment backwall and the deck occurs at about 2.62 seconds when the expansion gap is closed. This collision triggers compression passive forces along the abutment backwalls (Figure 3.9a).

Figure 3.9 b shows the compression forces in the spring at the acute and obtuse corners of the abutment. The figure illustrates that intermittent collisions with similar magnitudes occur simultaneously at both corners, which is an indication of a predominantly uniform distribution of the passive pressure along the abutment backwalls during the ground motion.

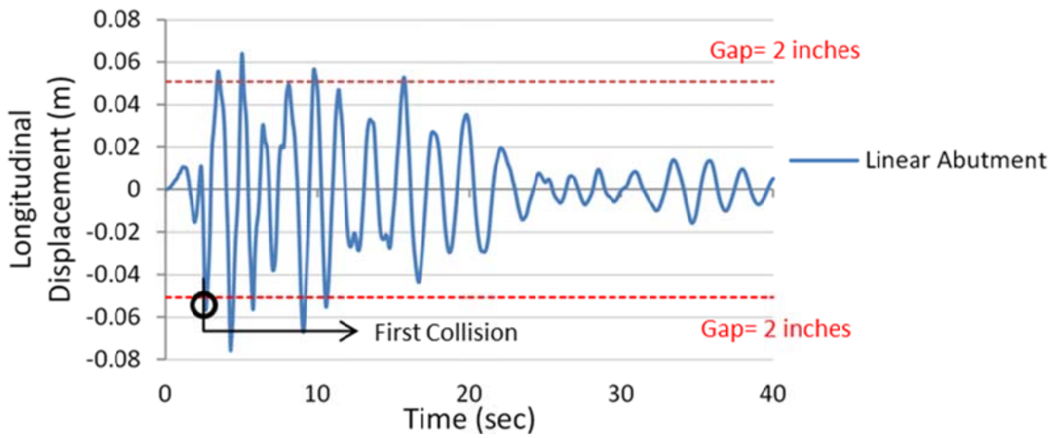

(a) Longitudinal displacement at the center of mass

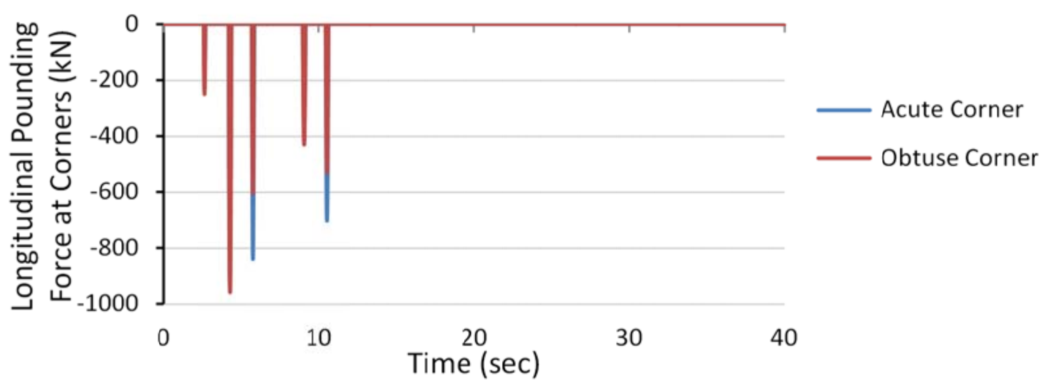

(b) Longitudinal pounding forces at abutment corners

Figure 3.9 Longitudinal displacement and pounding forces for linear abutments (Bridge Type 1 skewed at 45 degrees – Loma Prieta Earthquake)

For bilinear abutments, in which the backfill reaches its plastic capacity, the induced in-plane rotations are larger than for linear abutments. The rotations are all negative, indicating a permanent clockwise rotation of the longitudinal axis of the deck during the ground motion (Figure 3.8). After the first collision at 2.62 seconds has occurred, permanent passive pressures along the backwalls are observed (Figure 3.10).

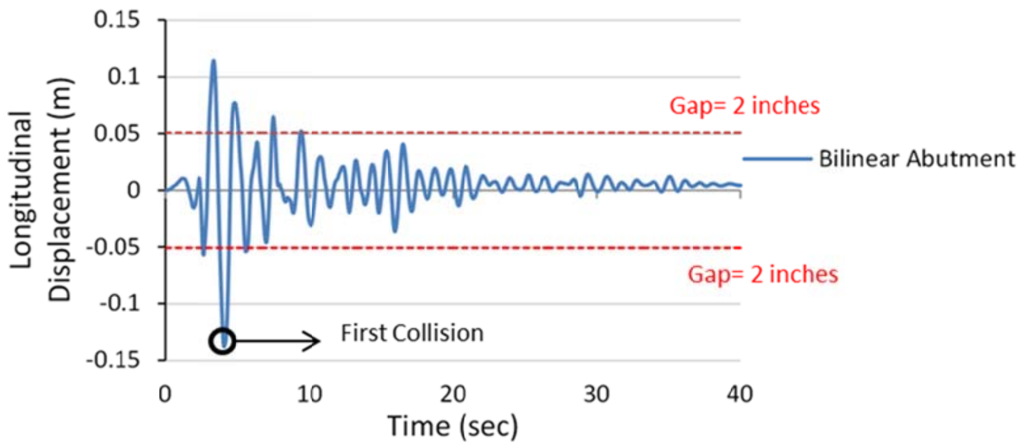

(a) Longitudinal displacement at the center of mass

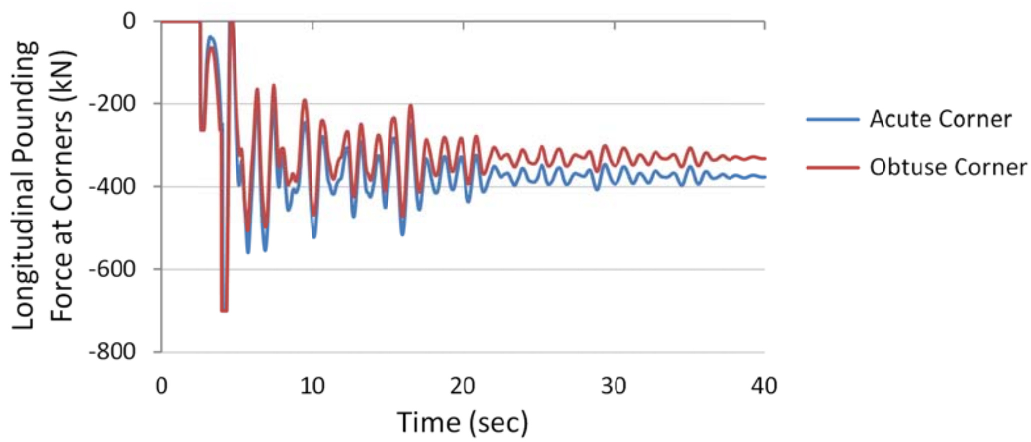

(b) Longitudinal pounding forces at abutment corners

Figure 3.10 Longitudinal displacement and pounding forces for bilinear abutments (Bridge Type 1 skewed at 45 degrees – Loma Prieta Earthquake)

The largest in-plane rotations are obtained for fusing abutments, in which plastic deformation of the backfill along with brittle failure of the abutment shear keys are expected. A permanent clockwise rotation of the deck is observed (Figure 3.8). This permanent rotation has been also reported by Tirasti and Kawashima (2008), and Shamsabadi and Kapuskar (2010). A non-uniform distribution of passive pressure along the backwalls was observed, as reflected by larger compressions at the obtuse corner than at the acute corner

Figure 3.11).

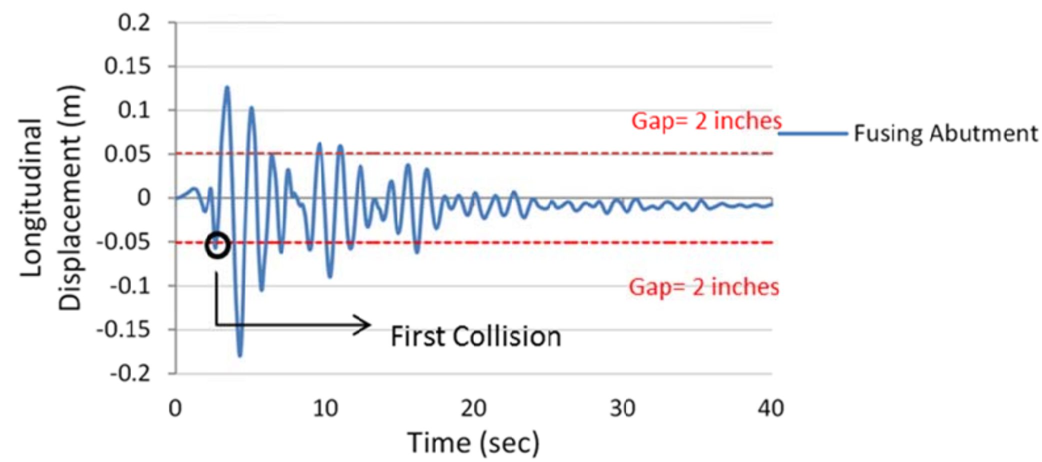

(a) Longitudinal displacement at the center of mass

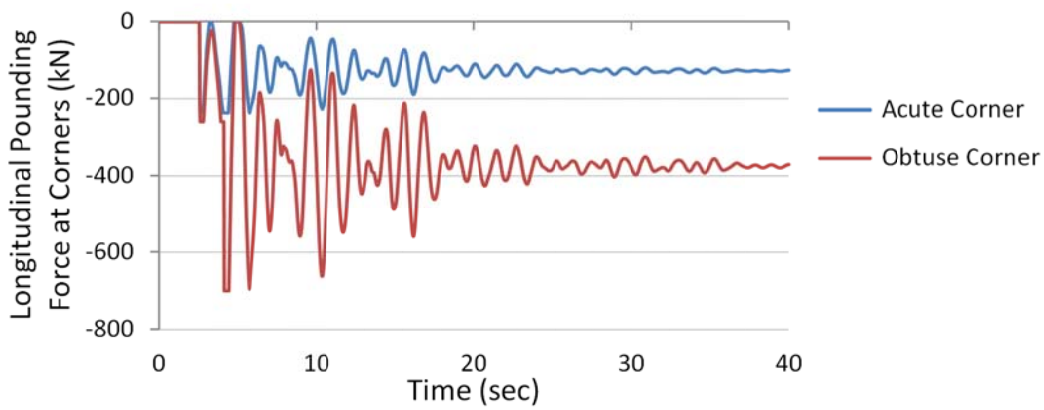

(b) Longitudinal pounding forces at abutment corners

Figure 3.11 Longitudinal displacement and pounding forces for fusing abutments (Bridge Type 1 skewed at 45 degrees – Loma Prieta Earthquake)

3.4.2 Peak In-plane Deck Rotation and Additional Pier Drift

In standard engineering practice it is important to assess the peak in-plane rotational demands of skewed bridges as they contribute to the calculation of the support length that the engineer should provide at the abutments in order to prevent superstructure unseating. These peak in-plane rotational demands also induce additional drift demands to the piers. This additional drift is calculated for the column furthest from the center of mass as illustrated in Figure 3.12. Figure 3.13 provides an overview of the peak in-plane rotations and the additional pier drifts for the Bridge Type 1 during the 1989 Loma Prieta earthquake and the 2010 Maule earthquake, for different skew angles and abutment performance levels. The additional drift is a useful measure to highlight the displacement demand missing at the pier when the in-plane deck rotation induced by earthquake pounding is ignored in the analyses. Thus, the additional drift could be used as a tool to decide when running only linear elastic analysis is acceptable.

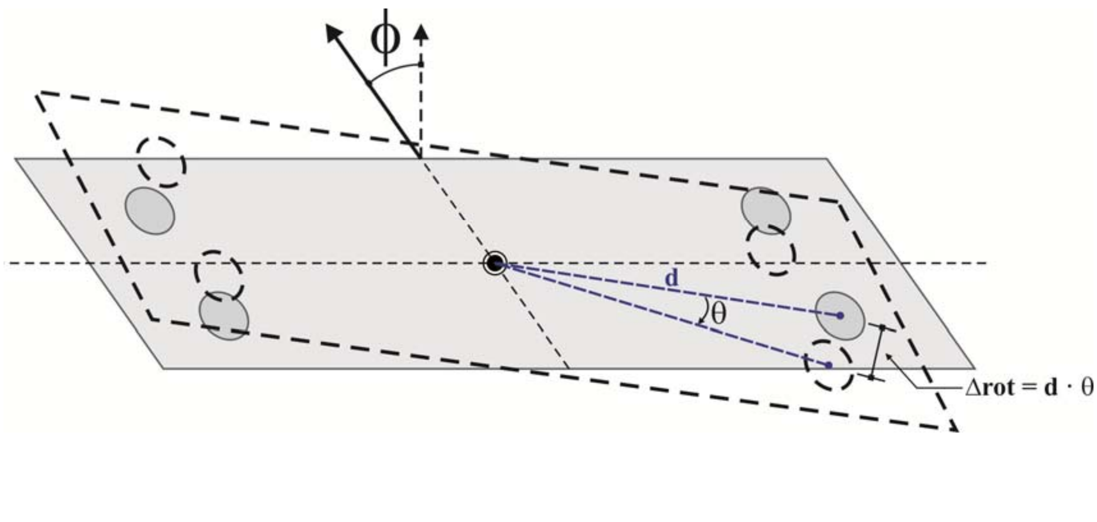

Figure 3.12 Illustration of additional pier displacement (Δ_{rot}) due to in-plane deck rotation

For the 1989 Loma Prieta and the 2010 Maule earthquakes, there is an increment in the peak in-plane rotation as a function of the skew angle for all the abutment types modeled in this study (Figure 3.13). Similar results are observed for the others input ground motions used.

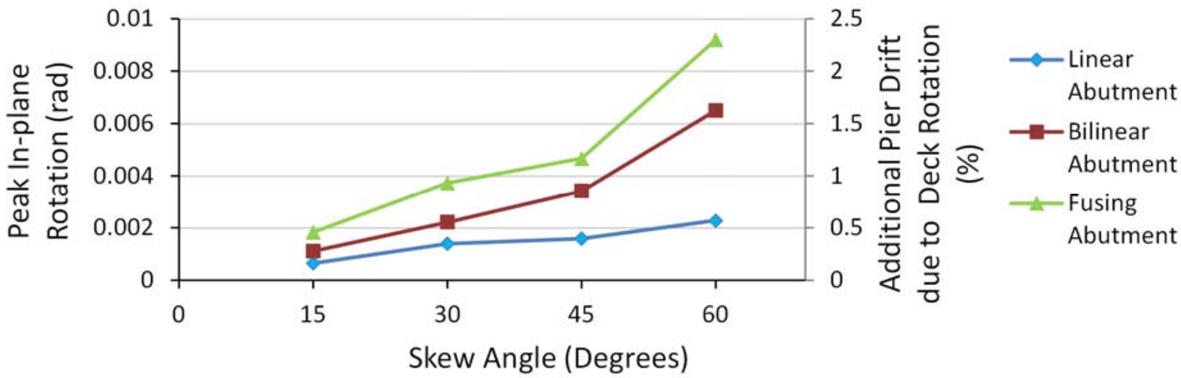

(a) Loma Prieta (1989)

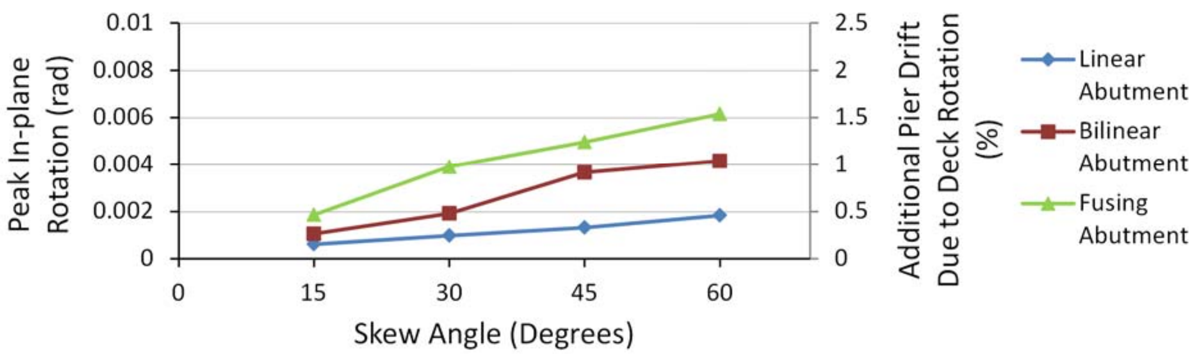

(b) Maule (2010)

Figure 3.13 Peak in-plane rotations and additional pier's drift (Bridge Type 1 subjected to the 1989 Loma Prieta and 2010 Maule Earthquakes).

The mean and the dispersion of the peak in-plane rotations and additional drifts obtained for Bridge Type 1 for all ground motions are presented in Figure 3.14. The response is very sensitive to the type of abutment. It is noted that the largest demands are experienced by skewed bridges with abutment shear keys that fuse during the earthquake. This could be explained, in part, by the reduction in the lateral and rotational stiffnesses of the bridge once the shear keys fails. This type of response could also be expected for existing bridges with poor lateral restraint. The additional drift could be up to 1.8 % for skew angles of 60 degrees. The lowest demands are observed for linear abutments, for which the lateral restraint remains in place throughout the earthquake. In this case, the additional drift could be up to 0.5 %. For the bilinear abutments, the largest additional drift is average 1.4 %, and for all skew angles the response is bounded between the response of the linear and the fusing abutments.

A linear dependency in the magnitude of the peak in-plane rotation and additional drift as a function of the skewed angle is observed. This trend suggests the magnitude of the demands is proportional to the skew angle. The dispersion is in generally small, and the largest standard deviation (0.4%) was obtained for the bridge with fusing abutments skewed at 60 degrees.

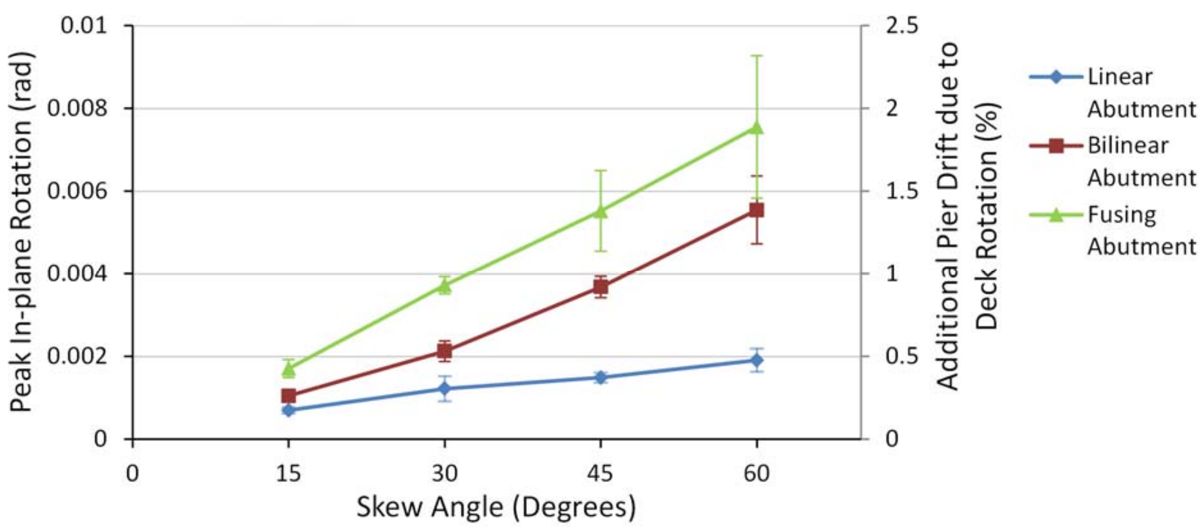

Figure 3.14 Bridge Type 1- Peak in-plane rotations and additional pier's drift for all ground motions

For Bridge Type 2, which is also a three-span bridge but shorter than Bridge Type 1; with a single pier per bent, similar trends and results are observed (Figure 3.15). The lowest rotations occurred in bridges with linear abutments with a largest additional drift of 0.5 %. And the largest rotations are observed for fusing abutment with a largest additional drift of 2.3%. However, the dispersion for bridges with fusing abutments (0.7 %) is larger than those for Bridge Type 1 (0.4 %).

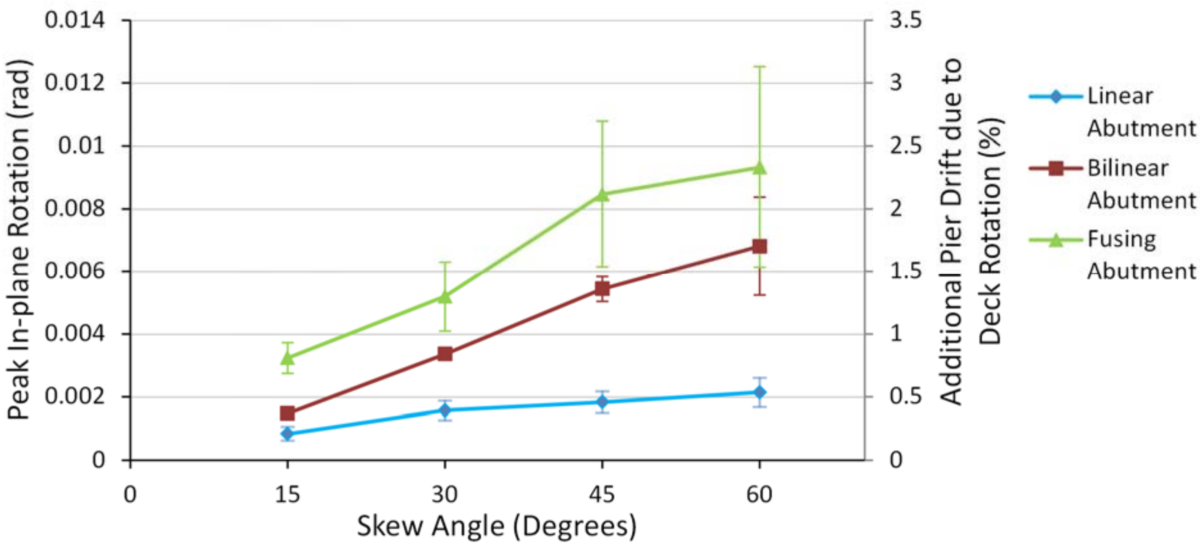

Figure 3.15 Bridge Type 2- peak in-plane rotations and additional pier's drift for all ground motions

An interesting finding regarding the Bridge Type 3, is that there were no in-plane rotations of the deck for all skew angles, abutment performances and input ground motions considered. Bridge Type 3 is a wide/short (46m), two-span structure, with a 5 m high four columns bent. Its configuration is similar to the Hwy 24 bridge tested and discussed in section 2.2.1. The reason why in-plane rotations of the deck are not observed is because the two-inch (5 cm) dimension of the longitudinal gap is not exceeded during the ground motion, and so pounding does not occur and the induced in-plane rotations are not triggered (Figure 3.16). However, it is noted that the skew angle still influences the direction of the lateral demands. The transverse displacement is in the direction of the skew, and the longitudinal displacement is perpendicular to this. The absence of in-plane rotations for Bridge Type 3 illustrates that simply because a bridge is skewed and torsionally sensitive, does not mean that it is necessarily going to be torsionally activated, the onset of in-plane rotations will depend on the size of the gap and whether or not it is closed.

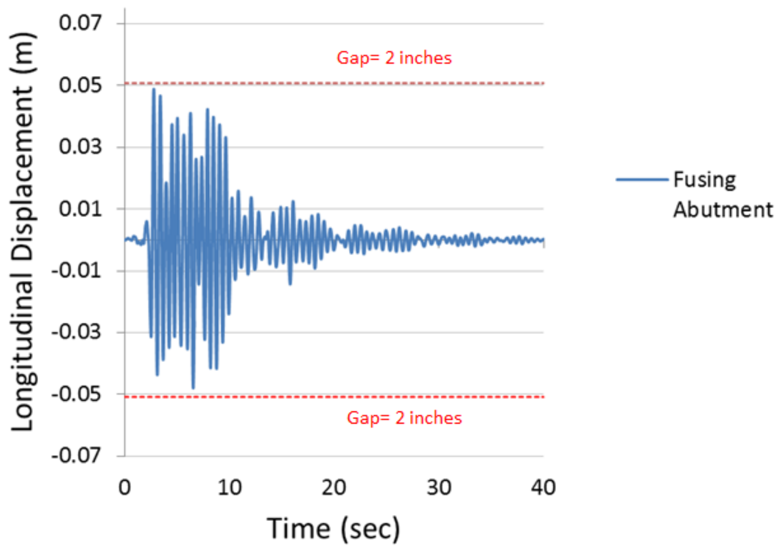

Figure 3.16 Longitudinal response for Bridge Type 3 with fusing abutments and skewed at 60 degrees subjected to the 1989 Loma Prieta Earthquake

In contrast, for Bridge Type 4, which is also a two-span bridge with the same length as Bridge Type 3 but with a narrower deck and two columns per bent (10 m high), in-plane rotations of the deck were observed. Since it is a two-span structure the in-plane rotations primarily increase the longitudinal drift of the pier. The pier drift increases proportionally with the skew angle. Similar to the other bridges, the lowest drift values, and dispersions are found for the linear abutments, with the largest being for the fusing abutments which can reach up to 1.25 % with standard deviation of 0.25 % for the structure skewed at 60 degrees (Figure 3.17).

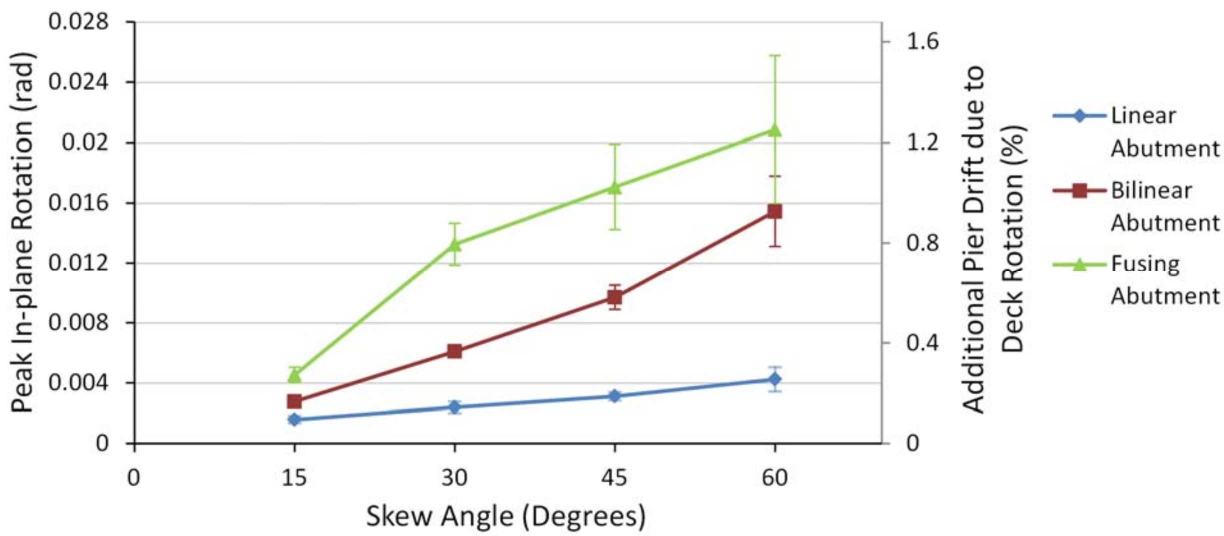

Figure 3.17 Bridge Type 4- peak in-plane rotations and additional pier drift for all ground motions

3.4.3 Total Pier Drift

The total drift of a pier in the transverse direction is a combination of the drift due to the deck transverse displacement and in-plane rotation (Figure 3.18). This research examines the total pier drift in the direction in which the in-plane rotation of the deck has a major influence. For three-span bridges (Bridge Type 1 and 2) this direction is the transverse direction, whereas for two-span bridges this direction (Bridge Type 3 and 4) is the longitudinal direction.

Bridge Type 1 with bilinear abutments and skewed at 45 degrees; subjected to the 1989 Loma Prieta Earthquake is used to illustrate the characteristics of the response history. Figure 3.19 shows the response history of pier drift due to the deck transverse displacement obtained from a linear elastic analysis, and the response history due to in-plane rotation of the deck as well as the total drift of the pier obtained from a nonlinear analysis. It is noted that the peak drift of each response history occurs at a different time.

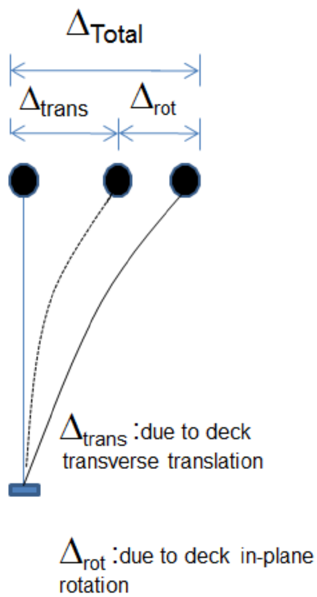

Figure 3.18 Total drift at piers in the transverse direction

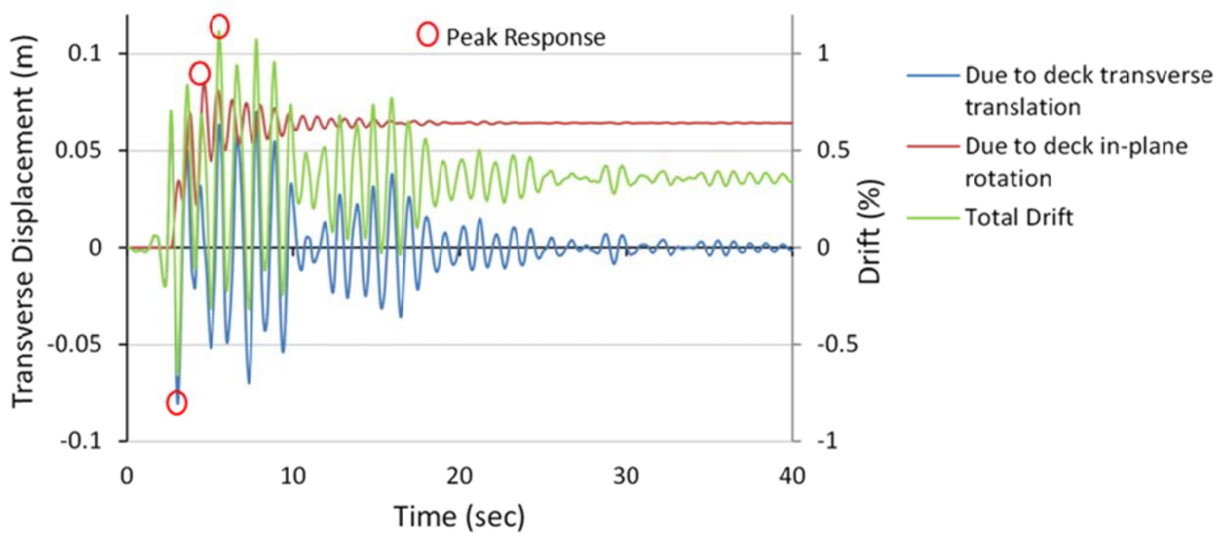

Figure 3.19 Response histories of transverse drift (Bridge Type 1 with bilinear abutments skewed at 45 degrees – Loma Prieta Earthquake)

The analysis is extended to bridges with linear and fusing abutments and to all the skew angles and input ground motions considered previously. Figure 3.20 to Figure 3.22 show for each abutment type the peak of the total pier drift obtained from the nonlinear analysis and obtained by computing an absolute combination of the peak responses, in which the peak value of the drift due to the transverse translation of the deck is added to the peak values of the drift due to the in-plane rotation of the deck. The absolute combination was selected as it resulted in the best match to the actual peak drift of the pier given by the nonlinear analysis. A comparison between the total drift of the pier obtained from nonlinear analysis and the drift due to transverse translation of deck indicates that for linear abutments the contribution of the in-plane rotation of the deck becomes significant for skew angles greater than 30 degrees. In the cases of bilinear and fusing abutments the contribution is significant regardless of the skew angle.

Parametric analyses similar to those conducted with Bridge Type 1 were also conducted for Bridge Types 2 and 4. The trends in the peak drift of the pier are similar to those previously observed for Bridge Type 1. The findings indicate that the peak drift at columns can be estimated based on an absolute combination of the peak transverse drift obtained from linear elastic analysis and the peak drift due to the in-plane rotation of deck obtained from nonlinear analysis.

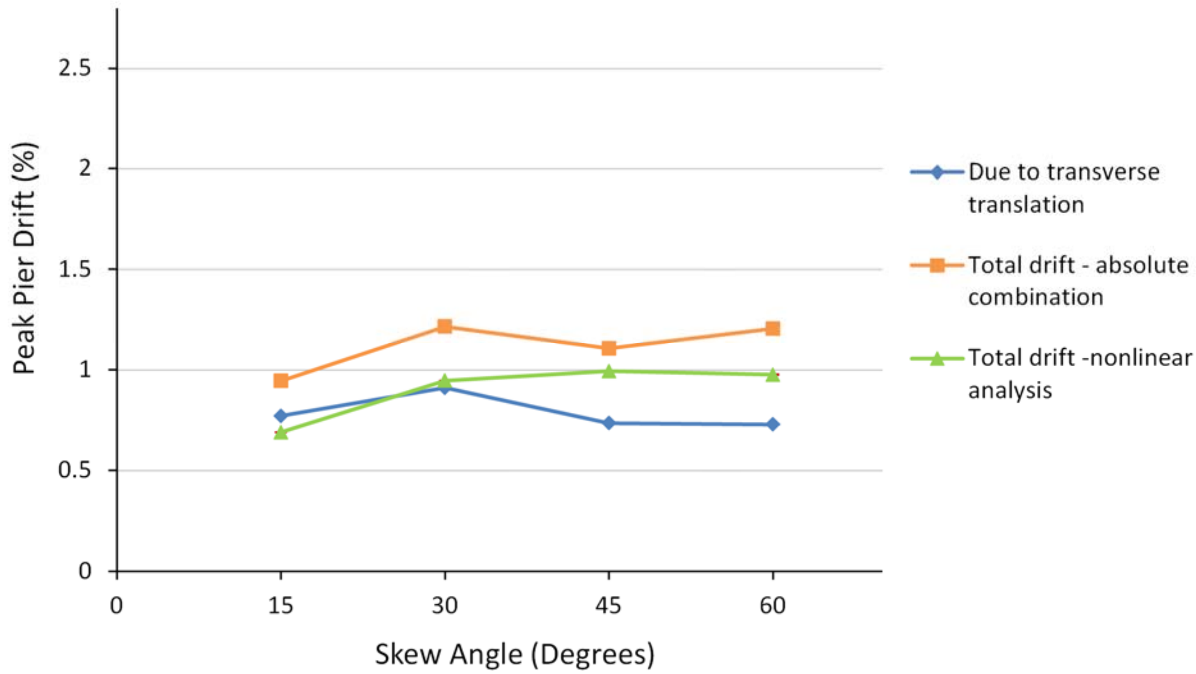

Figure 3.20 Total drift for the linear abutments (Bridge Type 1-all ground motions)

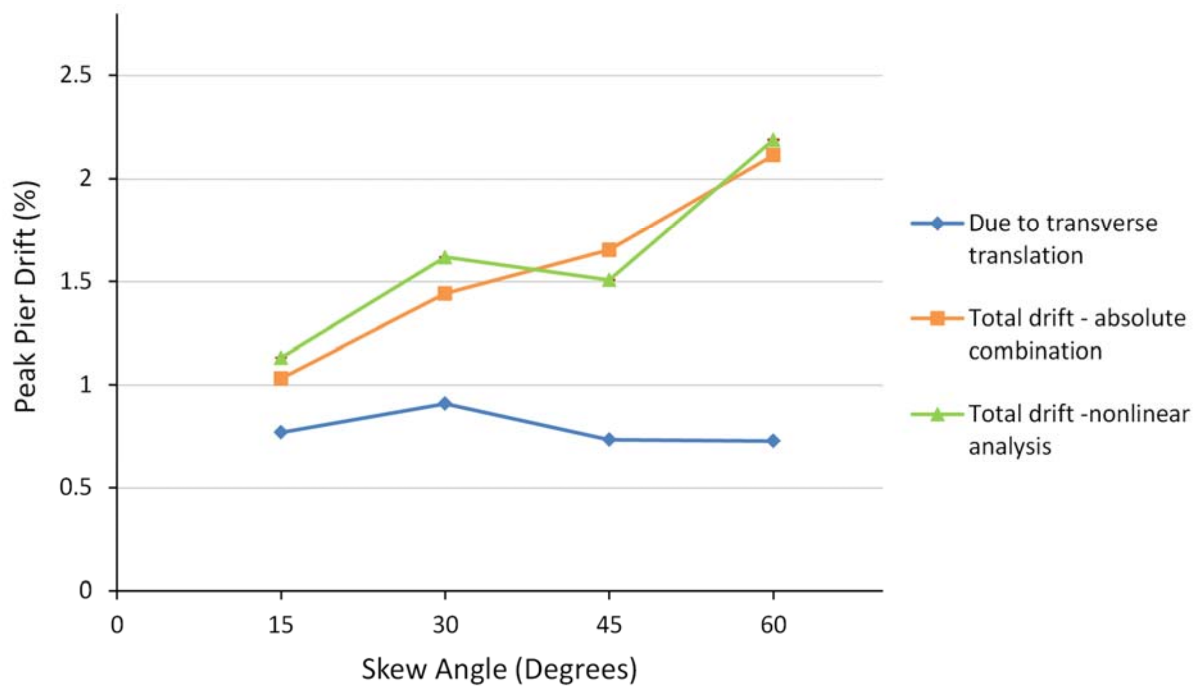

Figure 3.21 Total drift for the bilinear abutments (Bridge Type 1-all ground motions)

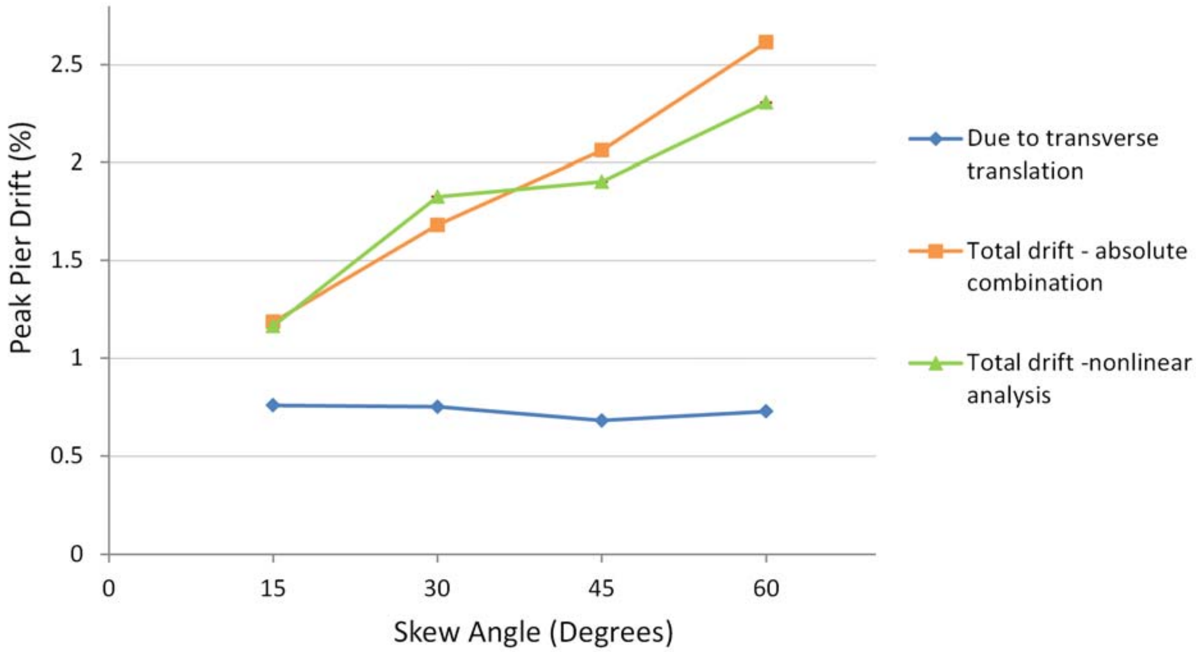

Figure 3.22 Total drift for the fusing abutments (Bridge Type 1-all ground motions)

3.4.4 Soil-Foundation-Structure Interaction Effects (SFSI)

There are three approaches to account for Soil-Foundation-Structure Interaction (SFSI) effects. The first approach is the direct method which entails modeling the pile group, the bridge and the surrounding soil using continuum models. This type of modeling includes all the inertial and flexibility effects involves in the SFSI problem; however the computational effort can be very time consuming (Finn 2005, Rahmani et al. 2013).

In the second approach, the soil around the piles at each level is simulated by a series of springs and dashpots. This approach includes two steps. In the first step, site response analysis is conducted to obtain the time histories at each level. Then in the second step, the calculated time histories are applied to the free ends of the spring-dashpot systems. This approach captures the flexibility (kinematic) and damping effects of the SSI problem. The inertial effects of the bridge in the soil-foundation system are not captured in this approach (Rahmani et al., 2012).

In the third approach, the pile group is replaced by equivalent translational and rotational springs representing the soil and foundation system underneath the bridge. The spring stiffnesses are estimated using approximate simplified methods of variable reliability. This approach captures the foundation flexibility effects and was used to conduct the comprehensive parametric study in this research. The inertial effects of the bridge in the soil-foundation system are not captured in this approach.

Foundation flexibility effects might increase displacement demands of piers. In this section models which incorporate these effects are considered by using springs at the base of the piers (Figure 3.23). The nonlinear models developed in the previous stage for Bridge Type 1 and Bridge Type 4 are adjusted to account for the effect of foundation flexibility in the displacement demands of piers.

The analysis is aimed to identify the role of the skew angle in the increment or reduction of soil-foundation-structure interaction effect (SFSI) on the displacements demands of the bridge. The result of the parametric study will primarily help to quantify the contribution of the rotation of the deck to the total lateral response of the pier under these conditions.

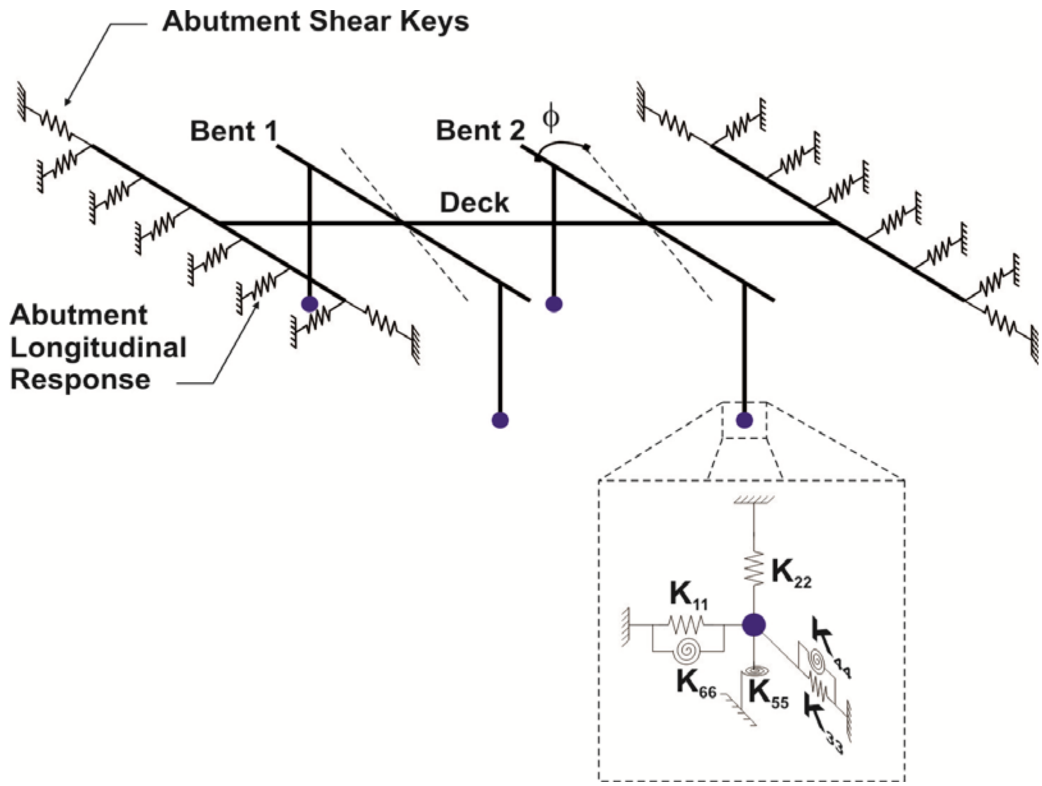

Figure 3.23 Bridge Type 1 – model for Soil-Foundation-Structure-Interaction effects

3.4.4.1 Description of the Foundation and Soil Profiles

Each pier is assumed to be supported on a 5×5 pile group of steel piles. The piles are 10m long and the outer diameter of each pile is 0.30 m with 2cm wall thickness. The piles are spaced at a center-to-center distance of three pile diameters (0.90 m). The pile cap is not embedded and located at ground level (Figure 3.24).

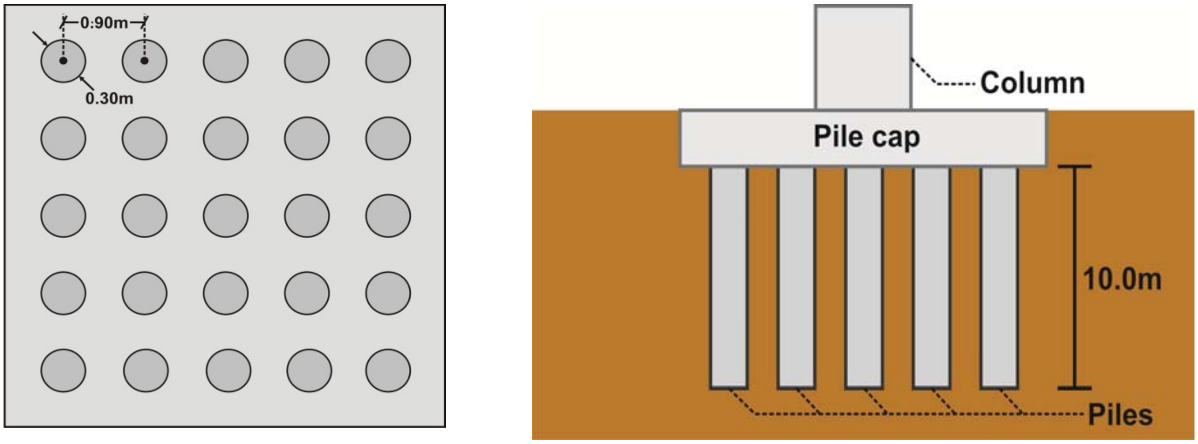

(a) Plan view **(b) Elevation**

Figure 3.24 Description of bridge foundation

The effects of foundation flexibility in the seismic demands of skewed bridges are investigated using different soil profiles. Christensen (2006) performed a full-scale lateral load test of a 3 x 3 pile group embedded in a realistic soil profile comprised by eight layers (Fayyazi et al., 2012). Christensen's soil profile is used here as reference deposit and to derive each of the four soil profiles used in this research. The uppermost four meters is replaced accordingly by a homogeneous layer of dense sand, medium sand, stiff clay, and soft clay (Figure 3.25). The substitution of the uppermost four meters is considered representative because soil-foundation interaction effects in piles mainly depend on the soil deposit in the upper 10 pile diameters (Lam and Martin, 1986), which in this case is 3 meters.

Figure 3.25 Soil deposits used to analyze the SFSI effects

3.4.4.2 Kinematic Pile Cap Stiffnesses

The pile cap stiffnesses were calculated using the substructure method, in which the pile group is analyzed separately from the bridge to obtain a 6×6 stiffness matrix that contains the effective stiffnesses of the pile group at the ground level of the foundation in the six degrees of freedom. This matrix is then replaced in the bridge model to carry on the seismic analysis. It is noted that this matrix is kinematic and only considers the foundation flexibility effects (massless soil-foundation system).

State of the practice substructure methods for SFSI effects on layered soil used by Caltrans (Shamsabadi, 2013) propose to perform a pushover to the pile group until reaching a target displacement. In this study the pushovers were performed by using the program GROUP (Reese et al., 2010), which uses a p-y curves approach and accounts for the nonlinear response of the soil deposit. A group factor effect of 0.42 was assigned based on the recommendations of

AASHTO (2012). The subgrade modules were obtained from the recommendations in FHWA (2006), values reported by Murchison and O'Neill (1984) were selected for sands and values by Lam et al., (1991) for clays. The strain at 50% stress level of clay (ε_{50}) was obtained from the recommendations by Reese et al. 2010, typical values of friction angle for sands were used. The input parameters used for the upper 4 meters of each soil deposit are summarized in Table 3.5.

Soil Deposit	Effective Unit Weight (kN/m^3)	Friction Angle (degrees)	Cohesion (KN/m^2)	Strain at 50% Stress Level, ε_{50}	Subgrade Modulus (KN/m^3)
1. Dense Sand	16.7	37	-	--	49928
2. Medium-Dense Sand	16.7	33	-	-	26351
3. Stiff Clay	16.7	-	70	0.005	6657
4. Submerged Soft Clay	9.1	-	20	0.02	2773

Table 3.5 Input soil properties for pile cap stiffnesses calculation

An uncoupled stiffness matrix was obtained by pushing independently in each degree of freedom. For instance, the longitudinal lateral stiffness (K_{11}) is given by the secant stiffness resulting from pushing the pile group horizontally in the longitudinal direction to a target displacement of 5 cm. This target displacement was selected as most of the AASTHO recommendations for piles group are based on experimental tests that target a similar displacement. In the vertical direction, the target displacement was defined assuming a settlement of 20 cm for the average bearing capacity; a similar procedure is used by Shamsabadi (2013). Judgment was exercised to define the target rotations for the flexural and torsional stiffnesses, the primary consideration was that bridges analyzed are modern short and medium span structures for which significant rocking at foundations is not the preferable performance expected by the Canadian Highway Code CAN/CSA-S6-06. In consequence a small target rotation of 0.0002 radians was used. The resulting pile cap stiffnesses in each direction are given in Table 3.6.

Soil Profile	Long. Lateral K_{11} (kN/m)	Vertical Axial K_{22} (kN/m)	Transverse Lateral K_{33} (kN/m^3)	Transverse Moment K_{44} (kN-m/rad)	Torsional Moment K_{55} (kN-m/rad)	Long Moment K_{66} (kN-m/rad)
1. Dense Sand	1.03E+05	6.10E+06	1.03E+05	4.00E+07	7.00E+07	4.00E+07
2. Medium-Dense Sand	9.00E+04	6.10E+06	9.00E+04	3.60E+07	2.45E+07	3.60E+07
3. Stiff Clay	8.00E+04	7.30E+06	8.00E+04	4.00E+07	4.00E+07	4.00E+07
4. Soft Clay (Submerged)	4.10E+04	7.00E+06	4.10E+04	4.00E+07	1.40E+07	4.00E+07

Table 3.6 Pile cap stiffnesses accounting for nonlinearity of soil deposit

3.4.4.3 Comparison to Pile Cap Stiffnesses Estimated Using Elastic Methods

The pile cap stiffnesses previously obtained accounting for a nonlinear response of the soil deposit are compared with those obtained assuming an elastic response of the deposit. The elastic approach produces a fully coupled 6×6 pile cap stiffness matrix. The stiffnesses of the pile group are calculated by multiplying the corresponding stiffness of a single pile by the number of piles and the group factor effect of 0.42 (AASHTO, 2012). The lateral, rotational and cross coupling terms for each pile are estimated using charts by Lam and Martin (1986). The additional contributions to the rotational and torsional stiffness from the bending actions among piles of the pile head forces are also considered. The terms of the coupled pile cap stiffness matrix for each soil deposit are given in

Table 3.7.

Each term of the coupled stiffness matrix was compared with its corresponding value obtained for the uncoupled stiffness matrix developed in the previous section. As the terms are bigger, this matrix represents a stiffer foundation condition than the obtained when the nonlinear response of the soil deposit was considered. As a result, the pile cap stiffnesses calculated considering a nonlinear response of the soil deposit are chosen to represent the soil-foundation system in the analysis undertaken.

Soil Profile	Long. Lateral K_{11} (kN/m)	Vertical Axial K_{22} (kN/m)	Transverse Lateral K_{33} (kN/m^3)	Transverse Moment K_{44} (kN-m/rad)	Torsional Moment K_{55} (kN-m/rad)	Long Moment K_{66} (kN-m/rad)	Cross Coupling K_{16},K_{34} (kN-m/rad)
1. Dense Sand	1.47E+06	9.43E+06	1.47E+06	5.44E+08	5.12E+07	5.44E+08	2.22E+06
2. Medium-Dense Sand	1.00E+06	9.43E+06	1.00E+06	4.79E+08	4.96E+07	4.79E+08	1.72E+06
3. Stiff Clay	4.39E+05	9.43E+06	4.39E+05	3.65E+08	4.78E+07	3.65E+08	9.91E+05
4. Soft Clay (Submerged)	2.60E+05	9.43E+06	2.60E+05	3.08E+08	4.72E+07	3.08E+08	6.98E+05

Table 3.7 Pile cap stiffnesses assuming elastic response of soil deposit

3.4.4.4 SFSI Effects in the In-plane Rotation of the Deck

The effect of SFSI in the in-plane rotation of the deck is investigated by comparing the results previously obtained in rigid base with the in-plane rotations obtained from flexible foundations.

The analyses for Bridge Type 1 on different soil deposits and for different abutment types show that effect of foundation flexibility in the in-plane rotations of the deck and subsequently the contribution to the total drift due to rotation is negligible regardless the skew angle (Figure 3.26).

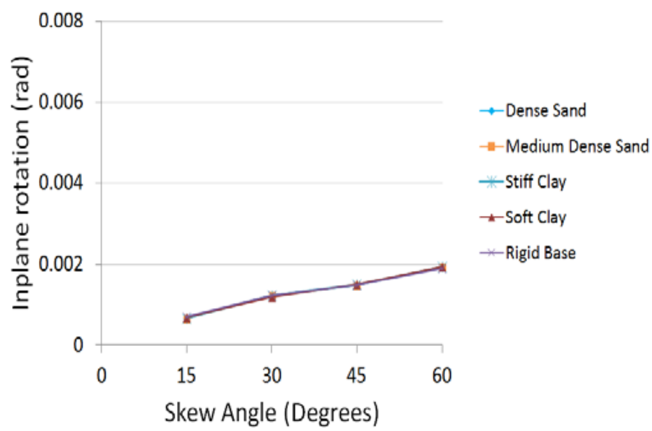

(a) Linear Abutments

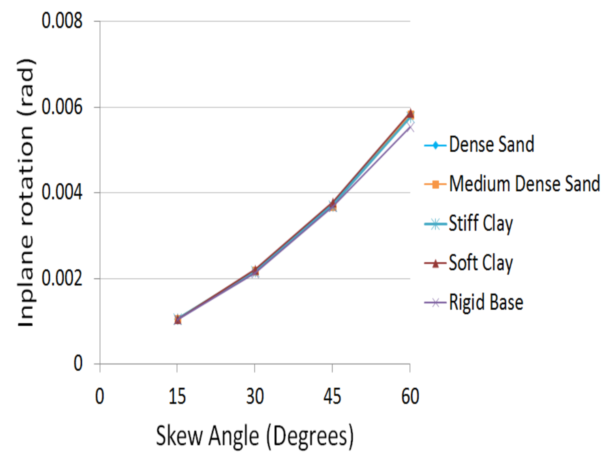

(b) Bilinear Abutments

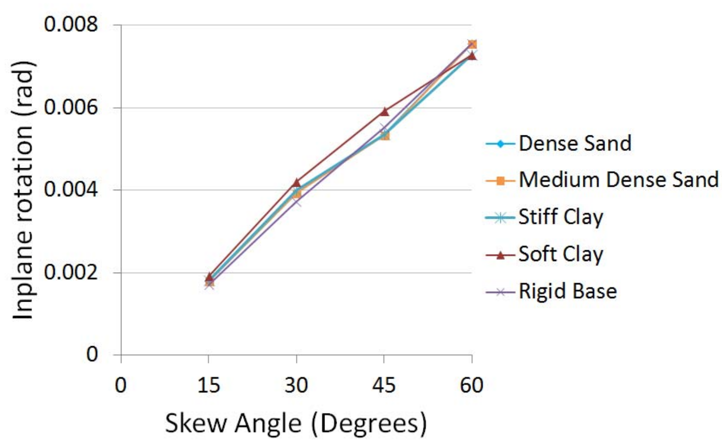

(c) Fusing Abutments

Figure 3.26 SFSI effects in the in-plane deck rotation for different soil deposits and abutments types

The negligible foundation flexibility effects can be explained by the low shifting of the bridge periods among the different foundation conditions. For example, for the Bridge Type 1 skewed at 45 degrees the transverse and the in-plane rotational period only changed from 1.03s and 0.74s on a rigid base condition to 1.12s and 0.75s on a submerged soft clay deposit. This means that the softest soil deposit only produces a shift of 8% in the transverse period of bridge and less than 2% in the in-plane rotational period. Similar trends are observed for the analysis conducted on Bridge Type 4.

Finn (2005) investigated the changes in the structural period as a tool to evaluate the impact of soil foundation flexibility effects on the seismic response of bridges. The study concluded that period shifting depends on the relation between the foundation stiffness (K_L^F) and the bridge stiffness on rigid base (K_P^S). Finn conducted a parametric study on a two-span bridge to define the relation of period shift and the relative bridge to bridge foundation stiffness (K_P^S / K_L^F). The study evaluated the period shift for the first mode of vibration and was run for different pile groups and soil deposits. The results of the study are shown in Figure 3.27, which relates the bridge to bridge foundation stiffness ratio (K_P^S / K_L^F) to a non-dimensional period ratio (T_P/T_F) where T_P is the period of the bridge on rigid base and T_F is the period of the bridge on a flexible base.

The transverse stiffness of Bridge Type 1 on rigid base (K_P^S) is 8466 KN/m and the stiffness of the foundation for soft clays (K_L^F) is 1040 x 10^3 KN/m, then the ratio K_P^S / K_L^F is 8.14x10^{-3} which using Figure 3.27 leads to a non-dimensional period ratio (T_P/T_F) of 0.93. This 7%

difference predicted by Finn's approach is in good agreement with the period shifting observed during the analysis and the subsequent negligible foundation flexibility effects.

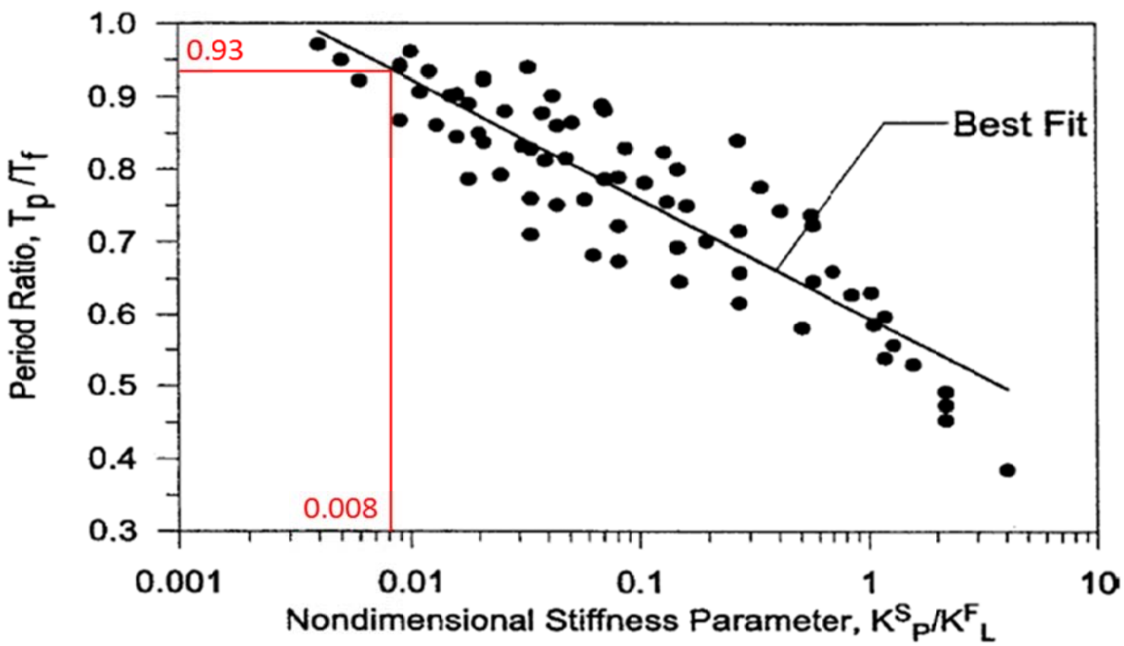

Figure 3.27 Period shift for bridge-foundation system (adopted from Finn, 2005).

3.5 Discussion

The displacement demands for skewed bridges with different abutment types subjected to a suite of input ground motions were calculated. The analyses provide an illustration of the amplification of the pier drift due to deck rotation as a function of the skew angle and the structural response of each abutment type. The analyses demonstrate that the additional drifts due to deck rotation increase in linear proportion with the skew angle. The results also indicate that the type of abutment (linear, bilinear or fusing) has a strong influence on the displacements demands of the bridge and suggest that the structural response of skewed bridges in seismic regulations should be discussed separately for each type of abutment.

The analyses of the total pier drift for bridges with linear abutments and longitudinal gap show that the contribution of the in-plane rotations becomes significant (>20 %) for skewed angles greater than 35 degrees, whereas for bilinear and fusing abutments the contribution is significant (>20 %) regardless of the skew angle. The peak drift at piers was conservatively estimated by the absolute combination of the peak drift due to the translation of the deck obtained from linear elastic analysis and the peak drift due to in-plane rotation of the deck obtained from nonlinear analysis.

The sensitivity analysis for the foundation properties used in this research showed that the foundation flexibility effects in the in-plane rotation of the deck due to seismic induced pounding are negligible for all the abutment types and skew angles considered.

Chapter 4: PROPOSED METHOD TO EVALUATE THE DISPLACEMENT DEMANDS

4.1 Introduction

Linear multimodal spectral or linear time history analyses are widely used in standard engineering practice to calculate the displacement demands on skewed bridges. These linear elastic procedures have been endorsed by most seismic provisions including AASTHO (2011) and the Canadian Highway Bridge Code, CAN/CSA-S6-06 (CHBDC). In view of the limitations of the linear elastic analysis with respect to the evaluation of the seismic effects on bridges with expansion joints, AASTHO (2011) states that: "*Two global dynamic analyses should be developed to approximate the nonlinear response of a bridge with expansion joint because it possesses different properties characteristics in tension and compression*" (Clause 5.1.2). The two bounding models suggested by AASTHO are: the tension model, in which the superstructure is free to move at both ends; and the compression model, in which both ends are restrained by linear springs to simulate the effects when the gap is closed. However, in the case of skewed bridges neither of these two models can properly capture the in-plane rotation of the deck due to the pounding between the superstructure and the abutments. This in-plane rotation of the deck can significantly increase the lateral displacement of the piers as demonstrated by this research and the work of others (Shamsabadi 2007, Tirasti and Kawashima 2008, Kavianijopari 2011). The challenge that designers face to estimate these demands in skewed bridges is further complicated by the fact that the demands not only depend on the skew angle, but also the dimensions and dynamic properties of the bridge, the abutment type, and the size of the gap at expansion joints.

A new method is proposed in this section to estimate the peak drift of the piers. The method uses the results of validated simplified nonlinear models to generate torsional sensitivity charts for selected bridge prototypes. The torsional sensitivity charts are then used to calculate the drift due to deck rotation. The total drift of the pier is estimated by superimposing the drift due to deck rotation on to the drift due to deck translation, which is obtained by using the traditional linear elastic analysis. An advantage of this approach is that it does not require the designer to run a nonlinear time history analysis, but instead the total pier drift is estimated by the simple superposition rule.

The method is intended to the abutment's structural response expected by the Ministry of Transportation and Infrastructure of British Columbia (BCMoT) in which the abutment-backfill and the abutment shear keys are expected to respond elastically for low seismic demands, whereas for higher demands the abutment-backfill is expected to reach its capacity throughout the earthquake. This structural response corresponds to the so-called bilinear abutments in this research.

4.2 Proposed Simplified Nonlinear Model

Typical nonlinear models are usually computationally expensive and are not often used in practical design. Here, a generalized 3-DOF simplified nonlinear model is proposed to calculate the in-plane rotations of skewed bridge decks. Unlike the detailed nonlinear model previously discussed in chapter 3, in the simplified nonlinear model the deck is represented by a rigid bar and the contribution of the columns and shear keys is included by static condensation and is represented by linear springs at the center of stiffness in the longitudinal, transverse and rotational directions (Figure 4.1). In a similar fashion to the detailed model, the abutment backfill and the two-inch [5cm] expansion joints are represented by a set of nonlinear springs oriented perpendicular to the skew angle. The formulation of this model considers only the mass of the superstructure (deck + cap beams) and a damping ratio of 5%.

This simplified nonlinear model is primarily conceived for the prediction, and parametric study, of the in-plane rotations of continuous multi-span skewed bridges with different pier dimensions and boundary conditions. This model also helps to study the effects in the in-plane rotations of different levels of lateral restraint given by abutment shear keys with different stiffnesses.

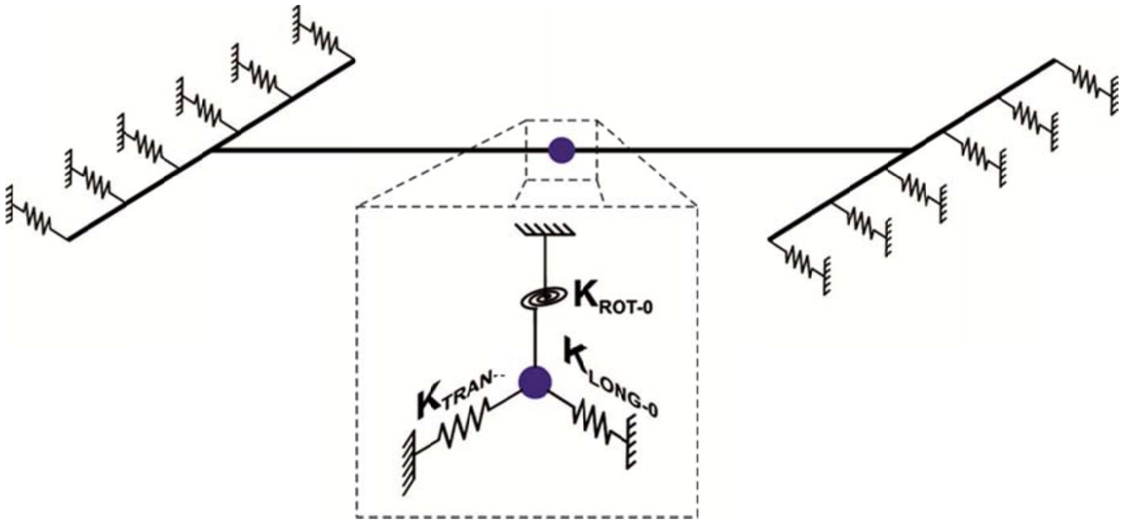

Figure 4.1 Simplified nonlinear model

The expressions to calculate the static condensation are given in Equations 4-1 to 4-3:

$$\boldsymbol{K_{LONG-O} = N_c \times k_{colx}} \tag{4-1}$$

$$\boldsymbol{K_{TRAN} = N_c \times k_{coly} + N_c \times \left({k_{sh}}/{2}\right)} \tag{4-2}$$

$$\boldsymbol{K_{ROT-O} = k_{colx} \times bb^2 + k_{coly} \times dd^2 + 2 \times k_{sh-eff} \times \left(\frac{L}{2}\right)^2 \times cos^2(\phi)} \tag{4-3}$$

where,

$K_{LONG\text{-}O}$: Stiffness at the center of mass in the longitudinal direction due to columns contribution (longitudinal stiffness of the bridge when the gap at expansion joints is open) .

K_{TRAN}: Stiffness at the center of mass in the transverse direction due to columns and shear keys contributions.

$K_{ROT\text{-}O}$: Rotational stiffness at the center of mass due to columns contribution and shear keys contribution (in-plane rotational stiffness of the bridge when the longitudinal gap at expansion joints is open).

k_{colx}, k_{coly}: Pier stiffness in the transverse and longitudinal directions.

$k_{sh\text{-}eff}$: Effective abutment shear key stiffness.

dd, bb: Distance between columns in X and Y directions.

L: Total span.

ϕ: Skew angle.

N_C: Number of piers in the bridge

4.3 Simplified Nonlinear Model Validation

Simplified nonlinear models of Bridge Type 1 and 4, with bilinear abutments and skewed at different angles are developed, in order to evaluate the accuracy of the estimate of the deck in-plane rotation predicted by the simplified nonlinear model. The models are developed using the computer program SAP 2000 and were subjected to the ground motions suite considered in this research.

Figure 4.2 compares the peak in-plane rotations estimated by using the simplified nonlinear model with respect to the peak in-plane rotations obtained by the detailed nonlinear models used in Chapter 3. It is observed that for the three-span structure (Bridge Type 1) the peak in-plane rotations predicted by the simplified nonlinear model are in good agreement with the predictions of the detailed nonlinear model for the different skew angles studied.

For the two-span structure (Bridge Type 4) the largest difference in the peak in-plane rotation predicted by the simplified and detailed models is 16 %. This difference is only observed for the structure skewed at 45 degrees (Figure 4.2 b). The results of the comparison undertaken indicate that the simplified nonlinear model provides realistic predictions of the in-plane rotation of the deck.

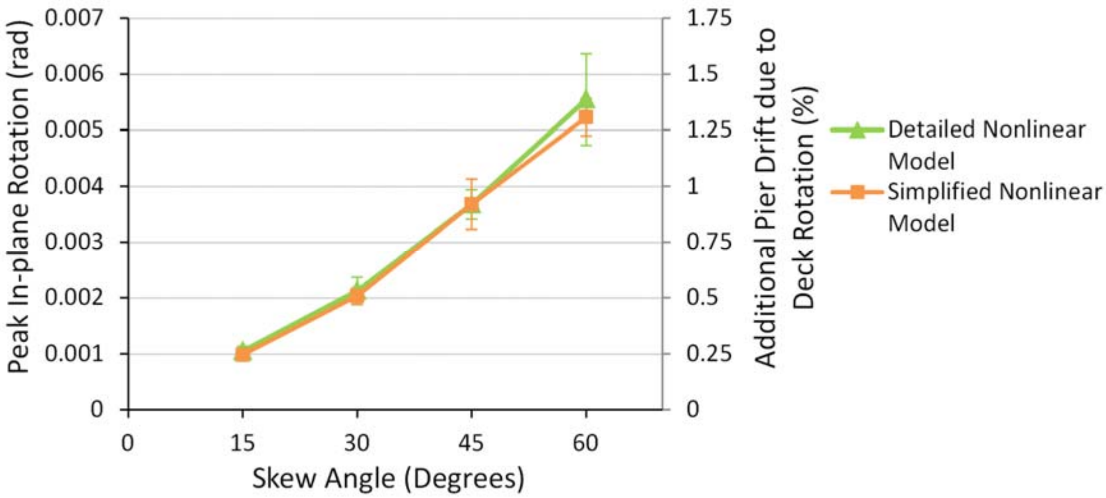

(a) Bridge Type 1 (three-span structure)

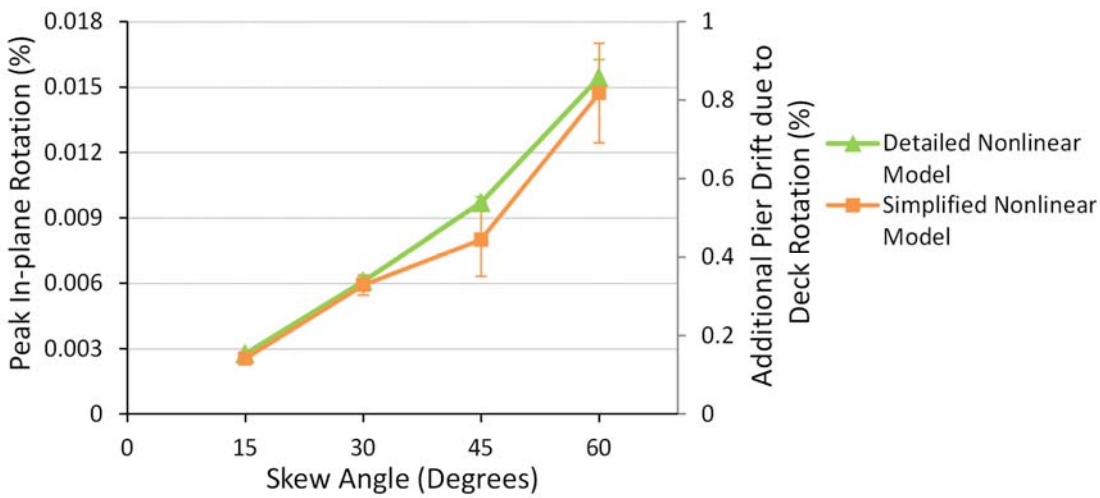

(b) Bridge Type 4 (two-span structure)

Figure 4.2 Validation of the simplified nonlinear model

4.4 Torsional Sensitivity

The in-plane rotation of the deck is the critical parameter to be calculated in order to estimate the additional drift of the piers. The magnitude of the in-plane rotation and the sensitivity of the bridge to rotate depend on a number of parameters, namely: the skew angle, the dimension of the bridge, the distance between piers, the stiffness of the abutment shear keys and the abutment backfill, as well as whether the connection of the pier to the superstructure is rigid or pinned. The in-plane rotational period of the bridge is proposed in this thesis as the property that can capture all these parameters at once (Equation 4-4).

$$\boldsymbol{T_{rot-o} = 2\pi\sqrt{\frac{I_o}{K_{ROT-O}}}} \tag{4-4}$$

Where:

T_{rot-o} : In-plane rotational period with longitudinal gap open

I_o : Mass moment of inertia of superstructure.

$$K_{ROT-O} = k_{colx} * bb^2 + k_{coly} * dd^2 + 2 * k_{sh-eff} * \left(\frac{L}{2}\right)^2 * cos^2(\phi)$$

(In-plane rotational stiffness with the longitudinal gap at expansion joints open)

The in-plane rotational period is used to examine the rotation of the deck in a wider range of bridges. For this, height and diameter of the piers of Bridge Type 1 and 4 are varied to generate structures with different in-plane torsional periods. The variations aim to be consistent with practical dimensions of piers of short and medium multi-span bridges. The height varied from 5 to 23 m and the diameter from 1.2 to 3 m. The bridges are then represented with simplified nonlinear models and analyzed for the different skew angles and input ground motions considered in this research. The results are summarized in the torsional sensitivity charts, which provide the in-plane rotation of the deck as a function of the skew angle and the in-plane rotational period of the bridge, with the longitudinal gap open (Figure 4.3). For convenience, the chart is presented as function of the in-plane rotational period of the bridge with the longitudinal gap open (T_{rot-o}) because it represents the rotational period of the structure when the abutment backwalls are not engaged, which is easier to calculate for designers and is usually the rotational period identified during ambient vibration tests on seat type abutment bridges.

4.4.1 Torsional Sensitivity Charts for Bridges with Piers Monolithically Connected to the Superstructure

Figure 4.3 shows the torsional sensitivity chart for three-span bridges with piers monolithically connected to the superstructure. It is noted that the onset of in-plane rotations occurs at a specific rotational period that varies according to the skew angle. For instance, for bridges skewed at 60 degrees, the in-plane rotation is triggered when the rotational period is greater than approximately 1.16 seconds. There is an upper limit in the rotational period that can be reached in a bridge with bilinear abutments, which is defined by the contribution to the rotational stiffness of the abutment shear keys that remain elastic throughout the earthquake. The chart illustrates that for three-span skewed bridges similar to Bridge Type 1, subjected to the seismicity of British Columbia and bilinear abutments, the maximum in-plane rotation of the deck around the center of stiffness is approximately 0.007 radians (0.40 degrees). Based on the reference of Bridge Type 4 the torsional sensitivity charts were also developed for two-span bridges (Figure 4.4). In this case, the maximum in-plane rotation observed was 0.018 rad (1.03 degrees).

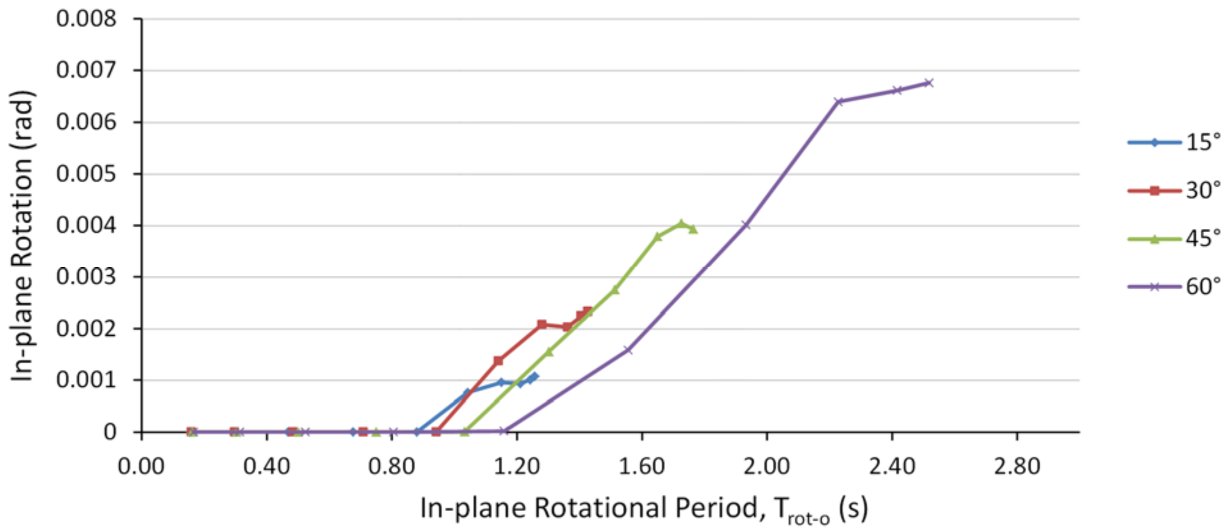

Figure 4.3 Torsional sensitivity chart for three-span skewed bridges with piers monolithically connected to the superstructure

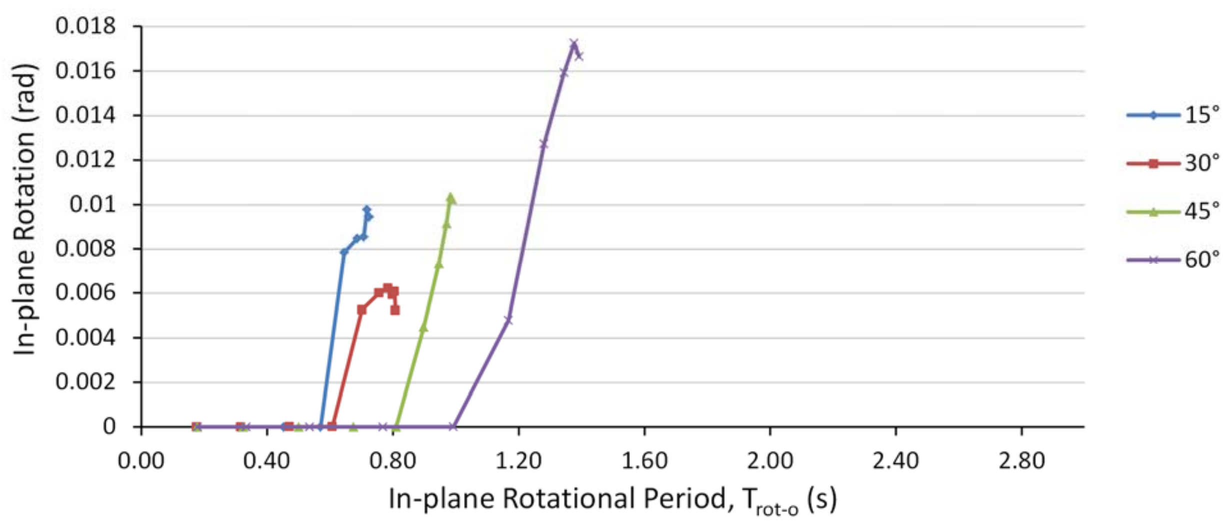

Figure 4.4 Torsional sensitivity chart for two-span skewed bridges with piers monolithically connected to the superstructure

4.4.2 Torsional Sensitivity Charts for Bridges with Piers Pinned Connected to the Superstructure

The analyses were extended to generate torsional sensitivity charts for two- and three-span skewed bridges with the piers pinned connected to the superstructure (Figure 4.5 and 4.6). The chart indicates that as a result of this increment in the longitudinal flexibility the onset of in-plane rotations occurs at a shorter rotational period than in bridges with the piers rigidly connected to the superstructure. For instance, in three-span bridges skewed at 60 degrees, the rotation is now triggered at a rotational period of 0.43 seconds instead of 1.16 seconds as it was for bridges with piers rigidly connected to the superstructure. However, the maximum in-plane rotation remains below 0.007 rad (0.40 degrees).

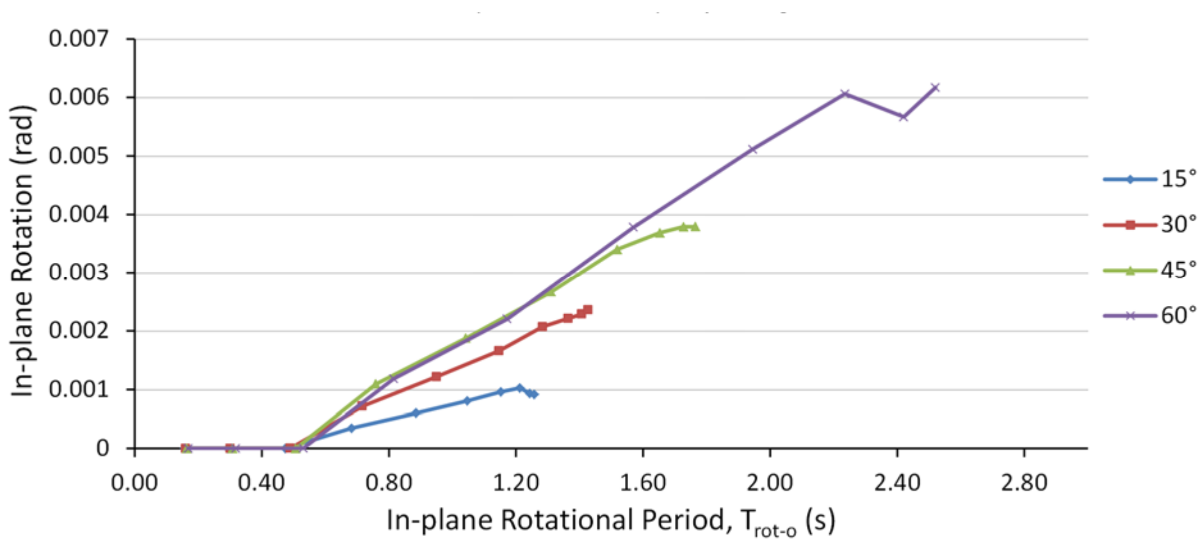

Figure 4.5 Torsional sensitivity chart for three-span skewed bridges with piers pinned connected to the superstructure

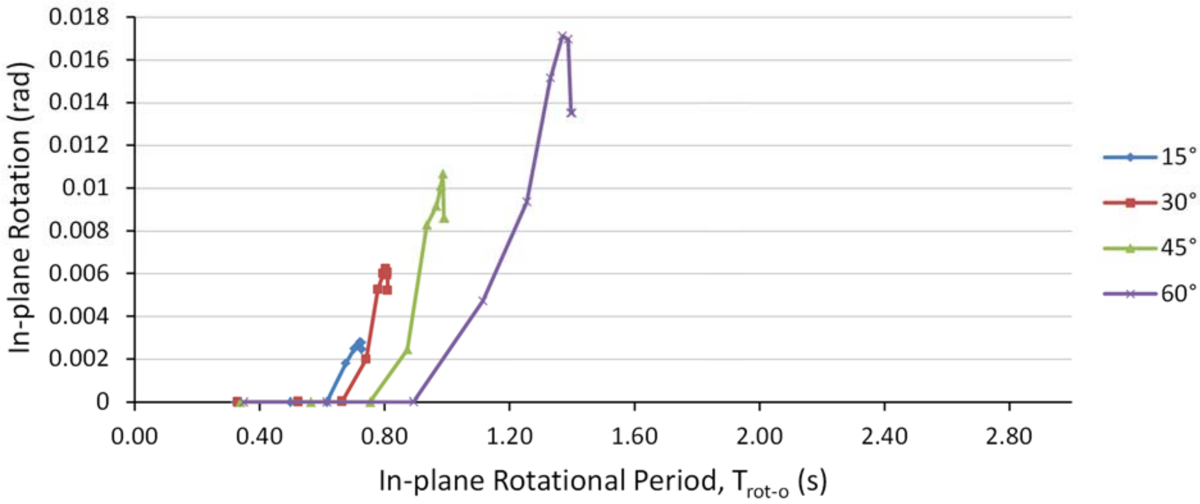

Figure 4.6 Torsional sensitivity chart for two-span skewed bridges with piers pinned connected to the superstructure

4.4.3 Effect of Different Levels of Lateral Restraint

The stiffness of the abutment shear keys used in this research was characterized based on the large-scaled monotonic and cyclic test conducted by Silva et al. (2009). There is limited experimental data of abutment shear keys testing and the results of Silva's experiments have also been used by others researches to characterize the stiffness of the abutment shear keys (Shamsabadi 2007; Kavianijopari 2011). However, these experiments were conducted for external shear keys designed according to the California's construction practice and for bridges of specific width.

A sensitivity study is conducted to understand the effect of the abutment shear keys stiffness in the in-plane rotation of the bridge deck. The different levels of lateral restraint are obtained by changing the abutment shear keys stiffness in the simplified nonlinear model of the three-span structures. Two cases were explored, one reducing to half the shear keys stiffness obtained from Silva's experiments (standard lateral restraint) and the other doubling it.

Figure 4.7 shows the changes in the torsional sensitivity curve of a three-span structure skewed at 45 degrees and with piers monolithically connected to the superstructure. The increased lateral restraint reduced by 40% the maximum in-plane rotation obtained using the standard lateral restraint, as well as reduced the in-plane rotational period of the structure. On the other hand, a reduction in the lateral restraint produces an increment of 52% in the in-plane rotation obtained with the standard lateral restraint and increases the in-plane rotational period of the structure. The analyses were extended to the others skew angle considered in this research and similar results were observed (Figure 4.8).

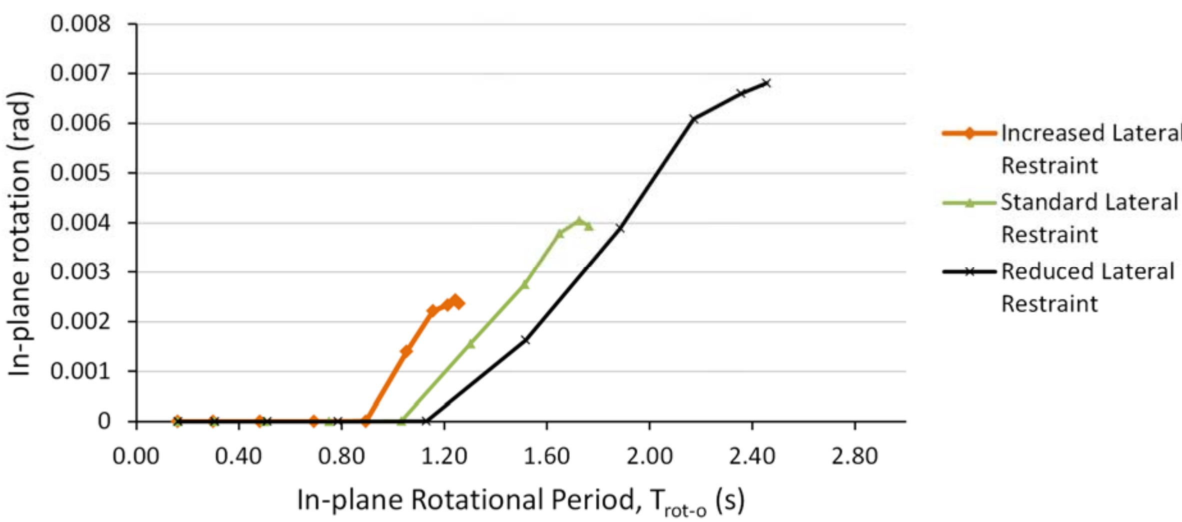

Figure 4.7 Effect of shear keys lateral restraint in the torsional sensitivity curve of three-span bridges skewed at 45 degrees with piers monolithically connected to the superstructure

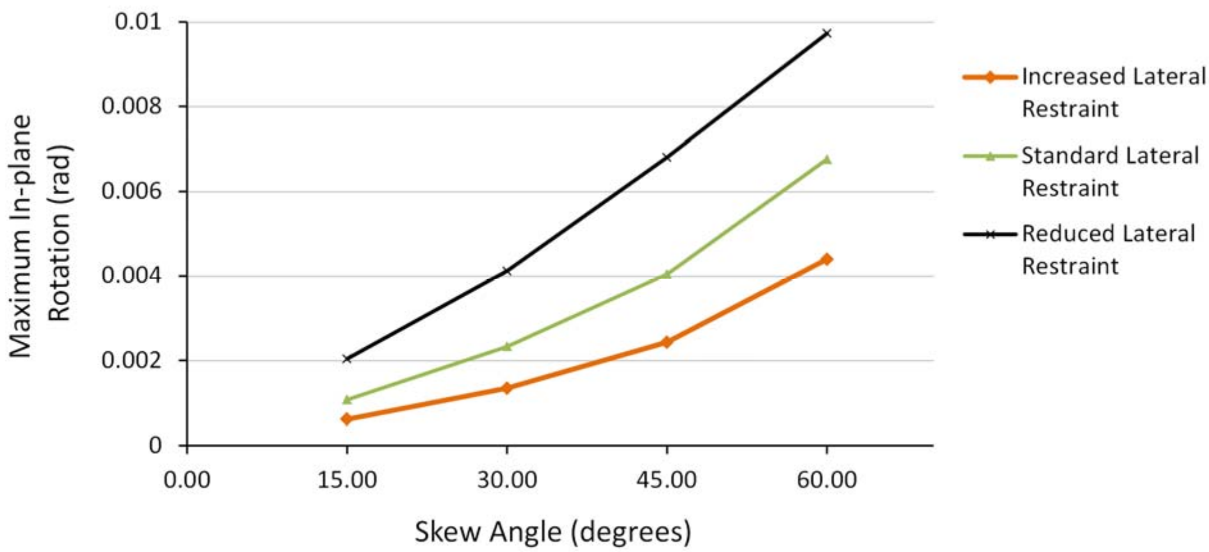

Figure 4.8 Effect of shear keys lateral restraint in three-span structures skewed at different angles

4.4.4 Considerations in Areas with Low Seismicity

The torsional sensitivity charts presented correspond to regions of high seismic hazard such as the cities of Vancouver (PGA=0.48g) and Victoria in British Columbia (PGA=0.55g), Canada. Bridges located in areas of low seismic hazard are expected to have smaller in-plane rotations than those predicted by the given charts. To quantify this reduction, the simplified nonlinear models for the three-span structures skewed at 60 degrees were subjected to the suite of grounds motion used in this research but scaled to the 2% risk of exceedance in 50 years Uniform Hazard Spectrum (UHS) for the City of Kelowna in British Columbia. The seismic hazard in the City of Kelowna is considered low (PGA=0.14g). The results show a reduction of 40% in the maximum in-plane rotation that was predicted for areas of high seismicity (Figure 4.9).

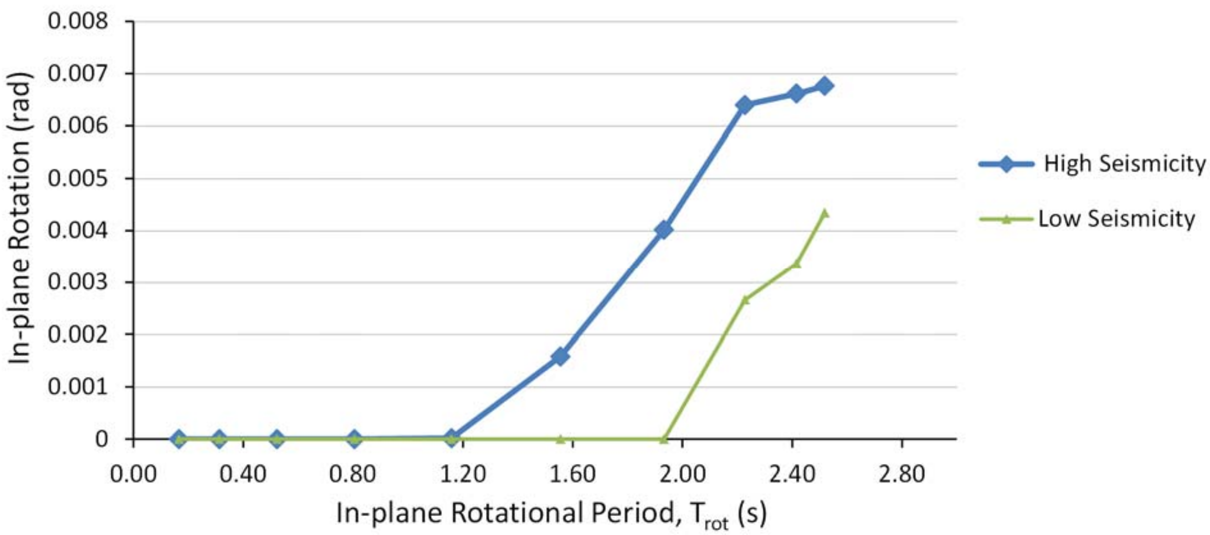

Figure 4.9 Reduction of in-plane rotation in areas of low seismicity (three-span structures skewed at 60 degrees with piers monolithically connected to superstructure)

4.5 Proposed Procedure for Calculating the Total Pier Drift

A simplified procedure to estimate the total pier drift of skewed bridges is described in the following paragraphs. The description is followed by an example that illustrates the application of the procedure. The proposed procedure requires the use of results from the traditional linear elastic model of the bridge, and the torsional sensitivity charts.

Step 1. Calculate Longitudinal and In-plane Rotational Period of the Bridge with the Gap at Expansion Joints Open:

The longitudinal period of the bridge with the gap at expansion joints open can be obtained by equation 4-5. The expression to obtain the in-plane rotational period was given in equation 4-4.

$$T_{long-o} = 2\pi\sqrt{\frac{m}{K_{LONG-O}}} \quad (4\text{-}5)$$

Where:

T_{long-o}: Longitudinal period of the bridge with the gap at expansion joints open

m : Mass of superstructure

$K_{LONG-O} = N_c * k_{coly}$, Longitudinal stiffness of the bridge when the gap at expansion joints is open (N_c: number of piers, K_{coly}: pier stiffness in the longitudinal direction)

Step 2. Check for the Occurrence of Pounding by Using a Prescribed Displacement Response Spectrum

Pounding between the deck and the abutments is a condition required to trigger the in-plane rotation of the superstructure. Modeling the longitudinal direction as a SDOF system, the spectral displacement at the longitudinal period of the bridge is compared to the size of the gap to check if the gap is exceeded and the pounding is triggered. To have a consistent hazard, a prescribed displacement spectrum is derived from the 2005 Uniform Hazard Spectrum (UHS) for Vancouver with 2% risk of exceedance in 50 years.

If the gap is not exceeded the bridge can be analyzed by linear elastic methods noting that the critical longitudinal and transverse displacements occur in the directions of the predominant response. This is, in the azimuth of the skew and perpendicular to the skew.

Step 3. Estimate Peak In-plane Rotation of the Deck (θ)

The peak in-plane rotation of the deck can be estimated by using the torsional sensitivity charts reading the in-plane rotation at the corresponding in-plane rotational period, or by developing a simplified nonlinear model following the recommendations of section 4.2.

Step 4. Obtain Peak Drift due to In-plane Rotation (Δ_{rot})

The peak drift due to in-plane rotation is estimated by equation 4-6.

$$\Delta_{rot} = \frac{\theta * L_C}{H} \tag{4-6}$$

Where:

Δ_{rot} : Peak drift due to in-plane rotation.

θ: Peak in-plane rotation of the deck.

L_c: Maximum Horizontal distance from the pier to center of stiffness.

H: Height of the Pier.

Step 5. Obtain Peak Drift due to lateral Translation of the Deck (Δ_{trans})

The peak response due to lateral translation of the deck is obtained from linear elastic analysis, whether multimodal spectral analysis or linear time history, of the bridge with the gap closed. This is convenient as it is the traditional approach used by designers to obtain the lateral drift.

Step 6. Obtain Total Drift

The total drift is obtained as the absolute combination of the peak drift due to in-plane rotation of the deck (Δ_{rot}) and the peak drift due to lateral translation of deck (Δ_{trans}).

4.5.1 Example

To illustrate its application the proposed procedure is applied to Bridge Type 1 skewed at 45 degrees. The steps are described below.

1. Periods with gap open: Longitudinal Period, T_{long-o} = 2.25 seconds

   In-plane Rotational Period, T_{rot-o} = 1.56 seconds.

2. Check for the occurrence of pounding:

   For S_D (2.25 s) = 15.3 cm > Gap= 5 cm, pounding will occur (Figure 4.10).

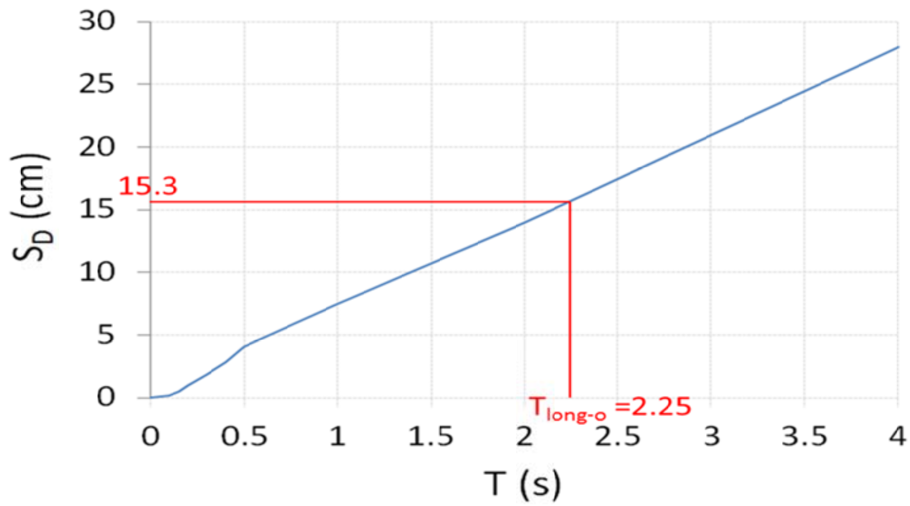

Figure 4.10 Estimation of longitudinal displacement using Vancouver displacement spectrum (derived from Vancouver UHS, 2% in 50 years).

3. Peak In-plane Rotation of Deck *(θ)*:

For T_{rot-o} = 1.56 seconds $\rightarrow$ Peak In-plane Rotation θ = 0.0029 rad (Figure 4.11)

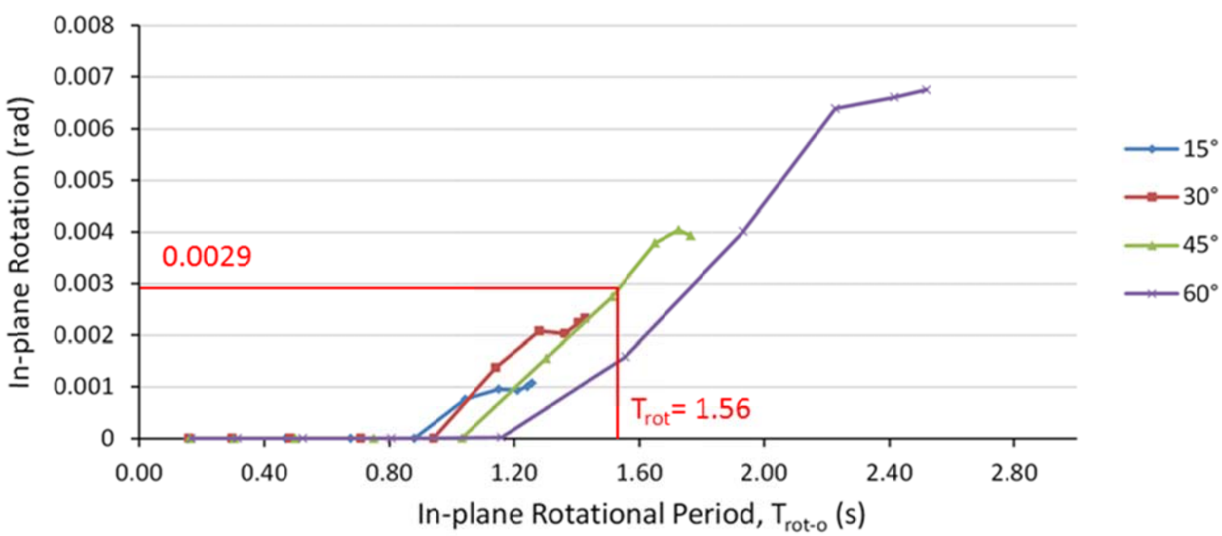

Figure 4.11 Estimation of peak in-plane rotation using torsional sensitivity chart for three-span bridges with piers monolithically connected to the superstructure.

4. Peak Drift due to In-plane Rotation *(Δ_{rot})* :

Given L_c= 25 m , H= 10 m, θ= 0.0029 rad $\rightarrow \Delta_{rot} = \frac{\theta * L_C}{H}$

$\rightarrow \Delta_{rot} = \frac{0.0029*25}{10}$

$\rightarrow \Delta_{rot} = 0.0072 = 0.72\ \%$

5. Peak Drift due to lateral Translation of the Deck *(Δ_{trans})*

From the results of a multimodal spectral analysis $\rightarrow$ Δ_{trans} = 0.71 %

6. Total Pier Drift

$\Delta_{Total} = \Delta_{trans} + \Delta_{rot}$ = 0.71 % + 0.72 % = 1.43 %

In Figure 4.12, the total pier drift (1.43%) calculated in this example is plotted against the results from the nonlinear time history analysis obtained in Chapter 3. The plot shows that for this example the difference with the results from the total pier drift from the nonlinear analysis (1.50%) was equal to a 5% difference,

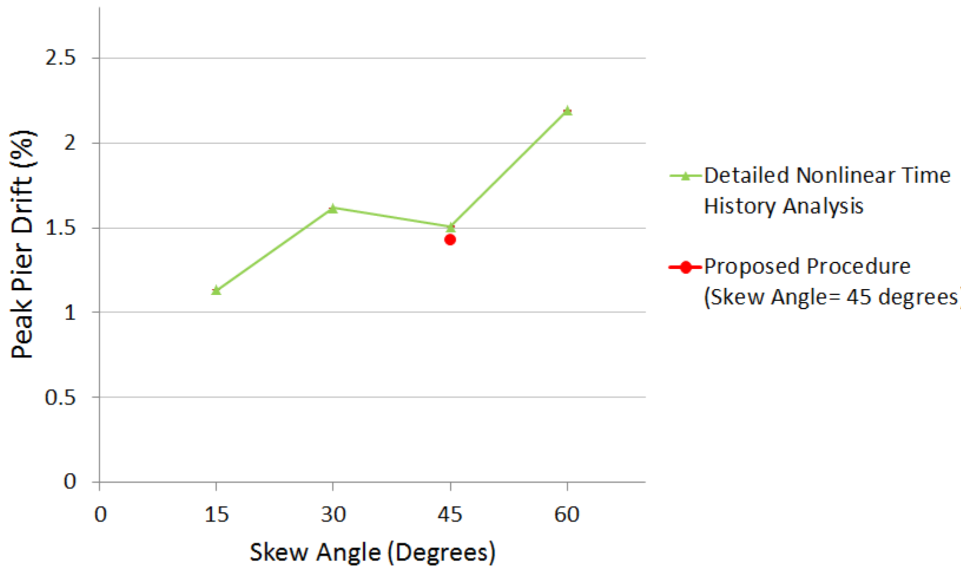

Figure 4.12 Total pier drift obtained with the proposed procedure for Bridge Type 1 (skewed at 45 degrees-bilinear abutments) compared to total drift obtained from the detailed nonlinear time history analysis.

4.6 Considerations about the Minimum Skew Angle to Call for Dynamic Analysis

As it has been previously discussed AASTHO (2011) recommends the use of multimodal spectral analysis for the calculation of the displacement demands of skewed bridges. In addition, AASTHO (2011) states that: *"Two dimensional models are adequate for bridges with a skew angle less than 30°"* (Commentary Clause C5.1.2). This clause suggests that multi-span bridges with a skew angle less than 30 degrees can be analyzed as non-skewed bridges ignoring the torsional effects of the in-plane rotation of the deck. A similar clause is adopted by other codes to simplify the analysis of skewed bridges. However, this research has demonstrated that the rotation of the deck strongly depends on the structural response of the abutment and additional pier drift due to in-plane rotations up to 0.5 % could be observed in bridges with fusing abutments with skew angles as low as 15 degrees. This research has also demonstrated that it might not be conservative to always use multimodal spectral analysis as it cannot capture in-plane rotation of the superstructure due to seismically induced pounding.

In view of the interest of the Ministry of Transportation of British Columbia and based on the results of this research, it is recommended to ignore the effects of the in-plane rotation due to seismically induced pounding for bridges with skew angle less than 20 degrees and abutments that reach their capacity in the longitudinal direction but remain elastic in the transverse direction (bilinear abutments). For abutments that respond elastically (linear abutments with a gap in the longitudinal direction) the limit in the skew angle can be increased to 30 degrees. It is noted that in the cases covered by the previous criteria drifts of up to 20 % induced by the deck rotation are being ignored.

When the in-plane rotations due to seismically induced pounding are ignored, the analysis can be performed by multimodal spectral analysis or by using two dimensional models. However, when a two dimensional model is utilized, the displacement demands should be obtained in the azimuth of the skew bent and perpendicular to this direction.

Chapter 5: CONCLUSIONS AND FUTURE WORK

A comprehensive damage survey of the performance of skewed bridges during past earthquakes demonstrated that medium and short multi-span skewed bridges with seat type abutments had suffered more damage than their non-skewed pairs. Primary damage generally occurs in the piers and has been associated with additional drift from in-plane rotation of the superstructure induced by pounding between the deck and its abutments. This type of rotation in skewed bridges was confirmed by analysis of strong motion records from the instrumented Second Northern Freeway (TCUBAB) in Taiwan.

Displacement-based design provisions, such as AASTHO (2011), require an accurate assessment of the displacement demands that bridges will be subjected to during earthquake shaking. AASTHO recommends two bounding models to calculate the demands using linear time history or multimodal spectral analysis, termed tension and compression models, respectively. In the tension model, the gap at expansion joints is considered open, whereas in the compression model, the gap is considered closed. This thesis demonstrated that in the case of skewed bridges the two types of models recommended by AASTHO, which are adapted by other seismic bridge provisions and widely used in standard engineering practice, do not properly capture in-plane rotations of the deck that might occur in skewed bridges with seat type abutment due to seismically induced pounding. This thesis proposed an alternative method to calculate the peak displacement demand of the piers accounting for the contribution to the displacement due to in-plane rotation of the deck.

The method proposed here used validated simplified nonlinear models to generate torsional sensitivity charts for specific bridge prototypes that provide the peak in-plane rotation of the deck as a function of skew angle and in-plane rotational period of the bridge. The peak in-plane rotation of the deck is used to estimate the drift due to deck rotation. On the other hand, the drift due to lateral translation of the deck is calculated from linear elastic analysis with a closed longitudinal gap. The total drift of the pier is estimated by the absolute combination of the peak drifts due to deck rotation and translation. An advantage of the proposed approach is that it only requires the designer to run traditional linear dynamic analysis. The nonlinear analysis required to assess the in-plane rotation of the deck is replaced by the torsional sensitivity charts.

This thesis demonstrated that the contribution of the in-plane deck rotation to the total drift of the pier strongly depends on the Embankment-Abutment-Structure Interaction (EASI) effects and the structural response expected at abutments by the approach used to design the bridge. The largest contribution (up to 2%) to the total drift from the in-plane deck rotation was obtained here for bridges with abutment shear keys expected to fuse due to brittle failure during the ground motion. The lowest contribution was obtained for bridges with abutments that are expected to remain elastic throughout the earthquake. These results suggest that the structural response of skewed bridges in seismic regulations should be discussed separately for each type of abutment response (elastic, elasto-plastic, and fusing).

For bridges with abutments that have an elasto-plastic response, such as those intended by the Ministry of Transportation and Infrastructure of British Columbia, and have a skew angle less than 20 degrees, the in-plane rotation effects may be effectively ignored; for abutments that respond elastically, the skew angle limit may be increased to 30 degrees. The total demand may be estimated by multimodal spectral analysis or by using two-dimensional (2D) models. However, when a 2D model is used, the displacement demands should be calculated in the predominant direction of response. This directionality in the lateral response of skewed bridges with seat type abutments was illustrated from ambient vibration tests and analysis of acceleration records from an instrumented bridge, in which the predominant direction of the transverse mode occurs in the azimuth of the skew bents, whereas the predominant direction of the longitudinal mode is perpendicular to the azimuth of the skew. This result provides experimental support for the recommendations to define the direction of the maximum displacement demands in skewed bridges.

This thesis also investigated conditions that trigger rotation of the superstructure. The bridge in-plane rotational period that onset the in-plane rotation of the deck was calculated via nonlinear dynamic analysis for different bridge prototypes as a function of skew angle. The analyses showed that in-plane rotation of the superstructure is only triggered when the longitudinal gap is exceeded. This observation implies that simply because a bridge is skewed, does mean that it is necessarily going to be torsionally activated. The analyses also showed that torsional activation depends on the size of the gap and whether or not it is closed.

In summary, this thesis contributes to the understanding of displacement demands on skewed bridges with seat type abutments and enhances the recommendations for performance based design of skewed bridges. The contribution of in-plane rotations to the total pier drift considering abutments with different structural response was explained in detail. The effect of Soil-Foundation-Structure interaction, the mechanism that triggers the deck rotation and directionality in the lateral response, were also investigated. A simplified method to estimate the total drift accounting for in-plane deck rotation contribution was proposed to provide the designer with a simple but complete approach for the assessment of the displacement demand of skewed piers.

5.1 Future Work

The scope of this research was limited to the response of symmetric skewed bridges with seat type abutments and continuous superstructure. Further studies are recommended to study the response of:

- ✓ Skewed bridges with seat type or integral abutments with discontinuous superstructure. This study will be relevant for existing bridges that generally have intermediate expansion joints in which pounding between adjacent superstructures may occur.

- ✓ Skewed bridges with seat type abutment with irregularities that cause eccentricities between the center of mass of the deck and the center of resistance of the lateral resistance system. Typical irregularities that can be investigated are different pier heights, unsymmetrical boundary conditions, and unequal skew angles.

In addition, the torsional sensitivity charts developed for bridges with the abutment structural response expected by the Ministry of Transportation and Infrastructure of British Columbia could be extended for other bridges prototypes and additional abutments nonlinearities.

References

AASHTO - American Association of State Highway and Transportation Officials. (2009). *Guide specifications for LRFD seismic bridge design.*

AASHTO - American Association of State Highway and Transportation Officials. (2011). *Guide specifications for LRFD seismic bridge design.*

AASHTO American Association of State Highway and Transportation Officials. (2012). *LRFD bridge design specifications.*

ATC-6-2. (1983). *Seismic retrofitting guidelines for highway bridges*. Palo Alto, California: Applied Technology Council.

Bjornsson S, Stanton J, Eberhard M. (1997). Seismic response of skew bridges. *6th U.S. National Conference on Earthquake Engineering,* pp. 1-12.

Caltrans. (2010). Seismic design criteria version 1.6.

CAN/CSA-S6-06. (2006). *Canadian highway bridge design code*. Toronto (Ontario, Canada).

Carvajal, J. C., Ventura, C. E., & Huffman, S. (2009). Ambient vibration testing of multi-span bridges with integral deck-abutments. Paper presented at the *Proceedings of the IMAC-XXVII,* Orlando, Florida USA.

Chao, W., Zhao, L., & Wu, Y. (2001). Centroid fault-plane inversion in three-dimensional velocity structure using strong-motion records. *Bulletin of the Seismological Society of America, 101*(3)

Chen, M., & Penzien, J. (1977). *Nonlinear soil- structure interaction of skew highway bridges* No. UCB/EERC-77/24). California: College of Engineering, University of Berkeley.

Christensen, D. (2006). Full scale static lateral load test of a 9 pile group in sand. (M.S., Brigham Young University, Department of Civil and Environmental Engineering).

Computers and Structures. (2012). *sap2000 version 15.1*. Berkeley, CA

Coordinator, I. G. B., Coordinator, M. G., Contributor, R. C. O., Contributor, B. D. O., Contributor, G. H. O., Contributor, R. I. O., et al. (1990). Bridge structures. *Earthquake Spectra, 6*(S1), 151-187.

Coordinator, J. M., Contributor, G. F. O., Contributor, R. M. O., Contributor, J. M. O., Contributor, N. P. O., Contributor, F. S. O., et al. (1995). Highway bridges and traffic management. *Earthquake Spectra, 11*(S2), 287-372.

Dimitrakopoulos, E. G. (2010). Analysis of a frictional oblique impact observed in skew bridges. *Nonlinear Dynamics, 60*(4), 575-594.

EERI, Earthquake Engineering Research Institute. (2001). 1999 Chi-Chi, Taiwan, earthquake reconnaissance report. *Earthquake Spectra, Special Supplement A, 17.*

Fayyazi, M. S., Taiebat, M., Finn, W. D. L., & Ventura, C. (2012). Evaluation of group factor method for analysis of pile groups. *Fifteenth World Conference on Earthquake Engineering,* Lisbon, Portugal. ID: 5546, 9 pages.

FHWA. (2006). *Seismic retrofitting manual for highway structures: Part 1- bridges* Federal Highway Administration.

Finn, W. D. L. (2005). A study of piles during earthquakes: Issues of design and analysis. *Bulletin of Earthquake Engineering, 3*, 141-234.

Ghobarah, A. A. (1974). Seismic analysis of skewed highway bridges with intermediate supports. *Earthquake Engineering and Structural Dynamics, 2*(3), 235-240.

Goel, R., & Chopra, A. (1995). *Seismic response study of the hwy 101/Painter street overpass near eureka using strong motion records* No. CSMIP 95-01). Berkeley, California: California Strong Motion Instrumentation Program.

Housner, G. W., Hudson, D. E., Trifunac, M. D., Frazier, G. A., Wood, J. H., Scott, R. F., et al. (1971). *Engineering features of the san fernando earthquake of february 9, 1971* No. EERL 71-02). Pasadena, California.

Housner, G. W., & Thiel, C., Jr. (1990). Competing against time; report of the governor's board of inquiry on the 1989 loma prieta earthquake. *Earthquake Spectra, 6*(4), 681-711.

Jablonski, A. M., Law, K. T., Lau, D. T., & Pierre, J. R. (1992). Collapse of the struve slough bridge during the 1989 loma prieta earthquake in different seismic code perspectives. *10 Vols,* pp. 5757-5757.

Kavianijopari, P. (2011). Performance-based seismic assessment of skewed bridges. (Doctor of Philosophy in Civil Engineering, University of California, Irvine).

Klosek, J., Deodatis, G., & Shinozuka, M. (1995). The gavin canyon undercrossing: Failure analysis under seismic loading and a retrofitting proposal using spring-damper systems. *Proceedings of the National Seismic Conference on Bridges and Highways:"Progress in Research and Practice",* San Diego- California. pp. 10-13.

Lam, I. P., & Martin, G. R. (1986). Seismic design for highway bridge foundations. *Lifeline Earthquake Engineering Performance, Design and Construction,* pp. 7-21.

Lam, I., Martin, G., & Imbsen, R. (1991). Modeling bridge foundations for seismic design and retrofitting. *Transportation Research Record,* (1290).

MAE, M. E. C. (2010). *The maule (chile) earthquake of february 27, 2010: Consequence assessment and case studies* No. 10-04).

Maleki S. (2001). Free vibration of skew bridges. *Journal of Vibration and Control, 7*, 935-952.

Maragakis, E. A., & Jennings, P. C. (1987). Analytical models for the rigid body motions of skew bridges. *Earthquake Engineering & Structural Dynamics, 15*(8), 923-944.

McCallen, D. B., & Romstad, K. M. (1994). Dynamic analyses of a skewed short-span, box-girder overpass. *Earthquake Spectra, 10*(4), 729-756.

Mitchell, D., Tinawi, R., & Sexmith, R. (1991). Performance of bridges in the 1989 loma prieta earthquake - lessons for canadian designers. *Canadian Journal of Civil Engineering, 18*, 711-734.

Moehle, J., Fenves, G., Mayes, R., Priestley, N., Seible, F., Uang, C. M. and Aschheim, M. (1995). Highway bridges and traffic management. *Earthquake Spectra*, *11*, 287

Monahan P.A., Levson, P. and Sy A. (2000). *Geoscience map 2000-3a- relative liquefaction hazard map of greater victoria* .

Mosquera, V., Smyth, W., & Betti, R. (2009). Utilization of strong motion data for assessment of integrity in instrumented highways bridges. *CSMIP09 Seminar,* California.

Murchison, J. M., & O'Neill, M. W. (1984). Evaluation of py relationships in cohesionless soils. *Analysis and Design of Pile Foundations,* pp. 174-191.

NIST. (1996). In Chung R. (Ed.), *The january 17, 1995 hyogoken-nambu (kobe) earthquake: Performance of structures, lifelines, and fire protection systems*. Gaithersburg: Building and Fire Research Laboratory.

Ortiz, A., Ventura, C., & Catacoli, S. (2013). Sensitivity analysis of the lateral damping of bridges for low levels of vibration. *Conference and Exposition on Structural Dynamics, IMAC XXXI,* Garden Grove, California.

Pina, F. E., Ventura, C. E., Taylor, G., & Finn, W. D. L. (2010). Selection of ground motions for the seismic risk assessment of low-rise school buildings in south-western british columbia, canada. (Toronto, ON).

Priestley, M. J. N. (1988). Whittier narrows, california earthquake of october 1, 1987-damage to the I-5/I605 separator. *Earthquake Spectra, 4*(2), 389-405.

Priestley, M. N., Seible, F., & Uang, C. M. (1994). *The Northridge earthquake of January 17, 1994: Damage analysis of selected freeway bridges* (Vol. 94, No. 6). Dept. of Applied Mechanics & Engineering Sciences, University of California, San Diego.

Rahmani, A., Taiebat, M., Finn, W. D. L., & Ventura, C. (2012). Determination of dynamic p-y curves for pile foundations under seismic loading. *Fifteenth World Conference on Earthquake Engineering,* Lisbon, Portugal. ID: 5228, 8 pages

Rahmani, A., Taiebat, M., and Finn, W.D.L. (2013) "Nonlinear dynamic analysis of Meloland Road Overpass using three-dimensional continuum modeling approach." *accepted for publication in Soil Dynamics and Earthquake Engineering.*

Reese, L., Wang, S., Isenhower, W., & Arrellagana, J. (2010). *Group version 8.0 technical manual*. Austin, Texas: Ensoft, Inc.

Shamsabadi, A. (2007). Three-dimensional nonlinear seismic soil-abutment-foundation-structure interaction analysis of skewed bridges. (Doctor of Philosophy (Civil Engineering), University of Southern California).

Shamsabadi, A. (2013). *Seismic soil-foundation-structure interaction (SFSI), practical bridge seismic foundation specifications design and analysis.* Unpublished manuscript.

Shamsabadi, A., & Kapuskar, M. (2010). Nonlinear soil-abutment-foundation- structure interaction analysis of skewed bridges subjected to near-field ground motions. *Transportation Research Record,* (2202), 192-205.

Shin, T., Tsai, Y., Yeh, Y., Liu, C., & Wu, T. (2002). Strong-motion instrumentation in programs in Taiwan. In Int'l Assoc. Seismol. & Phys. Earth's Interior, Committee on Education. (Ed.), *International handbook of earthquake and engineering seismology*.

Silva, P. F., Megally, S., & and Seible, F. (2009). Seismic performance of sacrificial exterior shear keys in bridge abutments. *Earthquake Spectra, 25*(3), 643-663.

Srinivasan, R. S., & Munaswamy, K. (1978). Dynamic response of skew bridge decks. *Earthquake Engineering & Structural Dynamics, 6*, 139-156.

Stewart, J. P., Abrahamson, N. A., Atkinson, G. M., Baker, J. W., Boore, D. M., Bozorgnia, Y., et al. (2011). Representation of bidirectional ground motions for design spectra in building codes. *Earthquake Spectra, 27*(3), 927-937.

SVS Structural Vibrations Solutions. (1999-2011). *Artemis extractor software*. Denmark.

Tirasti, P., & Kawashima, K. (2008). Seismic torsion response of skewed bridge piers. *JSCE Journal of Earthquake Engineering,* Turek, M., & Ventura, C. (2005). Vibration testing of the deltaport way bridge. *Proceedings of the IMAC-XXIII,* Orlando, Florida USA.

Ventura, C., Brincker, R., & Anderson, P. (2005). Dynamic properties of the painter street overpass for different levels of ground motions. *Eurodyn,* Rotterdam.

Ventura, C. E., Finn, W. D. L., Wagner P.R., & Felber A.J. (1996). Ambient vibration studies of three short-span reinforced concrete bridges. *Eleventh Conference on Earthquake Engineering,* pp. 921.

Yang, M., Rau, R., Yu, J., & Yu, M. (2000). Geodetically observed surface displacements of the 1999 Chi-Chi, earthquake. *Earth Planets Space, 52*, 403-413.

Yoshioka, S. (2001). Coseismic slip distribution of the 1999 Chi-Chi, Taiwan, earthquake deduced from inversion analysis of GPS data. *Bulletin of the Seismological Society of America, 95*(5).

Appendices

APPENDIX A. SUMMARY OF SEISMIC DAMAGE TO SKEWED BRIDGES DURING MAJOR EARTHQUAKES.

Structure	Event	Skew Angle	Total Length (m)	Typical Span (m)	No. Spans	Width (m)	Column Height (m)	Abutment Type	Found. Type	Damage description	Additional notes
Foothill Boulevard Undercrossing	San Fernando 1971	60	83.82	25	4	17	5.8	seat-type	Spread footings	Shear failure of columns, damage of wing wall, deck rotation and permanent offset at abutments (7.5 cm).	Monolithic piers-superstructure connections. Expansion joins at abutments.
Northbound Truck Route Undercrossing	San Fernando 1971	≈>30	---------	----------	-------	------	---------	-------------	---------	Columns damage, abutment translation, backfill slumping,	Monolithic piers-superstructure connections
West Sylmar Overhead	San Fernando 1971	> 60	--------	---------	6	-----	> 6 (variable)	seat-type	--------	Spalling at deck joints. Damage at the corners of stem wall.	Monolithic piers – superstructure (box girders) connections. Transversal restraint at abutments.

Structure	Event	Skew Angle	Total Length (m)	Typical Span (m)	No. Spans	Width (m)	Column Height (m)	Abutment Type	Found. Type	Damage description	Additional notes
San Fernando Road Overhead	San Fernando 1971	≈30	--------	---------	7	------	---------	seat-type	---------	Collapse of central span, column damage, abutment translation, deck rotation, and permanent offset at abutments.	Superstructure comprises by steel and prestressed concrete girders. Fallen span was steel.
Sierra Highway Undercrossing	San Fernando 1971	≈>20	--------	---------	3	------	--------	Integral	----------	Lateral damage of abutment wall.	Cantilever wall abutment separated from embankment retaining wall.
The I-5/I-605 Separation Bridge	Winter Narrows 1987	37.5 (max)	172	21	9	------	4.0 (shortest)	seat-type	Concrete piles. (pinned columns)	Shear failure of columns at central bent, spalling of girders at abutments, fracture of bearing keeper plates and permanent lateral displacements (2.5 cm)	Rocker bearings at abutments, transverse displacement restraint. Monolithic joint at box girders and cable restrainers at deck joints.

Structure	Event	Skew Angle	Total Length (m)	Typical Span (m)	No. Spans	Width (m)	Column Height (m)	Abutment Type	Found. Type	Damage description	Additional notes
Struve Slough Bridge	Loma Prieta 1989	30.5	243.84	11.3	22	10.54	> 24 m	Integral	Extended pile shaft	Combined shear and flexural failures of columns at top. Permanent deck displacement. Punching of piles through the deck. Significant lateral displacement of pier at the base.	Concrete diaphragm at piers, cast in place superstructure. Piers without cap beams. Supported on very soft clay and peat.
Rio Banano Bridge	Costa Rica, 1991	30	91	28	3	--------	9.0	seat-type	Concrete piles	Rotation of south abutment, backfill slumping, failure of piles and span unseating	Liquefaction occurred at south abutment.
Gavin Canyon Undercrossing	Northridge, 1994	66	226	28 (shortest)	5	20.73	9.44 (Shortest)	seat type	-----------	Span unseating and failure of restrainer cables, minor damage in columns, abutment translation.	short seat length (200 mm). Monolithic bent- girders connection.
Fairfax-Washington Undercrossing	Northridge, 1994	1 to 47	310	14 to 34	7	22.45	6.10	Sear type	Spread footings for abutments. Concrete piles for bents.	Columns collapse, flexural cracks in box girders.	Rocker bearings. Wall piers, multi-column bents, longitudinal restrainers at deck joints.

Structure	Event	Skew Angle	Total Length (m)	Typical Span (m)	No. Spans	Width (m)	Column Height (m)	Abutment Type	Found. Type	Damage description	Additional notes
Mission Gothic Undercrossing	Northridge, 1994	25-45	164	50	4	60	7	Seat type	Concrete Piles	Failure of columns at flares, span unseating, shear keys failure, deck rotation at abutments.	Elastomeric bearings and shear keys.
The Mukogawa bridge	Kobe, 1995	30	280	46.5	6	10	------	Seat type	Large diameter shaft (24 m depth)	Failure of bearings and longitudinal restrainers. Plastic distortion of steel girders at abutments. Damage of cross bracing, minor flexural damage in buried columns.	Rocker bearings. Longitudinal couplers installed to prevent unseating at abutments.
The Kawaraginishi bridge	Kobe, 1995	35	---------	--------	3	-----	----------	Seat type	---------	Span unseating and shear failure of wall piers.	Wall piers and multi-columns bents. Fixed joint only at one end, expansion joint without transverse restrainer elsewhere.

Structure	Event	Skew Angle	Total Length (m)	Typical Span (m)	No. Spans	Width (m)	Column Height (m)	Abutment Type	Found. Type	Damage description	Additional notes
Arifiye Overpass	Kocaeli, 1999	60	104	26	4	12.5	8	Seat type	Concrete Piles (40-50 m depth)	Span unseating, damage of MSEW walls at approaches.	The fault crossed transversally near the northern abutment. Elastomeric bearings, shear keys, and simple supported spans.
Shi-Wie bridge	Chi-Chi, 1999	55-85	75	25	3	23.5	9	Seat type	Caissons	Span unseating, columns tiltup	The fault crossed near the southern abutment Elastomeric bearings
Las Mercedes Bridge	Maule, 2010	11	28.5	-14.2	2	------	--------	Seat type	---------	Unseating of one girder, damage of shear keys	Elastomeric bearings, poor designed of shear keys and seismic restrainers. Absence of diaphragms.

Structure	Event	Skew Angle	Total Length (m)	Typical Span (m)	No. Spans	Width (m)	Column Height (m)	Abutment Type	Found. Type	Damage description	Additional notes
Paso Claudio Arrau	Maule, 2010	50	77.5	-------	4	------	---------	Seat type	------------	Cracking of shear keys, minor damage.	Elastomeric bearing, diaphragms. Poor seismic restrainers and shear keys.
Route 5 Overpass	Maule, 2010	≈>45	-------	-------	2	-----	----------	Seat type	-----------	superstructure translations Transverse (30 cm), longitudinal (41 cm), crack on east bridge embankment	Poor designed of shear keys. Absence of diaphragms.

APPENDIX B. SYSTEM IDENTIFICATION IN THE VERTICAL DIRECTION

The Enhanced Frequency Domain Decomposition (EFDD) technique available in ARTeMIS was used to undertake the modal identification analysis. For the Highway 99 and 24th Avenue Underpass seven modes of vibration in the vertical direction were clearly identified.

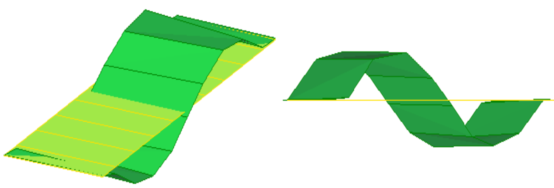

3D view elevation

1st vertical antisymmetric mode (f = 5.00 Hz)

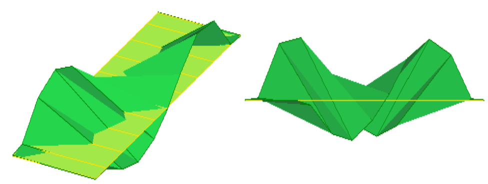

3D view elevation

1st Torsional mode (f = 5.88 Hz)

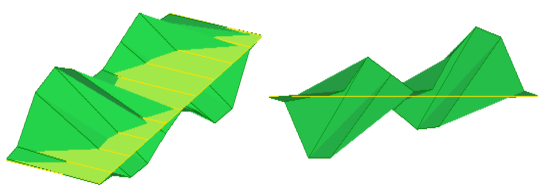

3D View Elevation

2nd Torsional mode (f = 7.00 Hz)

3D View Elevation

1st Torsional-vertical mode (f = 8.25 Hz)

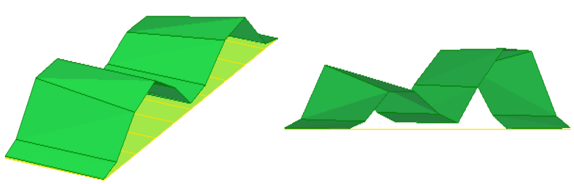

3D View Elevation

Vertical symmetric mode (f = 8.38 Hz)

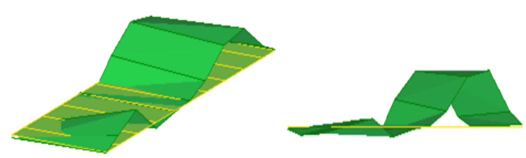

3D View Elevation

2nd Torsional-vertical mode (f = 10.69 Hz)

Vertical and torsional modes of vibration for HWY 24th

HWY 24		
Order	Freq. (Hz)	Mode Characteristic
1	5	1st Vertical Antisymmetric
2	**5.88**	1st Torsional
3	7	2nd Torsional
4	8.25	3rd Torsional
5	8.34	2nd Vertical Symmetric
6	10.69	4th Torsional

HWY 10		
Order	Freq. (Hz)	Mode Characteristic
1	5.406	1st Vertical Antisymmetric
2	5.688	2nd Vertical Symmetric
3	7.406	1st Torsional
4	7.781	2nd Torsional
5	10.41	1st Torsional-Vertical
6	10.78	2nd Torsional-Vertical
7	13.97	Torsional-Longitudinal

LHH-EB Underpass		
Order	Freq. (Hz)	Mode Characteristic
1	2.31	1st Vertical
2	2.77	1st Torsional
3	4.05	2nd Torsional
4	4.20	Torsional
5	5.06	Vertical
6	6.34	Vertical-Torsional
7	6.84	Vertical-Torsional
8	8.69	Torsional
9	9.59	Torsional
10	10.44	Vertical
11	11.63	Vertical
12	12.52	Vertical

Douglas Rd		
Order	Freq. (Hz)	Mode Characteristic
1	1.938	1st Torsional (Third Span)
2	2.625	1st Vertical
3	3.625	Longitudinal-Vertical
4	4.625	Longitudinal-Vertical
5	4.875	2nd Vertical Symmetric
6	5.313	3rd Vertical
7	6.688	Torsional
8	8.0	Vertical-Transverse
9	8.813	Vertical Antisymmetric-Transverse
10	9.063	Vertical Symmetric-Transverse
11	9.375	3rd Vertical
12	9.813	Vertical-2nd Transverse

Summary of system identification in the vertical direction

APPENDIX C. DISPLACEMENT AND ACCELERATION SPECTRA OF SELECTED GROUND MOTIONS.

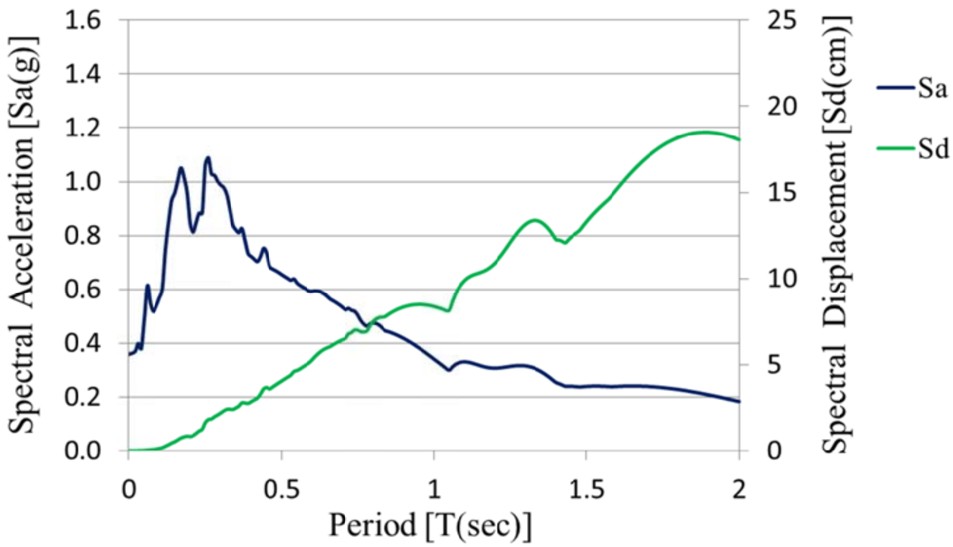

Loma Prieta (1989) - Station: CDMG-57007 Corralitos

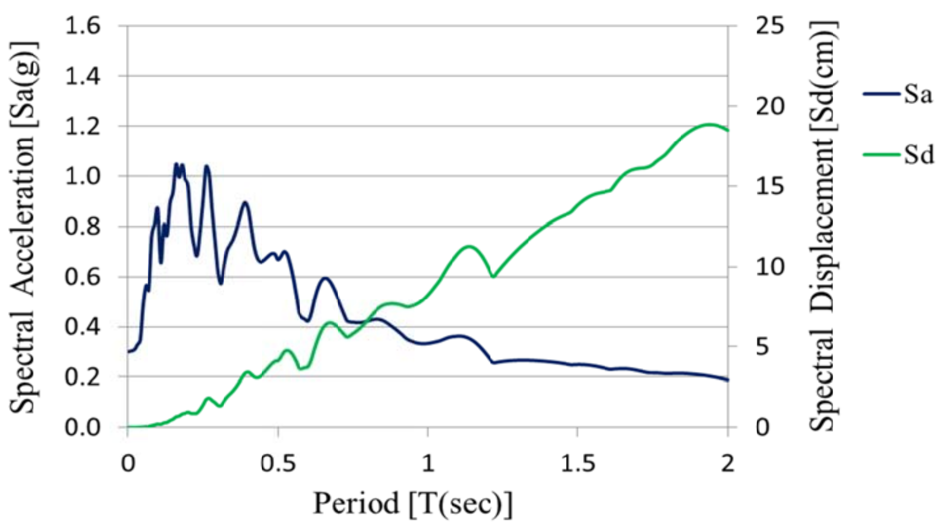

Northridge (1994)- Station: USGS 5108 Santa Susana Ground

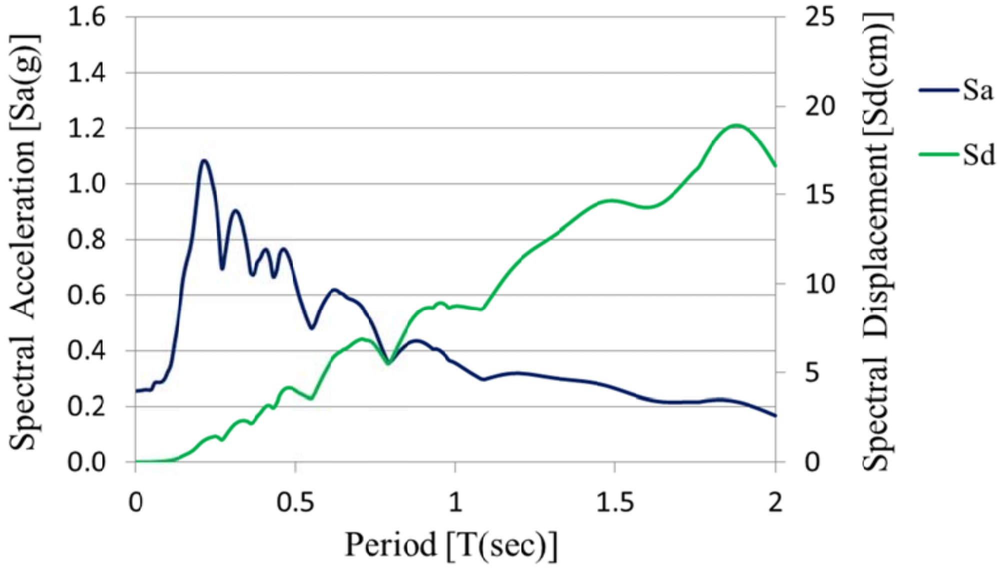

Nisqually (2001)- Station: Seattle (EVA)

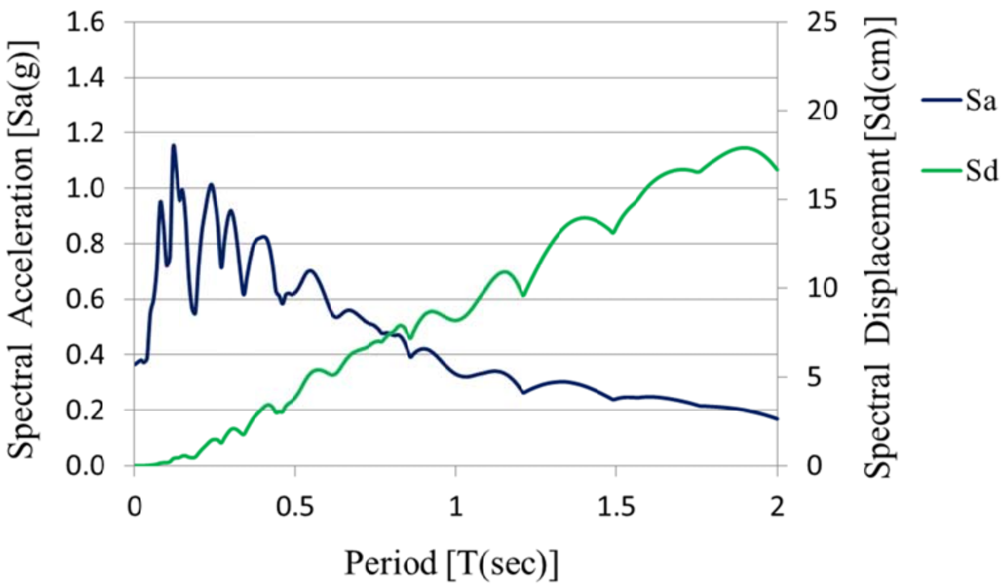

El Salvador (2001)- Station: Unidad de Salud Panchimalco (PA)

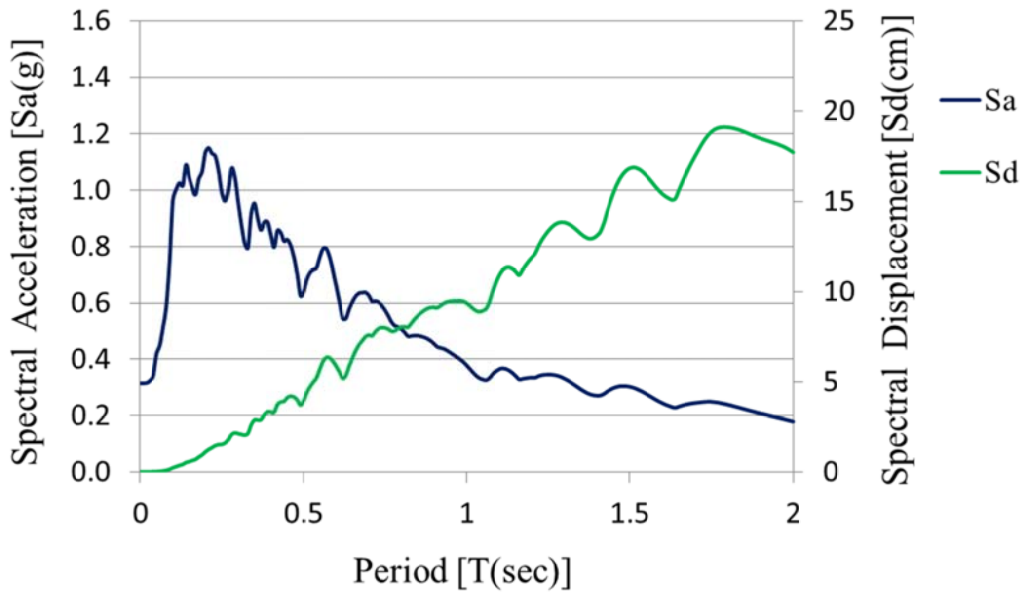

Maule (2010)- Station: Santiago Maipu (E-W)

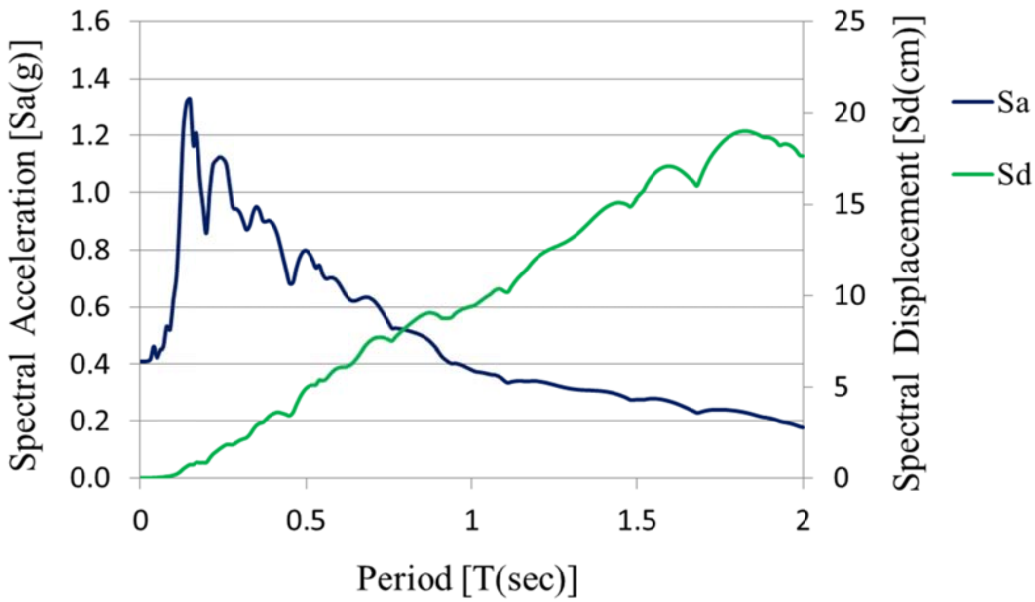

Michoacan (1985)- Station: La Union (UNIO)

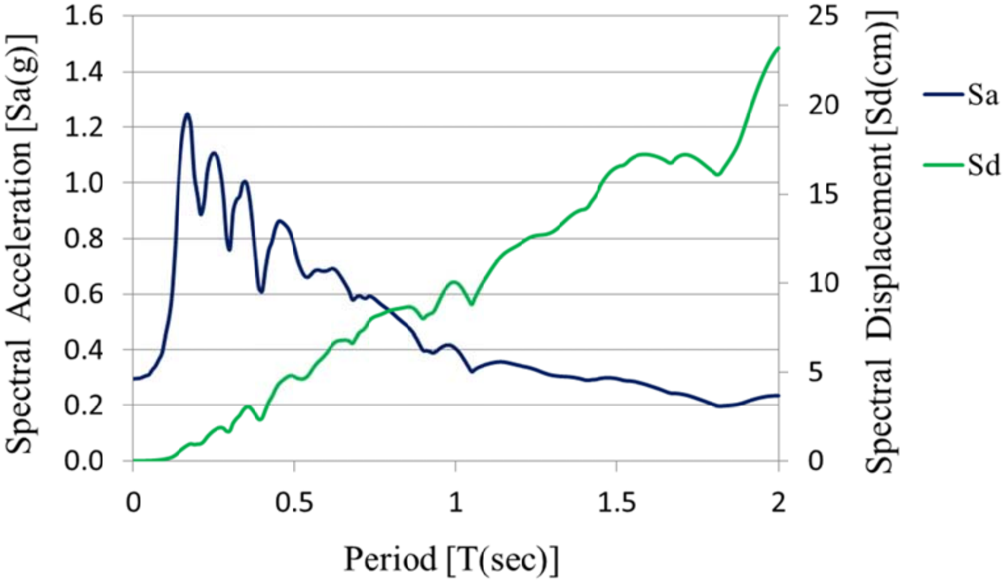

Tokachi-oki (2003)- Station: Noya (HDK107)